

# UC Santa Barbara

## UC Santa Barbara Electronic Theses and Dissertations

### Title

Xeno-Free Derivation of Retinal Pigmented Epithelium from Human Pluripotent Stem Cells

### Permalink

<https://escholarship.org/uc/item/54p650gq>

### Author

Pennington, Britney O.

### Publication Date

2014

Peer reviewed|Thesis/dissertation

UNIVERSITY OF CALIFORNIA

Santa Barbara

Xeno-Free Derivation of Retinal Pigmented Epithelium from  
Human Pluripotent Stem Cells

A dissertation submitted in partial satisfaction of the  
requirements for the degree Doctor of Philosophy  
in Biochemistry and Molecular Biology

by

Britney Ocean Pennington

Committee in charge:

Professor Dennis O. Clegg, Chair

Professor Dr. Carol A. Vandenberg

Professor Dr. Anthony W. De Tomaso

Dr. Lincoln V. Johnson, CSMD

December 2014



The dissertation of Britney Ocean Pennington is approved.

---

Lincoln V. Johnson

---

Carol A. Vandenberg

---

Anthony W. De Tomaso

---

Dennis O. Clegg, Committee Chair

December 2014

Xeno-Free Derivation of Retinal Pigmented Epithelium from  
Human Pluripotent Stem Cells

Copyright © 2014

by

Britney Ocean Pennington

## ACKNOWLEDGEMENTS

I have had the privilege to work with exceptionally inspiring individuals during my graduate experience. First and foremost, I want to thank my principal investigator, Dr. Dennis O. Clegg. He sets an outstanding example of how to conduct cutting edge research, to perform the intricate art of communicating science to specific, diverse groups, to survive the changing tides of the scientific field and how to focus on the pleasure and privilege of the project. Perhaps the most life-changing lesson I have learned from the living example of Dr. Clegg however, is to treat every human being and interaction with respect, kindness and joviality regardless of how famous, distinguished or engrossed in work you may be. Dr. Clegg has enthusiastically supported any idea that I have had, and the most fulfilling academic and career experiences that I've encountered are due to his mentorship style.

I would also like to thank Dr. Sherry T. Hikita and Dr. Dave E. Buchholz for mentoring me in the finer points of conducting experimental research, organization and musical inclinations. Dr. Duane Sears has been a devoted pedagogical mentor to me and I am so grateful for his guidance and support in my teaching endeavors. I am so appreciative of Graduate Dean Dr. Carol Genetti and Dr. Sandra Seale, two exceptionally strong female role models who have opened doors to a whole new world for me. I would like to thank Dr. Miguel de Los Rios for introducing me to a realm beyond academics. Thank you, my fellow Clegg Lab members and staff of the Center for Stem Cell Biology and Engineering.

And a big whopping thank you to my friends, past and present, particularly Daryl Taketa who is by far the most generous person I've ever met, and especially Jeff Bailey who has shared the most thrilling of life's adventures with me and has made these graduate school years the absolute best of my life. My heart is forever indebted to the unconditional love and support given to me by the Pennington and Ferencak families. Mom, you are one incredible lady.

## CURRICULUM VITAE

Britney Ocean Pennington

### EDUCATION

- Graduate: University of California Santa Barbara, 2008-Present  
Doctor of Philosophy in Biomolecular Science and Engineering  
Emphasis in Molecular Biology and Biochemistry  
GPA: 3.98
- Undergraduate: Florida Institute of Technology, 2004-2008  
Bachelor of Science in Molecular Biology  
Bachelor of Science in Biochemistry  
GPA: 4.0

### RESEARCH EXPERIENCE

- 2008-Present University of California Santa Barbara; Santa Barbara, CA  
Graduate Student Researcher in Lab of Dr. Dennis O. Clegg in the  
Biomolecular Science and Engineering Program, Center for Stem Cell  
Biology and Engineering, Neuroscience Research Institute and Institute for  
Collaborative Biotechnologies
- Summer 2007 National Renewable Energy Laboratory; Golden, CO  
Intern in the U.S. Department of Energy Science Undergraduate Laboratory  
Internship (SULI) program
- Summer 2006 Cornell University; Ithaca NY  
Intern in the Boyce Thompson Institute's Plant Genome Research Project
- 2004-2005 Florida Institute of Technology; Melbourne FL  
Undergraduate Researcher in Lab of Dr. David Carroll in Department of  
Biology and Dr. Mark Novak in Department of Chemistry

### PUBLICATIONS

**Britney O. Pennington**, "The Development of a Pluripotent Stem Cell Product in Combination with Substrate" *The Preclinical Development of Pluripotent Stem Cell-Based Therapeutics*. Springer Publishing. *In press*.

**Britney O. Pennington**, Sears DW and Clegg DO, "Interactive Hangman Teaches Amino Acid Structures and Abbreviations" *Biochemistry and Molecular Biology Education*. 2014

**Britney O. Pennington**, Clegg DO, Melkounian ZK and Hikita ST, "Defined Culture of Human Embryonic Stem Cells and Xeno-free Derivation of Retinal Pigmented Epithelial Cells on a Novel, Synthetic Substrate" *In review*.

Buchholz DE, **Britney O. Pennington**, Croze RH, Hinman CR, Coffey PJ and Clegg DO. "Rapid and Efficient Directed Differentiation of Human Pluripotent Stem Cells into Retinal Pigmented Epithelium," *Stem Cells Translational Medicine*. 2013. (2)5:384-93.

Clegg DO, Hikita ST, Hu Q, Buchholz DE, Rowland TJ, Conti L, **Britney O. Pennington**, Croze R, Leach L, Tsie M, and Johnson LV "Derivation of retinal pigmented epithelial cells from pluripotent stem cells" (2013) *The Stem Cell Handbook*, Second Edition, S. Sell, Ed., Springer Publishing.

Yongqing L, **Britney O. Pennington** and Hua J. "Multiple R-like genes are negatively regulated by *BON1* and *BON3* in *Arabidopsis*". *Molecular Plant-Microbe Interactions*. 2009. (22)7:840-8.

Carroll DJ, Mantilla A, **Britney O. Pennington**, and Wei H, "Regulation of mitogen activated protein kinase in single starfish oocytes during maturation and fertilization. " *FASEB Journal* 2007. (21)abstract 786.8.

## HONORS & AWARDS

- Sigma Xi Grants-In-Aid of Research Award (\$2000)
- UCSB Outstanding Teaching Assistant Award (\$1000)
- Richard & Katherine Gee Breaux Fellowship in Vision Research (\$10,000)
- Fight For Sight Summer Student Fellowship (\$2,100)
- Doreen J. Putrah Cancer Research Foundation Conference Fellowship (\$1000)
- Runner-up in the UCSB Grad Slam 3-minute Elevator Pitch Competition (\$1000)
- Sigma Xi Grants-In-Aid of Research Award (\$2500)
- California Institute for Regenerative Medicine Scholar (Fall 2011 – Fall 2012)
- Center for Science and Engineering Partnerships School for Scientific Thought Instructor (\$4000)
- Co-Designer of the winning T-shirt Design for MCDB and BMSE (Spring 2012)
- Audience's Favorite Poster Award, MCDB Department Retreat (Fall 2010)
- American Association of University Women's Award for Academic Excellence
- Florida Institute of Technology Faculty Honor Award (2008)
- Distinguished Student Scholar Award (Spring 2008)
- Florida Tech's Outstanding Senior in Biochemistry (Spring 2008)
- FIT Department of Biological Sciences Certificate of Appreciation (Spring 2008)
- Florida Institute of Technology's Outstanding Senior (Spring 2007)
- Florida Tech's Outstanding Senior in Molecular Biology (Spring 2007)
- Distinguished Student Scholar Award (Spring 2007)
- Florida Tech's Outstanding Junior in Molecular Biology (Spring 2006)
- First Place Chem-E Car Team at 2006 AIChE Southern Regional Competition
- Phi Eta Sigma Honor Society (Spring 2005- Fall 2008)
- Tri-Beta Biological Honor Society (Spring 2005- Fall 2008)
- First Place ScrapBook design for the Tri-Beta Southern Regional Conference

- Appointed to the College of Science Dean's Student Advisory Committee (Fall 2005 – Spring 2008)
- Florida Tech Trustee Scholarship (Total: \$40,000)
- Florida Academic Scholarship (Total: \$15,626)
- Dr. Richard and Charlotte Moore Scholarship (Total: \$9,281)
- Florida Roofing, Sheet Metal and Air Conditioning Contractors Association (FRSA) Educational Foundation Scholarship (Total: \$5,000)
- Valedictorian of Winter Park High School, Winter Park's Biology Department's Student of the Year, Winter Park Rotary Club's Student of the Month (Spring 2004).

## INVITED PRESENTATIONS

- Britney Pennington, "Directly Reprogramming Human Cells to Treat Ocular Diseases" 2014. Science and Engineering Council Invited Speakers Lunch, Goleta, CA.
- Britney Pennington, "Directly Reprogramming Human Cells to Treat Ocular Diseases" 2014. UCSB Evening Receptions, San Jose and Walnut Creek, CA.
- Britney Pennington, "Directly Reprogramming Human Cells to Treat Ocular Diseases" 2014. USCB Development Event San Diego Parent Reception, Del Mar, CA.
- Britney Pennington, "Directly Reprogramming Human Cells to Treat Ocular Diseases" 2013. Board of Trustees of the UCSB Foundation, Santa Barbara, CA.
- Britney Pennington, "Directly Reprogramming Human Cells to Treat Ocular Diseases" 2013. UCSB Grad Slam Finals, Santa Barbara CA.
- Britney Pennington, "Stem Cells and Regenerative Medicine" 2012. Family Science Night, Mountain View Elementary School, Goleta, CA.
- Britney Pennington, "Directly Reprogramming Human Somatic Cells into RPE" 2012. Neuroscience Research Institute's Annual Symposium, University of California Santa Barbara, CA.
- Britney Pennington, "Visualizing the Temperature Dependent Migration of Lignin Using Cytochemistry" 2007. National Renewable Energy Laboratory, Golden, CO.
- Britney Pennington, "The Quest for Natural Variations of *Lesion Cell Death* Loci in *Arabidopsis*" 2006. Boyce Thompson Institute at Cornell University, Ithaca, NY.

## TEACHING EXPERIENCE

Adjunct Professor	Cell Biology Lecture and Lab 2013 Westmont, Santa Barbra, CA
Associate Instructor	Stem Cell Biology in Health and Disease 2013-2014 UCSB, Santa Barbara, CA
Instructor	Stem Cells and Regenerative Medicine School for Scientific Thought Program Center for Science and Engineering Partnerships 2013, UCSB, Santa Barbara, CA

Science, Math and Reading Summer Camp  
Windover Community Church Multi-Family Housing Ministry  
2008, Windover Apartments, Melbourne, FL

Teaching Assistant    Biochemistry I, Neurobiology II, Introductory Biology Laboratory  
2008-2012 UCSB, Santa Barbara, CA

Volunteer                2012 - SciTrek Program at Harding Elementary, Santa Barbara, CA  
2010-Present - Family Ultimate Science Event (FUSE)  
2007 – Afterschool Program Tutor for middle school students  
2004 – Tutor at Stone Middle School with Advancement Via  
   Individual Determination (AVID) Program

#### PEDAGOGICAL CONFERENCES, WORKSHOPS AND POSTER PRESENTATIONS

Conferences    “21<sup>st</sup> Century Approaches to Teaching and Communicating in BMB”  
ASBMB Annual Meeting at Experimental Biology Conference in San Diego,  
CA. April 26-30, 2014

“Student-Centered Education in the Molecular Life Sciences” ASBMB  
Special Symposia, Hosted by: Vicky Minderhout and Jennifer Loertscher at  
Seattle University, WA. August 4-7, 2013

“Transitions, Education and Professional Development” ASBMB Annual  
Meeting at the Experimental Biology Conference in Boston, Massachusetts.  
April 22-26, 2013

Poster                Britney Pennington and Clegg DO “Ideas for Fun and Engaging Activities  
when Teaching Stem Cell Biology.” Student-Centered Education in the Life  
Sciences Symposia, Seattle, WA. August 6, 2013.

Workshops        “Learning Objectives, Assessments, and Learning Strategies” ASBMB  
Regional Full Day Workshop. Hosted by Dr. Duane Sears, Dr. Vicky  
Minderhout and Dr. Anne Wright, UCSB. February 8, 2014.

“ASBMB Assessment of Students – Reasoning with Core Concepts and  
Visualization in Biochemistry.” Full Day Workshop. Hosted by Dr. Trevor  
Andersen, Dr. Nancy Pelaez, and Dr. Hal White at Purdue University,  
Indiana. November 7, 2012

“Concept-Driven Teaching Strategies in Biochemistry and Molecular  
Biology.” Full Day workshop. Hosted by Dr. Duane Sears and Dr. Mike  
Klymkowsky at UCSB.

“Creating Interactive Sections with Active Learning.” And “Avoiding and  
Managing Conflict in a Classroom.” Hosted by Dr. Lisa Berry at UCSB.

“Jump Starting Discussion.” Hosted by Dr. Kim DeBacco at UCSB.

## ABSTRACT

### Xeno-Free Derivation of Retinal Pigmented Epithelium from Human Pluripotent Stem Cells

By

Britney Ocean Pennington

Age-related macular degeneration (AMD) is the leading cause of blindness in the elderly and is characterized by the death of the retinal pigmented epithelium (RPE), the cell layer located behind the retina. The RPE maintains the health of the primary cells responsible for vision, the photoreceptors. As AMD progresses, the RPE degrades, which causes the death of the photoreceptors and a debilitating loss of sight. Human embryonic stem cells (hESCs) can generate a limitless source of RPE for cellular therapies, therefore efforts to derive RPE from human embryonic stem cells (hESCs) to graft into AMD patients are under development. This thesis addresses two of the obstacles that hinder the production of these therapeutical cells. First, to manufacture cells for clinical use, it is desirable for procedures to be performed under defined conditions free of non-human reagents (xeno-free). Therefore, a novel, biomimetic, xeno-free RGD-containing copolymer designed for cell culture was investigated and found to support healthy hESC cultures and permit their differentiation into functional RPE. These stem cells and hESC-RPE demonstrate similar gene expression, protein localization and phagocytic function as cultures grown on a xenogeneic substrate. The second obstacle pertains to the intense time requirement needed



to differentiate hESCs into RPE. Therefore, we recapitulated the signaling events during early embryonic development to expedite the production of hESC-RPE from 1-3 months to 14 days. However, this protocol employs full length recombinant growth factors and animal derivatives. These components represent a challenge in employing these cells as therapies due to the risk of exposure to non-human immunogens. Preliminary work to replace the xenogeneic substrate and recombinant growth factors with small molecules is presented. These pilot studies demonstrate that a xeno-free substrate and dual-Smad inhibition via small molecules can rapidly and efficiently differentiate hESCs into a population of cells expressing a pigmentation marker. These studies contribute to the development of defined, xeno-free methods for cellular manufacture which can further the translation of stem cell therapies to the clinic.

## TABLE OF CONTENTS

I. Introduction .....	1
A. Pluripotent Stem Cell-Derived Retinal Pigmented Epithelium .....	2
B. Substrates for Stem Cell-Derived RPE .....	10
C. Combination of Stem Cell-Derived RPE with Substrate. ....	27
D. Future Directions .....	22
E. References .....	22
II. Novel Synthetic Substrate for Embryonic Stem Cells and RPE .....	28
A. Supports Human Embryonic Stem Cells .....	38
B. Xeno-Free Spontaneous Differentiation of hESCs into RPE.....	41
C. References .....	55
III. Rapid and Efficient Derivation of RPE from hESCs.....	59
A. Development of a Directed Differentiation Protocol.....	59
1. References.....	82
B. XenoFree Adaptation of Rapid and Efficient Directed Differentiation.....	84
1. References.....	100
IV. Development of Interactive Learning Exercises for Biochemistry .....	102
V. Conclusions.....	112
Appendix.....	114
A. Supplemental Tables.....	114
B. Supplemental Figures.....	115

## LIST OF FIGURES

Figure 1. hESC-RPE differentiation and enrichment .....	7
Figure 2. Structures of parylene variants .....	14
Figure 3. Photolithography of parylene-C into an ultrathin substrate .....	16
Figure 4. hESC-derived RPE on ultrathin parylene-C substrates .....	19
Figure 5. hESC characterization on Synthemax® II-SC .....	40
Figure 6. Efficiency of spontaneous differentiation on various substrates .....	42
Figure 7. Characterization of H9-derived hESC-RPE on various substrates .....	44
Figure 8. H9-derived hESC-RPE on Synthemax® II-SC are functional .....	47
Figure 9. hESC-RPE on parylene-C scaffolds .....	49
Figure 10. Factors rapidly direct pluripotent cells towards RPE fate .....	68
Figure 11. Pigmented RPE progenitors begin to pigment by day 14 .....	70
Figure 12. Gene & protein expression of directly differentiated UCSF4 and iPSC ..	71
Figure 13. Time course of early eye field gene and protein expression .....	74
Figure 14. Analysis of RPE enriched on day 14 and grown for 30 days in culture ..	76
Figure 15. Altering [msNoggin] and [Synthemax® II-SC] eliminates D14 Matrigel.	93
Figure 16. Achieving PMEL+ cells by replacing msNoggin with DMH1 .....	95
Figure 17. Replacing msNoggin with DMH1 yields similar gene expression .....	96
Figure 18. Achieving neural morphology with DMH1 and SB431542 .....	97
Figure 19. Dual-Smad inhibition yields a majority of PMEL+ cells .....	98
Figure 20. Example of the Amino Acid Hangman game .....	106
Figure 21. Percent of students assigning correct abbreviation pre/post Hangman .	109
Figure 22. Percent of students drawing correct structure pre/post Hangman .....	110

## LIST OF SUPPLEMENTAL TABLES & FIGURES

Supp. Table 1. Examples of Hints and Answers to Amino Acid Hangman .....	114
Supp. Figure 1. H9 & H14 hESC colony morphology on various substrates .....	115
Supp. Figure 2. Characterization of H14 hESCs on xeno-free substrates .....	116
Supp. Figure 3. H14-derived hESC-RPE on retain identity and function .....	117
Supp. Figure 4. Lacunae in hESC cultures on Synthemax <sup>®</sup> II-SC .....	118
Supp. Figure 5. Gene expression in H9 and H14-derived hESC-RPE .....	119
Supp. Figure 6. Morphology during D14 differentiation and after enrichment .....	120
Supp. Figure 7. Reference sheet of amino acid structures.....	121

# I. Introduction

Britney O. Pennington and Dennis O. Clegg\*

Center for Stem Cell Biology and Engineering, Neuroscience Research Institute, Program in Biomolecular Science and Engineering, Department of Molecular Cellular and Developmental Biology Department, University of California Santa Barbara, CA 93106.

Chapter 15: Development of a Pluripotent Stem Cell Product in Combination with Substrate  
*The Preclinical Development of Pluripotent Stem Cell-Based Therapeutics*  
Springer Publishing 2014.

## Abstract

Age-related macular degeneration (AMD) is the leading cause of blindness in the United States of America, which places an immense economic burden on society and severely decreases the quality of life in the patients. Pluripotent stem cells provide an unlimited source of retinal pigmented epithelium (RPE) which are being developed as a therapy for AMD. In order to ensure the precise delivery of functional RPE to the diseased site, scaffolds that support the cells during transplantation and post-surgery are also being tested. This chapter describes recent progress in generating RPE from human embryonic stem cells, and the characterization of a novel, biostable scaffold consisting of the polymer parylene-C. Stem cell-derived RPE monolayers on scaffolds hold great promise for the treatment of AMD and other retinal diseases.

**Abbreviations** Age-Related Macular Degeneration (AMD), chemically induced pluripotent stem cells (CiPSCs), hexamethyldisilazane (HMDS), human embryonic stem cells (hESC), induced pluripotent stem cells (iPSCs), inner cell mass (ICM), *in vitro* fertilization (IVF), mesh-supported submicron Parylene- C membrane (MSPM), pluripotent stem cell (PSC) Poly(D,L-lactic-co-glycolic acid) (PLGA), poly (ethylene glycol) (PEG), reactive ion etching (RIE), retinal pigmented epithelium (RPE), Royal College of Surgeons (RCS), scanning electron microscope (SEM), spectral-domain optical coherence tomography (SD-OCT)

## ***A. Pluripotent Stem Cell-Derived Retinal Pigmented Epithelium***

Geron Corporation's clinical trial for treating spinal cord injury in 2009 heralded the advent of human embryonic stem cell (hESC)-derived products as therapies for human maladies. In the infancy of this field, the eye is an excellent target organ for novel hESC therapies due to its potentially immune privileged state, its excellent endpoint parameters with non-invasive imaging techniques and sophisticated surgical protocols already in place. Diseases affecting the eye drastically affect the patient's quality of life and present an economic burden to society. Therefore, developing effective hESC-derived treatments for blindness has been an intense topic of research. All five of the recruiting clinical trials using hESC derivatives to treat diseases are targeting ocular pathologies. This section reviews the progress of developing a pluripotent stem cell (PSC) product to treat age-related macular degeneration.

### **Retinal Pigmented Epithelium & Age-Related Macular Degeneration**

Age-related macular degeneration (AMD) is the leading cause of blindness in people over 55 years of age and is predicted to cost the United States government at least \$845 million annually as the population ages [1, 2]. Two forms of AMD exist. The "wet", exudative form is characterized by blood vessel invasion into the retina and accounts for about 10% of AMD cases [3]. Vision loss occurs due to the formation of fibrotic scars and an accumulation of fluid between the neural retina and its supportive retinal pigmented epithelium (RPE) [1]. Currently, only palliative treatments are available for the wet form, which includes a regimen of intraocular injections of angiogenesis inhibitors such as Lucentis<sup>®</sup> and Avastin<sup>®</sup> and EYLEA<sup>®</sup>. The other form of AMD, nonexudative or "dry" AMD, afflicts the majority of patients and is characterized by "geographic atrophy" where

RPE, photoreceptors and choroid are degenerated or dysfunctional in the macula. The macular area of the retina is responsible for high acuity, central vision, and although it only accounts for 4% of the retinal area, it perceives 10% of the visual field [1]. Within the macula lies a region of the highest density of color-detecting cone photoreceptor cells in the retina. This fovea is just 2mm in diameter, but its cones allow for 20/20 vision and the discernment of fine details [1]. Therefore, vision crucially relies on the photoreceptors in the macular region, and these cells are supported and maintained by the underlying RPE.

The RPE is a polarized epithelial monolayer, meaning the two sides of the monolayer perform distinct, specialized functions. Located just behind the neural retina, the apical microvilli of the RPE interact with photoreceptors, while its basal side attaches to the basal lamina in Bruch's membrane, which separates the RPE from the vascular choroid. Although it does not directly participate in the transduction of light sensation like the neural retina, this epithelial layer performs a myriad of functions essential for vision. These include maintaining the health of the photoreceptors by transporting nutrients from the blood, removing old photoreceptor outer segments by phagocytosis, isomerizing all-trans to 11-*cis*-retinal to perpetuate the visual cycle, limiting oxidation in the eye, and absorbing stray light [1, 4, 5].

In dry AMD, fatty, proteinacious deposits called drusen accumulate between Bruch's membrane and the RPE monolayer. Drusen are associated with RPE dysfunction and degradation [6]. It is generally accepted that RPE dysfunction and death leads to deterioration of the photoreceptors and shriveled choroidal vessels. Although the molecular mechanisms that initiate AMD have not been fully elucidated, both environmental factors such as smoking and genetic polymorphisms in complement factors H, B, and Apolipoprotein E are associated with AMD [7-10].

Since RPE dysfunction primarily causes dry AMD, which accounts for 90% of the cases, several efforts have been made to replace the damaged cells with viable RPE to rescue visual function [3]. Early efforts to restore healthy RPE to patients with a degenerating macular region involved detaching and rotating the retina, or transplanting an autologous, peripheral RPE-choroid graft to the affected macular area. Although some patients regained light-sensitivity in the region of the graft (demonstrating some modicum of proof of concept), overall vision diminished and serious side effects such as retinal detachment were observed [11]. Transferring RPE from one region of the eye to the diseased site also requires substantial surgical skills and is technically challenging. Furthermore, in these autologous graft cases, aged RPE comprise the therapeutic cells, and if genetic factors caused the AMD, then the graft will consist of similarly flawed cells [12, 13].

### **Generating Stem Cell-Derived RPE for Clinical Applications**

Current efforts to restore healthy RPE to patients use allogenic RPE generated from human embryonic stem cells (hESCs) and induced pluripotent stem cells (iPSCs), for both pluripotent sources can theoretically produce an unlimited supply of RPE for cellular therapies [14, 15]. Clinical trials have already been initiated for both hESCs and iPSCs for the treatment of AMD [16-18].

### **Pluripotent Stem Cells**

hESCs are characterized as pluripotent cells, meaning they have the powerful ability to differentiate into any cell type in the body. During normal development, hESCs appear as the inner cell mass (ICM) region of the blastocyst, which is the embryonic stage five days post fertilization. This hollow cellular cluster contains about one hundred cells, and these



blastocysts are routinely generated outside of the body at *in vitro* fertilization (IVF) clinics [19]. Since only a subset of the created blastocysts are selected for implantation, the remaining embryos can be cryopreserved for potential future implantations, donated to other couples, donated to research after informed consent, or discarded [20]. Once designated for research, the hESCs in the ICM of donated blastocysts are harvested, and due to their perpetual self-renewing capabilities, can be grown continuously in culture in the lab [21].

Embryonic stem cells are not the only pluripotent source for generating RPE, for iPSCs are also capable of generating these specialized cells [22]. To accomplish induction of pluripotency in a differentiated somatic cell, a cocktail of exogenously applied stem cell transcription factors will commandeer the machinery maintaining the host cell's identity, which forcibly reprograms the cell into an embryonic stem cell-like state. Although relatively new to the science world, iPSCs have revolutionized our approach to studying and treating diseases. First created with murine cells in 2006 [23] and recapitulated in human cells in 2007 by independent labs [24, 25], iPSCs have already earned one of their discoverers the Nobel Prize in 2012. Since iPSCs originate from adult cells, fewer ethical and legal concerns hinder their progress towards the clinic. Additionally, iPSCs will be genetically matched to the donor cell type, thus providing the possibility of making patient-specific stem cells with limited immunogenicity for cellular therapies [26].

Early protocols for reprogramming involved virally inserting vectors in the host's genome, which could result in mutagenesis if the insertion disrupted the code for an essential gene. Newer methods use non-integrating vectors, including episomal Epstein Barr virus [27] or Sendai Virus [28]. Reprogramming has also been accomplished using mRNAs [29] and microRNAs [30]. As the field progresses towards clinical applications, several attempts to replace viral integration with small molecules for induction have culminated in a

successful virus-free reprogramming of murine somatic cells to pluripotency [31]. Exposing mouse embryonic, neonatal and adult fibroblasts to a cocktail of seven small molecules, which consisted of a cAMP agonist, GSK and TGF- $\beta$  inhibitors and chromatin modifiers, was sufficient to reprogram the somatic cells into chemically induced pluripotent stem cells (CiPSCs) [31]. Reprogramming with small molecules precludes unnecessary tampering with the genetic material, which could lead to adverse effects such as activation of oncogenes.

However, iPSCs are not identical to hESCs and may harbor genetic mutations and aging marks incurred by environmental insults on the original somatic cell [32]. Furthermore, the differentiation capability of iPSC lines is unpredictable [33], even when the lines originate from the same cell type. For example, four RPE lines were reprogrammed into iPSCs, but only two displayed preferential re-differentiation back into RPE, which was manifested by the expedited appearance of pigmented regions during the spontaneous iPSC differentiation [34]. The remaining two lines, however, did not exhibit this trend and actually produced fewer pigmented regions than the hESC control [34]. Other reports also suggest a disparity in the function of iPSC vs. hESC derived RPE [35]. Although iPSCs should not be eliminated as a potential source of therapeutic cells, extra precaution and characterization should be performed on their derivatives before proceeding to the clinic.

### **Differentiation of Pluripotent Stem Cells into RPE**

A plethora of protocols describe various ways of generating RPE from pluripotent stem cells [15, 16, 22, 33, 36-43]. It has been shown that stem cells grown as adherent monolayers or as 3D aggregates in suspension will spontaneously differentiate into a myriad of cell types including RPE. Spontaneous differentiation is accomplished by removing

molecules such as basic fibroblast growth factor (bFGF) from the stem cell culture conditions since these molecules are essential for maintaining hESC pluripotency *in vitro*. The differentiating monolayer or free-floating, spherical embryoid bodies, will then require several weeks to months to make patches of pigmented RPE surrounded by other differentiating cell types [36, 37, 44]. These pigmented patches may be manually isolated from contaminating cell types in order to obtain an enriched population of RPE (Fig. 1).

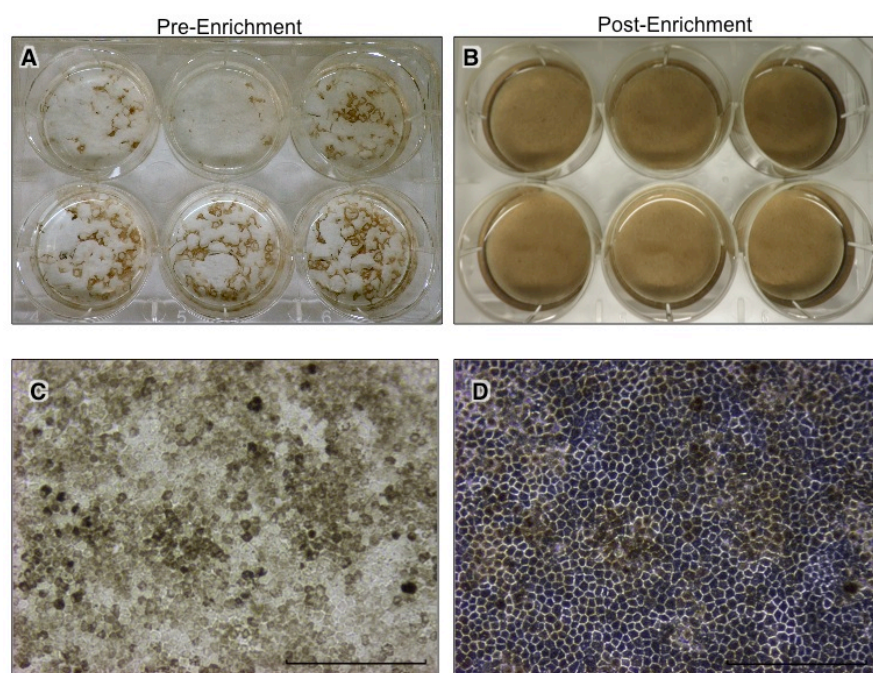


**Figure 1.** Human embryonic stem cells differentiating into RPE can be manually enriched to produce a more pure population of therapeutic cells. Upon removal of bFGF, hESC cultures will spontaneously differentiate into a myriad of cell types, including RPE. After about 30 days in culture, pigmented foci will appear in the culture dishes. (A) After 100 days in culture, large pigmented regions can be observed within the well of the tissue culture vessel by the naked eye. These regions may be manually separated from non-pigmented cells in a process termed “enrichment.” (B) By thirty-five days post-enrichment, a more pure population of pigmented hESC-derived RPE can be observed in the tissue culture vessel. (C) A brightfield and (D) phase contrast micrograph of an enriched hESC-derived RPE culture reveals the typical pigmented, cobblestone morphology with tight junctions between cells. Scale bar = 200µm.

Since spontaneous differentiation of stem cells into RPE requires an intense time investment, several labs have designed a variety of directed differentiation protocols to expedite this derivation. Furthermore, stimulating the directed differentiation of a particular cell type may discourage the growth of contaminating cells, thus increasing the final yield of desired cell product. In these endeavors, natural signaling mechanisms that occur during the *in vivo* development help researchers identify which molecular candidates should be exogenously applied to the *in vitro* stem cells to accelerate their differentiation into RPE. The primary events of RPE development *in vivo* involve neural induction prior to gastrulation, specification of the eye field within the embryonic brain, and then maturation of specific ocular cells as the eye develops through the optic vesicle and optic cup stages [5, 45].

In order to initially guide stem cell differentiation towards a neural fate, as opposed to other fates from the mesoderm and endoderm germ lineages, directed differentiation protocols have applied neuralizing growth factors such as nicotinamide, Dkk-1, Lefty-A, and commercial supplements such as N2 or B27<sup>®</sup> [33, 40, 41, 43]. Then, additional growth factors such as Activin-A, retinoic acid, and TGF $\beta$ 1 will predispose the neural cells to assume an RPE fate upon further differentiation [41]. A report in July 2012 claimed to accomplish neuralization in 5 days, and upon addition of Activin-A achieved an RPE yield of 95 $\pm$ 1% by day 30 [46]. To accomplish this efficient conversion of stem cells to RPE, cyst-like aggregates of undifferentiated hESC colonies were embedded in BD Matrigel<sup>™</sup> hESC-Qualified Matrix, which is an extract rich in extracellular matrix proteins derived from the Engelbreth-Holm-Swarm murine sarcoma. The embedded, three-dimensional culture system mimicked the *in vivo* environment during neural tube formation by surrounding the entire cluster of cells with a matrix that supplied contacts for cellular

adhesion. This approach facilitated the rapid attainment of a neural fate and varies from other culture methods, which use free-floating spherical aggregates in solution or a 2D monolayer. The embedded neural progenitors however, may produce RPE or neural retinal derivatives. In order to promote an RPE identity, the 3D neural cysts were recovered from their Matrigel encasement and plated on a 2D culture system in the presence of Activin-A to foster the development of a polarized monolayer. By day 18, pigmented regions appeared followed by the acquisition of the typical cobblestone RPE morphology and expression of RPE-specific molecular markers such as Mitf, RPE65 and Bestrophin. These hESC-derived RPE effectively performed phagocytosis on the photoreceptor outer segments when co-cultured with murine retinal explants. This differentiation protocol demonstrates the value of combining exogenously applied growth factors, embedded 3D conditions and 2D monolayers when directing the differentiation of hESCs to RPE [46].

To date, the most rapid directed differentiation protocol generates RPE from pluripotent stem cells in 14 days [47]. By combining protocols that efficiently generate neural progenitor cells with effective procedures for deriving RPE, 80% of the stem cell derivatives at the end of two weeks are positive for PMEL17, a pre-melanosomal protein and an RPE marker. [22, 41, 47, 48]. To prime the population of pluripotent stem cells for expedited RPE development, the culture first undergoes neural induction to generate an eye field precursor population. This is accomplished by adding nicotinamide and noggin to induce a neural fate [41, 49], the canonical wnt inhibitor Dkk-1 which promotes eye field development, and IGF-1 which stimulates forebrain and early eye field transcription factor expression [5]. Then, the addition of Activin-A and an FGF inhibitor SU5402 effectively guides the cells to an RPE fate instead of neural retina. The RPE generated by the 14<sup>th</sup> day may be enriched and cultured as a monolayer for an additional month. These cells express

RPE markers such as tyrosinase, PEDF and CRALBP, and demonstrate functional phagocytosis of rod outer segments. In addition to rapidly generating RPE, this expedited protocol is useful for studying signaling mechanisms during RPE development. Furthermore, this group identified a mechanism of partial PARP-1 inhibition as a possible explanation of how nicotinamide accelerates the development of RPE from hESCs [41, 47, 49].

However, these directed differentiation protocols use Matrigel™ in their procedures, which is an animal derivative. In order to manufacture cells for clinical use, it is desirable for procedures to be performed under defined conditions sans animal products, or xeno-free, and many studies are still optimizing the derivation with these parameters [50]. Ideally, small molecules could replace recombinant proteins and peptides and xeno-free substrates would support pluripotent stem cell maintenance and promote their differentiation to RPE.

### ***B. Substrates for Stem Cell-Derived RPE***

A biomedical substrate or scaffold aims to provide a supportive, structural surface for cells to attach, proliferate, differentiate and perform their normal functions after transplantation [51]. Recent results indicate that hESC-RPE monolayers on a substrate survive longer than bolus injections of hESC-RPE [52]. The chemical composition and physical traits of the substrate significantly influence how the transplanted cells will operate in a diseased setting. Perhaps most importantly, the substrate must support the therapeutic cells' health and function. This section describes the development of a transplantable substrate designed to support the pluripotent stem cell based product, hESC-derived RPE.

## Types of Substrates

In order to design an effective substrate for the transplantation of hESC-derived RPE, the qualities of the *in situ* RPE substrate should be considered. Naturally, the polarized RPE monolayer orients its apical side towards the photoreceptors of the neural retina while the basolateral side sits upon the supportive, underlying Bruch's membrane. This pentalaminar Bruch's membrane consists of an elastin layer sandwiched between two collagen strata, which separates the basal membranes of the RPE from the underlying endothelial cells of the choriocapillaris blood vessels [53]. In addition to emulating the chemical composition during substrate design, the relative thickness of the transplant must also be considered. The Bruch's membrane is 1-4 $\mu$ m thick, and substrates significantly exceeding this dimension could distort the contour of the overlying neural retina, and would thus result in a deformed visual perception [54].

Purified proteins or modifications of constituents within the Bruch's membrane have been investigated as candidates for RPE scaffolds. Gelatin, which is made of single peptide chains from the denatured collagen triple helix [55], has been investigated as a substrate since it is a derivative of a naturally occurring Bruch's membrane constituent. However, two layers of RPE opposed to a single monolayer appeared 28 days after transplanting a porcine RPE sheet on a gelatin substrate, possibly due to the sheet doubling back on itself [56]. Furthermore, employing natural products for substrate fabrication could lead to irreproducibility of results due to batch-to-batch variations in the acquisition of these proteins.

Synthetic polymers can be finely tuned to match the physical and chemical properties of the transplant's destination while also providing high reproducibility in large-scale manufacturing processes [51]. Both biodegradable and biostable synthetic polymers have

been investigated as substrates for RPE transplantation. The decomposition rate of biodegradable scaffolds can be controlled by varying the ratios of the constituents in the substrate and the types of bonds connecting them. Biodegradable scaffolds provide initial support to the therapeutic cells during and shortly after the transplantation, and these substrates do not leave a residual ectopic product in the eye since they are metabolized over time. However, both the biodegradable polymer and its degradation products must not elicit an immune response [51].

A vast array of synthetic, biodegradable candidate materials have been investigated for supporting RPE health and function. Poly(D,L-lactic-co-glycolic acid) (PLGA) for example, is a biodegradable FDA approved poly ( $\alpha$ -hydroxy ester) whose properties can be tuned by controlling the ratio of the lactide and glycolide constituents [57, 58]. Certain ratios of high molecular weight PLGA can support the adhesion and proliferation of human fetal RPE *in vitro* [57]. Hydrolysis of the ester bond of the two constituents produces molecules that are biocompatible and readily metabolized *in vivo* [51]. However, to our knowledge no biodegradable substrates have been used to transplant pluripotent stem cell derived RPE into the subretinal space [15]. Conversely, biostable scaffolds would offer permanent support to the therapeutic cells, but must not interfere with the natural transport of nutrients.

### **Parylene-C**

One biostable polymer used in many biomedical applications including transporting RPE into the subretinal space is parylene-C, a member of the *para*-xylylene polymerization products [59]. In 1947, Michael Mojzesz Szwarc, a physical chemist at the University of Manchester in the aftermath of World War II, noticed that a peculiar coating would



accumulate on his equipment when studying the decomposition of gaseous *para*-xylene [60, 61]. *P*-xylene consists of a benzene ring with methyl groups in the *para* positions, but during pyrolysis it converts to *p*-xylylene, which is kinetically prone to polymerize in the solid phase, thus producing the thin, peelable film on Szwarc's devices [59, 60, 62]. However in Szwarc's studies, only 10-15% of the polymerization precursor, *p*-xylylene was produced, which would cause a bottleneck in a larger-scale manufacturing attempt [60, 62]. In 1966, the production of the polymer was perfected by William Gorham at Union Carbide Corporation in New Jersey [59]. Gorham used a di-*p*-xylylene intermediate, or (2,2)*p*-cyclophane, during the production process which yielded 99% of the polymerizing *p*-xylylene product, now known as parylene [62]. In 1991, Union Carbide Corporation transferred the production of parylenes to Specialty Coating Systems which has since founded nine manufacturing locations around the world [63].

Today, the commercial synthesis of parylene exclusively uses the Gorham Process, which involves 1) the sublimation of di-*p*-xylylene in a vaporizer, 2) its conversion to the gaseous monomer *p*-xylylene in a pyrolysis chamber and 3) the chemical vapor deposition of the gaseous monomer on a given surface at room temperature [59, 62, 64]. Upon deposition, the monomer spontaneously polymerizes into poly-*p*-xylylene, or parylene-N [59]. Parylene-N is a linear chain of poly-*p*-xylylene whose aromatic rings are substituent free (Fig. 2). Functionalizing the benzene ring of the precursors with chlorine atoms produces polymer derivatives with varying mechanical, thermal and electrical properties known as parylene-C, which possesses one chlorine substituent per aromatic ring, and parylene-D, which possesses two (Fig. 2) [59, 65].

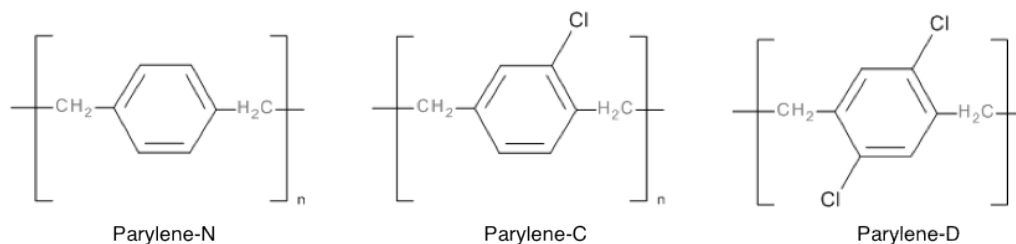


**Figure 2.** Structures of parylene variants. Members in the parylene polymer family have distinct physical properties and can be used in various applications. Parylene-C has been implemented in coating electronics and biomedical devices and has been recently engineered into ultrathin, semipermeable membranes to serve as a substrate for hESC-derived RPE.

Initially, the electronics industry capitalized on parylene-C's low water and gas permeability for producing protective coatings for circuit boards. Also, the chemical vapor deposition of parylene results in a conformal coating sans pinholes [59, 64]. Pinholes arise from bubbles that are trapped during the deposition process which later burst to create defects in the film, thus rendering any underlying circuitry vulnerable [66]. This conformal coating property expanded parylene's application to protecting delicate biomedical circuitry implanted into the relatively hostile environment of the body. Physicians have used parylene-C coated pacemakers, stents and electrodes acting as neural prostheses [64, 67]. Furthermore, parylene-C is chemically inert and has a Young's Modulus measure of stiffness of 3.2GPa, which confers recalcitrance to tearing [64, 65, 68].

### Engineering Parylene-C into a Biocompatible Substrate

As a hydrophobic polymer, parylene-C forms a protective barrier that isolates its cargo from the body and therefore must be modified in order to support adherent, therapeutic cells [64, 65, 69]. Etching parylene-C with oxygen plasma for one to two minutes significantly increases its hydrophilicity which enables the polymer to support adherent cells similarly to polystyrene, or tissue culture plastic [65, 70]. Additionally, parylene-C may be micropatterned into specific structures and stencils by photolithography, thus making it

amenable to a range of cellular applications [68, 71, 72]. For example, layered parylene-C stencils support patterned *in vitro* co-cultures of cells, such as stem cells with hepatocytes and fibroblasts. This allows for the regulated study of spatio-temporal effects of intercellular contacts between stem cells and their neighbors [68].

Photolithography is essential in order to use parylene-C as substrate for transplanting stem-cell derived RPE into the subretinal space. As mentioned above, parylene-C is impermeable to water, gases and small molecules, which would hinder the RPE function of transporting nutrients from the choriocapillaris below the Bruch's membrane to the photoreceptors in the neural retina. In order to overcome this barrier, ultrathin parylene membranes (.15-.80 $\mu$ m) have been designed and fabricated by the Tai Group using a two-step lithography approach [72, 73]. This method deposits a thicker parylene meshwork (6 $\mu$ m) as a base layer to support the subsequent delicate, ultrathin coating (Fig. 3). Briefly, the thick layer of parylene-C coats a silicon foundation treated with hexamethyldisilazane (HMDS) (Fig. 3a). HMDS affects parylene's adhesion to other chemicals during the lithography process [71, 72]. The next two layers include aluminum and a photoresist, a substance that confers protection to underlying layers until exposed to light (Fig. 3b). Lithography of the photoresist, wet aluminum etching, and reactive ion etching (RIE) of the parylene-C bores an array of 20 $\mu$ m diameter cylinders through the underlying strata to the silicon base (Fig. 3c,d). Once this supportive meshwork has been constructed, a final application of ultrathin parylene-C and photoresist are applied over the pre-existing layer, which results in an array of ultrathin parylene regions supported by the meshwork of thicker polymer (Fig. 3e,f,g) [72, 73]. Flipping the ultrathin meshwork after synthesis presents a continuous, semi-permeable, biostable substrate to the pluripotent stem cell-derived RPE (Fig. 3h). Ultrathin regions of 0.15-0.50 $\mu$ m thickness have been calculated to permit

diffusion of chemicals up to MW ~1,302 to 291 KDa, respectively, which includes most of the serum protein [72]. Vitamin A, a nutrient that must pass through the Bruch's membrane to perpetuate the visual cycle, and its carrier have a MW ~75KDa, which suggests ultrathin parylene-C meshwork is a viable substrate for emulating the Bruch's membrane when transplanting stem cell-derived RPE [72-75].

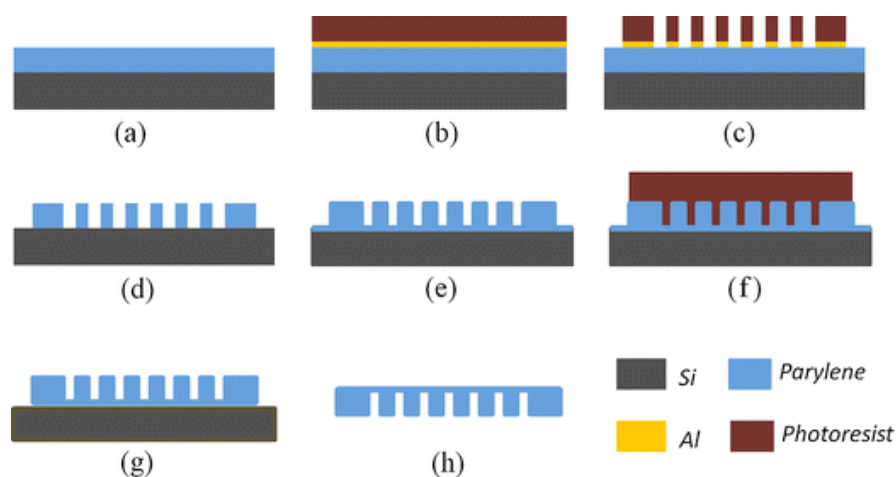


**Figure 3.** Photolithography of parylene-C into an ultrathin substrate. (a) A thicker, 6  $\mu\text{m}$  layer of parylene-C first coats HMDS treated silicon. (b) A second layer formed by the sequential coating of aluminum and photoresist (c) undergoes photolithography and wet-etching to form a template or mask that protects the underlying parylene-C during the (d) reactive ion etching (RIE). This removes the uncovered parylene-C and results in an array of hollow cylinders in the thick parylene layer. (e) A second, ultrathin (0.30  $\mu\text{m}$ ) layer of parylene-C and (f) a photoresist are applied, and a final round of lithography and RIE (g) give shape to the final substrate product. (h) The resulting, ultrathin parylene-C membrane is removed from the silicon base and inverted to present a continuous, semi-permeable, biostable substrate to the pluripotent stem cell-derived RPE. © *Biomedical Microdevices* (2012) 14(4) pp 659-667, "Mesh-supported submicron parylene-C membranes for culturing retinal pigment epithelial cells" Lu B, Zhu D, Hinton D, Humayun M, Tai YC, Fig 1. – with kind permission from Springer Science+Business Media.

Having confirmed the ability of parylene-C to permit nutrient transport, it is necessary to demonstrate its biocompatibility in the subretinal space. When compared to poly(imide), amorphous aluminum oxide-coated poly(imide), poly(vinyl pyrrolidone) and poly (ethylene glycol) (PEG) after transplantation into the subretinal space of Yucatan pigs, parylene-C and

PEG did not significantly alter the retinal architecture nor did they instigate abnormal RPE behavior for three months [76].

These studies demonstrate that parylene-C can be fabricated with the proper dimensions and characteristics to support cell adhesion, provide appropriate diffusion properties, and to not distort the contour of the neural retina nor illicit an immune response.

### ***C. Combination of Stem Cell-Derived RPE with Substrate for Cellular Therapies***

Bringing a cellular therapy from the lab to the clinic requires an astounding cooperation among diverse fields. Collaborations between cell biologists, material scientists, physicists, surgeons, and engineers reflect the truly interdisciplinary nature of regenerative medicine [77]. Designing a pluripotent stem cell-based product in combination with a synthetic substrate for subretinal transplantation to treat AMD exemplifies such synergy. This section discusses the combination of hESC-derived RPE with the synthetic parylene-C substrate, surgical strategies to transplant this fabricated product, and the next progressive steps in the field.

#### **Cell-Suspension vs. Adherent Cells on a Substrate for Cellular Therapies for AMD**

An intense topic of interest in the field is the relative efficacy of transplanting healthy RPE as a single cell suspension or as a monolayer on a supportive substrate to treat AMD. Both approaches have been investigated, and both are currently undergoing clinical trials or pre-clinical animal studies [17, 78-80].

Cells in a suspension would be easier to deliver into the eye and would cause less trauma during surgery. The first clinical study to use hESC-derived cells for ocular diseases

injected a suspension of hESC-derived RPE into the subretinal space of one dry-AMD patient and one Stargardt's Disease patient and in both cases, observed slight visual improvement after four months [17]. However, the degree of degeneration in diseased retinas will vary from patient to patient, therefore, it is difficult to extrapolate from this one instance the efficacy of injecting an RPE suspension as a viable therapy for the entire AMD population. Cells from a suspension could localize to any retinal area, thus providing a randomized, patchy support of photoreceptors [81]. Furthermore, loose cells in a suspension may aggregate, precluding the formation of a polarized monolayer and possibly incurring an immunological reaction.

An alternative approach utilizes, solid, transplantable substrates that enable delivery of a polarized monolayer to a specific destination while providing support in a diseased environment. Parylene-C is a candidate substrate for transplanting hESC-derived RPE. Lu et al. (2012) have demonstrated that RPE derived from the H9 hESC line can adhere and grow into a confluent monolayer with characteristic RPE morphology and pigmentation on an ultrathin parylene-C substrate (Fig. 4a-c). These hESC-derived RPE cells express the tight junction marker ZO-1, which demonstrates the formation of an epithelial layer (Fig. 4d). Typical apical microvilli develop, which are essential to the phagocytic function of RPE in maintaining photoreceptor outer segments *in vivo* (Fig. 4e-f). This proof of concept culture demonstrates that hESC-derived RPE can attain confluency and form a polarized monolayer on parylene-C.

Two recent studies demonstrated that hESC-derived RPE seeded on an ultrathin parylene-C substrate 1) do not elicit an immune response in immunocompromised nude rats [52] and 2) can be effectively transplanted into the subretinal space of a Royal College of Surgeons (RCS) rat, an animal model for blindness [80].

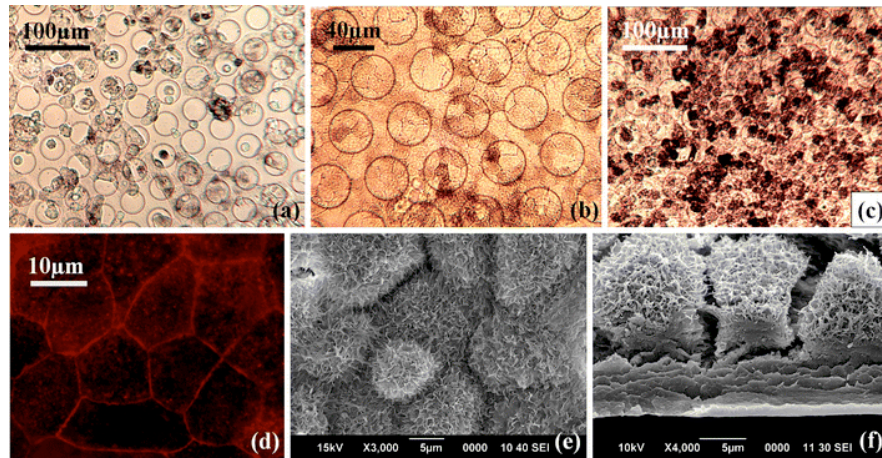


**Figure 4.** hESC-derived RPE cells cultured on the ultrathin parylene-C substrate. Images taken (a) one day (b) one week and (c) four weeks after seeding hESC-derived RPE onto the ultrathin parylene-C substrate demonstrate the cells' ability to attach, proliferate and form a confluent, pigmented monolayer. (d) Immunostaining for the tight junction marker, ZO-1, reveals the typical cobblestone morphology and the epithelial trait of the RPE. (e) Top-view and (f) cross-section scanning electron micrographs confirm an established, polarized monolayer on the parylene-C substrate with the RPE microvilli oriented on the apical side. © *Biomedical Microdevices* (2012) 14(4) pp 659-667, "Mesh-supported submicron parylene-C membranes for culturing retinal pigment epithelial cells" Lu B, Zhu D, Hinton D, Humayun M, Tai YC, Fig 9. – with kind permission from Springer Science+Business Media.

In order to compare the immunogenicity of an hESC-derived RPE cell suspension to a cellular monolayer on an ultrathin parylene-C substrate, each condition was applied to the subretinal space of an athymic nude rat, which is an immunocompromised rat lacking T-cells [52, 82]. Neither resulted in tumor formation, but the supportive parylene substrate significantly improved the viability of the hESC-derived RPE 12 months post implantation when compared to the injected suspension. Specifically, 50% of the 2700 cells that were transplanted on the substrate were detected by human RPE markers one year post-surgery, while only 25% of the 100,000 cells that were injected as a cell suspension could be found in the eye [52]. Additionally, the transplantable substrate significantly promoted the maintenance of a polarized monolayer while the suspension cells formed clumps in the subretinal space. It has previously been demonstrated that once in suspension, RPE

reattachment rate is directly proportional to cell survival [83]. This demonstrates obvious benefits to using a substrate. Cells attached to a scaffold have an increased likelihood to survive, form a polarized monolayer, and to be precisely delivered to a specific destination.

Demonstrating efficacious delivery of a stem cell-based product on a substrate and functional recovery in an animal model is an essential prerequisite before proceeding to clinical trials. Researchers have demonstrated the feasibility of transplanting hESC-derived RPE on parylene-C into the subretinal space of the RCS rat, an animal model of blindness [80]. In 1953, Professor Sorsby at the Royal College of Surgeons in London inbred rats prone to heritable cataracts for over nine generations. Later in 1960, Sidman and Pearlstein inbred these animals for 5-9 additional generations and entitled the resulting strain the Royal College of Surgeons (RCS) rat [84]. These animals are homozygous recessive for an allele of the pink-eyed dilution gene, *p*, which affected the RPE pigmentation *in vivo* but not *in vitro*, and to a much lesser extent, the body size [84]. This strain became notorious for its retinal degeneration which starts 18 days after birth due to accumulation of rod outer segments. [85]. The RPE in the RCS rat cannot perform phagocytosis to remove the excess outer segments due to a mutation in the receptor tyrosine kinase gene *Mertk* [86]. Therefore, these animals start to become blind by 18 days after birth due to an excess accumulation of photoreceptor outer segments and experience a total loss of vision within 3 months [86, 87]. Vision in RCS rats may be rescued by subretinal cell-suspension injections of fetal rat RPE [88], adult human ARPE19, genetically modified h1RPE7 [89] hESC-RPE [16] and iPSC-RPE [90]. However, the RCS rat does not emulate the disease phenotype of drusen deposits nor neovascularization as seen in AMD, but this strain does offer an animal model in which to test the viability, functionality, and potential immunogenicity of transplanted RPE cells on a substrate. The RCS rat model system has also been used to study retinitis pigmentosa.



Ultrathin parylene-C membranes carrying therapeutic hESC-derived RPE have also been successfully introduced into the subretinal space of the RCS rat and normal Copenhagen rats [80]. Proper placement of the transplant was confirmed by spectral-domain optical coherence tomography (SD-OCT). Although the procedure caused an expected retinal detachment, the tissue reattached within in one week. Comparing the numbers of hESC-derived RPE adhered to the substrate pre- and post-transplantation revealed less than 2% of the cells were dislodged during surgery. Specifically, the cell loss was observed primarily at the edges of the substrate, leaving the cells in the center of the patch seemingly undisturbed [80]. Optokinetic assays [90] that measure visual rescue by hESC-derived RPE on parylene-C substrates *in vivo* are currently being investigated.

### **Cell Delivery Methods**

Transplanting an intact hESC-derived RPE monolayer can be technically challenging, which has stimulated the optimization of surgical approaches to ensure reproducibility of the procedure with protection and proper orientation of the graft. A fork-like implantation device has been used to implant synthetic scaffolds of parylene-C, silicon oxide and iridium oxide into the subretinal space of RCS rats [91]. Prior to implantation, the scaffold slides between two prongs of the tool, which confers mechanical stability, and once in the subretinal space, the prongs slide away while a central bar keeps the implant in place. However, implants used with this device were thicker than 10 $\mu$ m and had not been coated with cells. This approach may be more appropriate for transplanting thicker electrical retinal prosthesis rather than ultrathin membranes coated with therapeutic cells [80, 91]. These bulky implantation tools may obstruct the surgeon's view, which could result in damage to the optic nerve and retina. An alternate technique demonstrated protection of

human fetal RPE by encapsulating the cells grown on a rigid-elastic polyester substrate, polyethylene terephthalate (PET) with gelatin, which preserved the implant during an *in vitro* injection through a specially designed cannula [79]. However, in order to avoid batch-to-batch variation of naturally derived products such as gelatin, synthetic platform devices are preferred over organic substrates when protecting the specialized monolayer grown on an ultrathin substrate.

To transplant hESC-derived RPE grown on an ultrathin parylene-C membrane into the subretinal space of the RCS rat, the Humayun group has developed an implantation tool that supports and protects the delicate cargo and allows for specific orientation during delivery. The cell and substrate implant rests on a thicker (10 $\mu$ m) parylene plate and is secured in place during the surgery by raised barriers which are 30 $\mu$ m high. Together, this implantation device and its cargo remains sufficiently sturdy to endure the shear force of the surgery, but is not too stiff to cause injury to the surrounding soft retinal tissue. The implantation plate and its therapeutic cargo are delivered into the subretinal space with forceps. Once in the desired location, forceps maintain the position of the implant while the tool is withdrawn. In contrast to cumbersome transplantation devices that may interfere with the surgeon's view and result in accidental damage, this thin parylene platform device is only slightly wider than the implant itself [80]. Additional tools must be designed when transplanting therapeutic cells on a substrate into larger mammals.

#### ***D. Future Directions***

Monitoring stem cell-derived RPE post-transplantation is essential to fully assess their integration into host tissue. To this end, human-specific markers such as Tra-1-85 can be used to distinguish the hESC-derived cells from the host animal tissue [52]. Furthermore,

fluorescent reporters of genes of interest could be used in animal models. Novel methods for labeling the transplanted human cells are needed to allow researchers to evaluate proper monolayer orientation and integration as well as to detect any unwanted migration or dedifferentiation.

Transplantation of healthy hESC-derived RPE on parylene-C as discussed in this chapter may only treat early stages of AMD since photoreceptors would already have perished in the progressed form of the disease. A plethora of protocols describe photoreceptor differentiation from hESCs [33, 40, 48], and hESC-derived retinal progenitors have been demonstrated to integrate with host neural tissue and restore some visual response in blind mice [92, 93]. However, photoreceptors cannot be restored in AMD patients unless the underlying RPE is also functional. Therefore, in order to rescue photoreceptors and RPE in late-AMD patients, scaffolds supporting both cell types must be designed.

In 2014, we stand at the threshold of using pluripotent stem cell based products as a powerful tool in regenerative medicine. Human embryonic stem cells possess the ability to generate any cell type in the body, which offers an unlimited source of material for replacement therapeutics. Synthetic substrates may ensure the support and directed delivery of the hESC-derived cells in a myriad of diseases. If successful, pluripotent stem cell-derived products in combination with substrates may cure currently untreatable diseases, replace expensive palliative medications, and restore quality of life to previously afflicted patients.

**Acknowledgments** This work was supported by the Richard & Katherine Gee Breaux Fellowship in Vision Research, Garland Initiative for Vision, Fight for Sight, Sigma Xi, The Foundation Fighting Blindness Wynn-Gund Translational Research Acceleration Program, the UCSB Institute for Collaborative Biotechnologies through grant W911NF-09-0001 from the U.S. Army Research Office, and the California Institute for Regenerative Medicine DR1-01444, CL1-00521, TG2-01151 (DOC) and Major Facilities grant FA1-00616. BOP was a fellow of the California Institute for Regenerative Medicine. The content of the information does not necessarily reflect the position or the policy of the Government, and no official endorsement should be inferred. We would like to thank Dr. Sherry Hikita and the Pennington and Ferencak families for their tremendous support and inspiration.

## References

1. Hageman GS, Gehrs K, Johnson LV, Anderson D (1995) Age-related macular degeneration (AMD). Webvision: The Organization of the Retina and Visual System [Internet]. Salt Lake City, UT: University of Utah Health Sciences Center
2. Rein DB, Zhang P, Wirth KE, et al. (2006) The economic burden of major adult visual disorders in the United States. *Arch Ophthalmol* 124:1754–1760. doi: 10.1001/archophth.124.12.1754
3. Carr A-JF, Smart MJK, Ramsden CM, et al. (2013) Development of human embryonic stem cell therapies for age-related macular degeneration. *Trends in Neurosciences* 36:385–395. doi: 10.1016/j.tins.2013.03.006
4. Strauss O (2005) The Retinal Pigment Epithelium in Visual Function. *Physiological Reviews* 85:845–881. doi: 10.1152/physrev.00021.2004
5. Clegg DO, Buchholz D, Hikita S, et al. (2008) Retinal pigment epithelial cells: development in vivo and derivation from human embryonic stem cells in vitro for treatment of age-related macular degeneration. 1–24.
6. Johnson LV, Forest DL, Banna CD, et al. (2011) Cell culture model that mimics drusen formation and triggers complement activation associated with age-related macular degeneration. *Proc Natl Acad Sci USA* 108:18277–18282. doi: 10.1073/pnas.1109703108
7. Baird PN (2004) The 2 and 4 Alleles of the Apolipoprotein Gene Are Associated with Age-Related Macular Degeneration. *Investigative Ophthalmology & Visual Science* 45:1311–1315. doi: 10.1167/iovs.03-1121
8. Haines JL (2005) Complement Factor H Variant Increases the Risk of Age-Related Macular Degeneration. *Science* 308:419–421. doi: 10.1126/science.1110359
9. Melville H, Carpinello M, Hollis K, et al. (2013) 1479-5876-11-53. *Journal of Translational Medicine* 11:1–1. doi: 10.1186/1479-5876-11-53
10. Hageman GS, Anderson DH, Johnson LV, et al. (2005) A common haplotype in the complement regulatory gene factor H (HF1/CFH) predisposes individuals to age-related macular degeneration. *Proc Natl Acad Sci USA* 102:7227–7232.
11. Chen FK, Uppal GS, Rubin GS, et al. (2008) Evidence of Retinal Function Using Microperimetry following Autologous Retinal Pigment Epithelium-Choroid Graft in Macular Dystrophy. *Investigative Ophthalmology & Visual Science* 49:3143–3150. doi: 10.1167/iovs.07-1648
12. John S, Natarajan S, Parikumar P, et al. (2013) Choice of Cell Source in Cell-Based Therapies for Retinal Damage due to Age-Related Macular Degeneration: A Review. *Journal of Ophthalmology* 2013:1–9. doi: 10.1002/jcb.22701
13. Binder S (2011) Scaffolds for retinal pigment epithelium (RPE) replacement therapy. *British Journal of Ophthalmology* 95:441–442. doi: 10.1136/bjo.2009.171926
14. Haruta M, Takahashi M (2005) Embryonic Stem Cells: Potential Source for Ocular Repair. *Semin Ophthalmol* 20:17–23. doi: 10.1080/08820530590921846
15. Rowland TJ, Buchholz DE, Clegg DO (2011) Pluripotent human stem cells for the treatment of retinal disease. *J Cell Physiol* 227:457–466. doi: 10.1002/jcp.22814
16. Lu B, Malcuit C, Wang S, et al. (2009) Long-Term Safety and Function of RPE from Human Embryonic Stem Cells in Preclinical Models of Macular Degeneration. *Stem Cells* 27:2126–2135. doi: 10.1002/stem.149
17. Schwartz SD, Hubschman J-P, Heilwell G, et al. (2012) Embryonic stem cell trials for macular degeneration: a preliminary report. *The Lancet* 379:713–720.
18. Mellough C First iPSC clinical trials to take place in Japan. In: [stemcellportal.com](http://www.stemcellportal.com/news-and-press/latest-news/571-first-ipsc-clinical-trials-to-take-place-in-japan.html). <http://www.stemcellportal.com/news-and-press/latest-news/571-first-ipsc-clinical-trials-to-take-place-in-japan.html>. Accessed 1 Sep 2013
19. Hardy K, Handyside AH, Winston RM (1989) The human blastocyst: cell number, death and allocation during late preimplantation development in vitro. *Development* 107:597–604.
20. Dickens BM (2008) International Society for Stem Cell Research (ISSCR) Guidelines for the Conduct of Human Embryonic Stem Cell Research (December 2006). *Med Law* 27:179–190.
21. Thomson JA (1998) Embryonic Stem Cell Lines Derived from Human Blastocysts. *Science* 282:1145–1147. doi: 10.1126/science.282.5391.1145
22. Buchholz DE, Hikita ST, Rowland TJ, et al. (2009) Derivation of functional retinal pigmented epithelium from induced pluripotent stem cells. *Stem Cells* 27:2427–2434. doi: 10.1002/stem.189
23. Takahashi K, Yamanaka S (2006) Induction of Pluripotent Stem Cells from Mouse Embryonic and Adult Fibroblast Cultures by Defined Factors. *Cell* 126:663–676. doi: 10.1016/j.cell.2006.07.024
24. Takahashi K, Tanabe K, Ohnuki M, et al. (2007) Induction of Pluripotent Stem Cells from Adult Human Fibroblasts by Defined Factors. *Cell* 131:861–872. doi: 10.1016/j.cell.2007.11.019
25. Yu J, Vodyanik MA, Smuga-Otto K, et al. (2007) Induced Pluripotent Stem Cell Lines Derived from Human Somatic Cells. *Science* 318:1917–1920. doi: 10.1126/science.1151526

26. Araki R, Uda M, Hoki Y, et al. (2013) Negligible immunogenicity of terminally differentiated cells derived from induced pluripotent or embryonic stem cells. *Nature* 494:100–104. doi: 10.1038/nature11807
27. Yu J, Hu K, Smuga-Otto K, et al. (2009) Human Induced Pluripotent Stem Cells Free of Vector and Transgene Sequences. *Science* 324:797–801. doi: 10.1126/science.1172482
28. Fusaki N, Ban H, Nishiyama A, et al. (2009) Efficient induction of transgene-free human pluripotent stem cells using a vector based on Sendai virus, an RNA virus that does not integrate into the host genome. *Proc Jpn Acad, Ser B* 85:348–362. doi: 10.2183/pjab.85.348
29. Mandal PK, Rossi DJ (2013) Reprogramming human fibroblasts to pluripotency using modified mRNA. *Nat Protoc* 8:568–582. doi: 10.1038/nprot.2013.019
30. Anokye-Danso F, Trivedi CM, Juhr D, et al. (2011) Highly Efficient miRNA-Mediated Reprogramming of Mouse and Human Somatic Cells to Pluripotency. *Cell Stem Cell* 8:376–388. doi: 10.1016/j.stem.2011.03.001
31. Hou P, Li Y, Zhang X, et al. (2013) Pluripotent Stem Cells Induced from Mouse Somatic Cells by Small-Molecule Compounds. *Science* 341:651–654. doi: 10.1126/science.1239278
32. Pera MF (2011) Stem cells: The dark side of induced pluripotency. *Nature* 471:46–47. doi: 10.1038/471046a
33. Meyer JS, Shearer RL, Capowski EE, et al. (2009) Modeling early retinal development with human embryonic and induced pluripotent stem cells. *Proc Natl Acad Sci USA* 106:16698–16703. doi: 10.1073/pnas.0905245106
34. Hu Q, Friedrich AM, Johnson LV, Clegg DO (2010) Memory in Induced Pluripotent Stem Cells: Reprogrammed Human Retinal-Pigmented Epithelial Cells Show Tendency for Spontaneous Redifferentiation. *Stem Cells* 28:1981–1991. doi: 10.1002/stem.531
35. Feng Q, Lu S-J, Klimanskaya I, et al. (2010) Hemangioblastic Derivatives from Human Induced Pluripotent Stem Cells Exhibit Limited Expansion and Early Senescence. *Stem Cells* 28:704–712. doi: 10.1002/stem.321
36. Klimanskaya I, Hipp J, Rezai KA, et al. (2004) Derivation and comparative assessment of retinal pigment epithelium from human embryonic stem cells using transcriptomics. *Cloning Stem Cells* 6:217–245. doi: 10.1089/clo.2004.6.217
37. Lund RD, Wang S, Klimanskaya I, et al. (2006) Human embryonic stem cell-derived cells rescue visual function in dystrophic RCS rats. *Cloning Stem Cells* 8:189–199. doi: 10.1089/clo.2006.8.189
38. Gong J, Sagiv O, Cai H, et al. (2008) Effects of extracellular matrix and neighboring cells on induction of human embryonic stem cells into retinal or retinal pigment epithelial progenitors. *Experimental Eye Research* 86:957–965. doi: 10.1016/j.exer.2008.03.014
39. Vugler A, Carr A-J, Lawrence J, et al. (2008) Elucidating the phenomenon of HESC-derived RPE: Anatomy of cell genesis, expansion and retinal transplantation. *Experimental Neurology* 214:347–361. doi: 10.1016/j.expneurol.2008.09.007
40. Osakada F, Ikeda H, Sasai Y, Takahashi M (2009) Stepwise differentiation of pluripotent stem cells into retinal cells. *Nat Protoc* 4:811–824. doi: 10.1038/nprot.2009.51
41. Idelson M, Alper R, Obolensky A, et al. (2009) Directed Differentiation of Human Embryonic Stem Cells into Functional Retinal Pigment Epithelium Cells. *Stem Cell* 5:396–408. doi: 10.1016/j.stem.2009.07.002
42. Liao JL, Yu J, Huang K, et al. (2010) Molecular signature of primary retinal pigment epithelium and stem-cell-derived RPE cells. *Hum Mol Genet* 19:4229–4238. doi: 10.1093/hmg/ddq341
43. Nistor G, Seiler MJ, Yan F, et al. (2010) Three-dimensional early retinal progenitor 3D tissue constructs derived from human embryonic stem cells. *Journal of Neuroscience Methods* 190:63–70. doi: 10.1016/j.jneumeth.2010.04.025
44. Rowland TJ, Blaschke AJ, Buchholz DE, et al. (2012) Differentiation of human pluripotent stem cells to retinal pigmented epithelium in defined conditions using purified extracellular matrix proteins. *J Tissue Eng Regen Med* 7:642–653. doi: 10.1002/term.1458
45. O'Rahilly R (1975) The prenatal development of the human eye. *Experimental Eye Research* 21:93–112.
46. Zhu Y, Carido M, Meinhardt A, et al. (2013) Three-Dimensional Neuroepithelial Culture from Human Embryonic Stem Cells and Its Use for Quantitative Conversion to Retinal Pigment Epithelium. *PLoS ONE* 8:e54552. doi: 10.1371/journal.pone.0054552.s010
47. Buchholz DE, Pennington BO, Croze RH, et al. (2013) Rapid and Efficient Directed Differentiation of Human Pluripotent Stem Cells Into Retinal Pigmented Epithelium. *Stem Cells Translational Medicine* 2:384–393. doi: 10.5966/sctm.2012-0163
48. Lamba DA, Karl MO, Ware CB, Reh TA (2006) Efficient generation of retinal progenitor cells from human embryonic stem cells. *Proc Natl Acad Sci USA* 103:12769–12774. doi: 10.1073/pnas.0601990103
49. Cimadamore F, Curchoe CL, Alderson N, et al. (2009) Nicotinamide rescues human embryonic stem cell-derived neuroectoderm from parthanatic cell death. *Stem Cells* 27:1772–1781. doi: 10.1002/stem.107
50. Maruotti J, Wahlin K, Gorrell D, et al. (2013) A Simple and Scalable Process for the Differentiation of Retinal Pigment Epithelium From Human Pluripotent Stem Cells. *Stem Cells Translational Medicine* 2:341–354. doi: 10.5966/sctm.2012-0106
51. Hynes SR, Lavik EB (2010) A tissue-engineered approach towards retinal repair: Scaffolds for cell transplantation to

- the subretinal space. *Graefes Arch Clin Exp Ophthalmol* 248:763–778. doi: 10.1007/s00417-009-1263-7
52. Diniz B, Thomas P, Thomas B, et al. (2013) Subretinal implantation of retinal pigment epithelial cells derived from human embryonic stem cells: improved survival when implanted as a monolayer. *Investigative Ophthalmology & Visual Science* 54:5087–5096. doi: 10.1167/iovs.12-11239
  53. Sumita R (1961) The fine structure of Bruch's membrane of the human choroid as revealed by electron microscopy. *Journal of Electron Microscopy* 10:111–118.
  54. Thomson RC, Giordano GG, Collier JH, et al. (1996) Manufacture and characterization of poly ( $\alpha$ -hydroxy ester) thin films as temporary substrates for retinal pigment epithelium cells. *Biomaterials* 17:321–327.
  55. Veis A, Cohen J (1960) Reversible transformation of gelatin to the collagen structure. *Nature* 186:720–721.
  56. Del Priore LV (2004) Survival of Allogeneic Porcine Retinal Pigment Epithelial Sheets after Subretinal Transplantation. *Investigative Ophthalmology & Visual Science* 45:985–992. doi: 10.1167/iovs.03-0662
  57. Giordano GG, Thomson RC, Ishaug SL, et al. (1997) Retinal pigment epithelium cells cultured on synthetic biodegradable polymers. *J Biomed Mater Res* 34:87–93.
  58. Chung T-W, Tsai Y-L, Hsieh J-H, Tsai W-J (2006) Different ratios of lactide and glycolide in PLGA affect the surface property and protein delivery characteristics of the PLGA microspheres with hydrophobic additives. *Journal of Microencapsulation* 23:15–27. doi: 10.1080/02652040500286110
  59. Beach WF (2004) Xylylene polymers. *Encyclopedia of Polymer Science and Technology*
  60. Szwarc M (1947) Some remarks on the CH<sub>2</sub>[graphic omitted]CH<sub>2</sub> molecule. *Discuss Faraday Soc* 2:46. doi: 10.1039/d9470200046
  61. SCS History of Parylene. In: History of Parylene. [http://scscoatings.com/what\\_is\\_parylene/history.aspx](http://scscoatings.com/what_is_parylene/history.aspx). Accessed 1 Sep 2013
  62. Gorham WF (1966) A New, General Synthetic Method for the Preparation of Linear Poly-p-xylylenes. *Journal of Polymer Science Part A-1: Polymer Chemistry* 4:3027–3039.
  63. Gillespie C Indiana Chamber of Commerce Member Spotlight: Specialty Coating Systems. In: indianachamber.com. <http://www.indianachamber.com/index.php/specialty-coating-systems>. Accessed 1 Sep 2013
  64. Tan CP, Craighead HG (2010) Surface Engineering and Patterning Using Parylene for Biological Applications. *Materials* 3:1803–1832. doi: 10.3390/ma3031803
  65. Chang TY, Yadav VG, De Leo S, et al. (2007) Cell and Protein Compatibility of Parylene-C Surfaces. *Langmuir* 23:11718–11725. doi: 10.1021/la7017049
  66. Kate (2009) SCH Technologies. 1–2.
  67. Li W, Rodger DC, Meng E, et al. Wafer-Level Parylene Packaging With Integrated RF Electronics for Wireless Retinal Prostheses. *J Microelectromech Syst* 19:735–742. doi: 10.1109/JMEMS.2010.2049985
  68. Wright D, Rajalingam B, Selvarasah S, et al. (2007) Generation of static and dynamic patterned co-cultures using microfabricated parylene-C stencils. *Lab Chip* 7:1272. doi: 10.1039/b706081e
  69. Wei L, Lakhtakia A (2012) Toward bioinspired parylene-C coatings of implant surfaces. In: Lakhtakia A (ed) *SPIE Smart Structures and Materials + Nondestructive Evaluation and Health Monitoring*. SPIE, pp 83390R–83390R–10
  70. Song JS, Lee S, Jung SH, et al. (2009) Improved biocompatibility of parylene-C films prepared by chemical vapor deposition and the subsequent plasma treatment. *J Appl Polym Sci* 112:3677–3685. doi: 10.1002/app.29774
  71. Ilic B, Craighead HG (2000) Topographical patterning of chemically sensitive biological materials using a polymer-based dry lift off. *Biomed Microdevices* 2:317–322.
  72. Lu B, Zhu D, Hinton D, et al. (2012) Mesh-supported submicron parylene-C membranes for culturing retinal pigment epithelial cells. *Biomed Microdevices* 14:659–667. doi: 10.1007/s10544-012-9645-8
  73. Lu B, Liu Z, Tai Y-C (2011) Ultrathin parylene-C semipermeable membranes for biomedical applications. 505–508.
  74. Moore DJ, Clover GM (2001) The effect of age on the macromolecular permeability of human Bruch's membrane. *Investigative Ophthalmology & Visual Science* 42:2970–2975.
  75. Lee CJ, Vroom JA, Fishman HA, Bent SF (2006) Determination of human lens capsule permeability and its feasibility as a replacement for Bruch's membrane. *Biomaterials* 27:1670–1678. doi: 10.1016/j.biomaterials.2005.09.008
  76. Montezuma SR (2006) Biocompatibility of Materials Implanted into the Subretinal Space of Yucatan Pigs. *Investigative Ophthalmology & Visual Science* 47:3514–3522. doi: 10.1167/iovs.06-0106
  77. Daar AS, Greenwood HL (2007) A proposed definition of regenerative medicine. *J Tissue Eng Regen Med* 1:179–184. doi: 10.1002/term.20
  78. Falkner-Radler CI, Krebs I, Glittenberg C, et al. (2011) Human retinal pigment epithelium (RPE) transplantation: outcome after autologous RPE-choroid sheet and RPE cell-suspension in a randomised clinical study. *British Journal of Ophthalmology* 95:370–375. doi: 10.1136/bjo.2009.176305
  79. Stanzel BV, Liu Z, Brinken R, et al. (2012) Subretinal delivery of ultrathin rigid-elastic cell carriers using a metallic shooter instrument and biodegradable hydrogel encapsulation. *Investigative Ophthalmology & Visual Science*

53:490–500.

80. Hu Y, Liu L, Lu B, et al. (2012) A Novel Approach for Subretinal Implantation of Ultrathin Substrates Containing Stem Cell-Derived Retinal Pigment Epithelium Monolayer. *Ophthalmic Res* 48:186–191. doi: 10.1159/000338749
81. Caramoy A (2011) A reply to human retinal pigment epithelium (RPE) transplantation: outcome after autologous RPE-choroid sheet and RPE cell-suspension in a randomised clinical study. *British Journal of Ophthalmology* 95:431–431. doi: 10.1136/bjo.2010.191882
82. Rolstad B (2001) The athymic nude rat: an animal experimental model to reveal novel aspects of innate immune responses? *Immunol Rev* 184:136–144.
83. Tezel TH, Del Priore LV (1997) Reattachment to a substrate prevents apoptosis of human retinal pigment epithelium. *Graefes Arch Clin Exp Ophthalmol* 235:41–47.
84. Sidman RLR, Pearlstein RR, Waymouth CC (1965) Pink-eyed dilution (p) gene in rodents: increased pigmentation in tissue culture. *Dev Biol* 12:93–116. doi: 10.1016/0012-1606(65)90023-0
85. Edwards RB, Szamier RB (1977) Defective phagocytosis of isolated rod outer segments by RCS rat retinal pigment epithelium in culture. *Science* 197:1001–1003.
86. D'Cruz PMP, Yasumura DD, Weir JJ, et al. (2000) Mutation of the receptor tyrosine kinase gene *Mertk* in the retinal dystrophic RCS rat. *Hum Mol Genet* 9:645–651.
87. Herron WL, Riegel BW, Myers OE, Rubin ML (1969) Retinal dystrophy in the rat—a pigment epithelial disease. *Investigative Ophthalmology & Visual Science* 8:595–604.
88. Sheedlo HJ, Li L, Turner JE (1991) Photoreceptor cell rescue at early and late RPE-cell transplantation periods during retinal disease in RCS dystrophic rats. *J Neural Transplant Plast* 2:55–63. doi: 10.1155/NP.1991.55
89. Lund RD, Adamson P, Sauvé Y, et al. (2001) Subretinal transplantation of genetically modified human cell lines attenuates loss of visual function in dystrophic rats. *Proc Natl Acad Sci USA* 98:9942–9947. doi: 10.1073/pnas.171266298
90. Carr A-J, Vugler AA, Hikita ST, et al. (2009) Protective Effects of Human iPS-Derived Retinal Pigment Epithelium Cell Transplantation in the Retinal Dystrophic Rat. *PLoS ONE* 4:e8152. doi: 10.1371/journal.pone.0008152.s004
91. Butterwick A, Huie P, Jones BW, et al. (2009) Effect of shape and coating of a subretinal prosthesis on its integration with the retina. *Experimental Eye Research* 88:22–29. doi: 10.1016/j.exer.2008.09.018
92. Lamba DA, Gust J, Reh TA (2009) Transplantation of Human Embryonic Stem Cell-Derived Photoreceptors Restores Some Visual Function in *Crx*-Deficient Mice. *Cell Stem Cell* 4:73–79. doi: 10.1016/j.stem.2008.10.015
93. Warre-Cornish K, Barber AC, Sowden JC, et al. (2014) Migration, Integration and Maturation of Photoreceptor Precursors Following Transplantation in the Mouse Retina. *Stem Cells and Development* 140218132743006. doi: 10.1089/scd.2013.0471

## II. Novel Synthetic Substrate for Stem Cells and RPE

### Defined Culture of Human Embryonic Stem Cells and Xeno-free Derivation of Retinal Pigmented Epithelial Cells on a Novel, Synthetic Substrate

Britney O. Pennington<sup>a</sup>, Dennis O. Clegg<sup>a,b</sup>, Zara K. Melkounian<sup>c</sup>, Sherry T. Hikita<sup>a,d</sup>

<sup>a</sup>Center for Stem Cell Biology and Engineering, Neuroscience Research Institute, Biomolecular Science and Engineering Program, <sup>b</sup>Department of Molecular, Cellular and Developmental Biology, University of California Santa Barbara, CA 93106. <sup>c</sup>Corning Life Sciences, Corning Inc., Corning, New York, USA, <sup>d</sup>Asterias Biotherapeutics, Inc., Menlo Park, CA 94025

This manuscript is undergoing review with *Stem Cells Translational Medicine*.

#### Abstract

Age-related macular degeneration (AMD), a leading cause of blindness, is characterized by the death of the retinal pigmented epithelium (RPE), which is a monolayer posterior to the retina that supports the photoreceptors. Human embryonic stem cells (hESCs) can generate an unlimited source of RPE for cellular therapies, and clinical trials have been initiated. However, protocols for RPE derivation using defined conditions free of non-human derivatives (xeno-free) are preferred for clinical translation and to avoid exposing AMD patients to animal-derived products which could incite an immune response. In this study, we compared the maintenance of hESCs and their differentiation into RPE using Matrigel®, Synthemax®-R Surface and Synthemax®II-SC Substrate. The latter is a novel, synthetic, animal-derived component-free (ACF), RGD peptide-containing copolymer produced under good manufacturing practices (GMP) and is designed for stem cell culture. This report demonstrates that Synthemax®II-SC supports long term culture of H9 and H14 hESC lines and permits efficient differentiation of hESCs into functional RPE. Expression of RPE-specific markers was assessed by flow cytometry, qPCR, and



immunocytochemistry, and RPE function was determined by phagocytosis of rod outer segments and secretion of pigment epithelium-derived factor (PEDF). Both hESCs and hESC-derived RPE maintained normal karyotypes after long-term culture on Synthemax®II-SC. Furthermore, RPE generated on Synthemax®II-SC are functional when seeded onto parylene-C scaffolds designed for clinical use. These experiments suggest that Synthemax®II-SC is a suitable, defined substrate for hESC culture and the xeno-free derivation of RPE for cellular therapies.

## **Introduction**

Age-related macular degeneration (AMD) is the leading cause of blindness in people over 65 years of age in industrialized countries, accounting for 8.7% of the world's blind population, and it is projected that annual costs to the US federal government will exceed \$845 million by 2021<sup>1-3</sup>. The early stages of this disease involve the dysfunction of the retinal pigmented epithelium (RPE). The RPE maintains the health of the photoreceptors through phagocytosis of damaged outer segments, transporting and secreting ions and growth factors across the blood-retina barrier, isomerizing all-*trans* to 11-*cis*-retinal to perpetuate the visual cycle, absorbing stray light and limiting oxidation in the eye<sup>4-6</sup>. AMD manifests in two types. Exudative or “wet” AMD is characterized by choroidal neovascularization into the retina, and can be mitigated by palliative intraocular injections of angiogenesis inhibitors like Avastin®, Lucentis® or EYLEA®. However, 90% of AMD patients suffer from the “dry” form, which can lead to the geographic atrophy of the RPE and photoreceptors in the macular region of the retina<sup>7</sup>. As AMD progresses, the RPE degrade, causing the photoreceptors to deteriorate which leads to an incapacitating loss of vision<sup>8</sup>.

Currently, clinical studies are investigating the efficacy of transplanting non-autologous RPE generated from human embryonic stem cells (hESC-RPE) and induced pluripotent stem cells (iPSC-RPE) as a means to restore vision in AMD patients<sup>9-11</sup>. These pluripotent stem cell-derived RPE have already demonstrated visual rescue in an animal model of retinal degeneration, the Royal College of Surgeons (RCS) rat<sup>12,13</sup>. A preliminary study of one dry AMD patient injected with a suspension of hESC-RPE cells reported no tumor formation or adverse events after four months<sup>9</sup>. However, diseased retinas among patients will display varying degrees of degeneration, and since a suspension of RPE cells is extremely dissimilar to the endogenous organization, it is difficult to predict the efficacy of bolus injections as a therapy for the entire AMD population. Alternatively, other groups are progressing to clinical trials using transplantable scaffolds, which provide a solid surface to promote a polarized RPE monolayer, enable site-specific delivery of the therapeutic cells, and confer support in a diseased environment<sup>14,15</sup>. To this end, ultrathin parylene-C scaffolds have been engineered to provide a transplantable, semi-permeable scaffold to support therapeutic hESC-RPE in the subretinal space<sup>16,17</sup>.

Methods to culture and differentiate pluripotent stem cells into RPE often use xenogeneic mouse embryonic fibroblasts (MEFs) or Matrigel®, a substrate derived from the Engelbreth-Holm-Swarm murine sarcoma<sup>9,11-13,18</sup>. These conditions present a possibility of exposing therapeutic cells to animal-derived immunogens, viruses and other undefined components such as growth factors, collagenases and plasminogen activators<sup>19-21</sup>. Recent efforts to derive hESC-RPE without using non-human animal products have co-cultured hESCs with human foreskin fibroblasts and substrates comprised of full-length human proteins<sup>22-24</sup>. However, due to the natural variability among fibroblast cell lines or batches of purified proteins, synthetic substrates may be more desirable for consistent generation of

clinical-grade therapies. Synthemax®-R is a synthetic, animal-derived component-free (ACF) substrate designed for cell culture and is composed of a biologically active peptide derived from the human extracellular matrix (ECM) protein vitronectin that is covalently conjugated to the tissue culture vessel by an acrylate moiety<sup>25</sup>. ACF conditions do not employ any animal-derived products, including human, and this distinguishes it from xeno-free conditions. Synthemax®-R has been shown to support hESC and iPSC growth<sup>25-31</sup> and their differentiation into ocular cell types<sup>26,31,32</sup>. However, Synthemax®-R is only available in limited styles of tissue culture plates, thus restricting its range of applications and its ability to scale-up the manufacture of therapeutic cells. Synthemax®-II SC Substrate, is a novel ACF, good manufacturing practices (GMP)-compliant peptide-copolymer that self-adsorbs onto tissue culture plastic or glass surfaces. This feature imparts versatility when scaling-up production of therapeutic cells and facilitates a wider array of characterization assays. The Synthemax®II-SC peptide includes the RGD containing sequence from the ECM protein vitronectin, KGGPQV**TRGD**VFTMP, which promotes adhesion in a variety of cells<sup>25,33,34</sup>. To date, Synthemax®II-SC has been shown to support human iPSCs and human mesenchymal stem cells<sup>35,36</sup>. Here we validate Synthemax®II-SC as a viable substrate for the defined culture of hESCs and hESC-RPE. We have found that pluripotent H9 and H14 hESC lines can be maintained on Synthemax®II-SC and retain a normal karyotype for more than 16 passages. These lines differentiate into hESC-RPE with a significantly higher yield than hESCs maintained on Synthemax®-R Surface. Also, hESC-RPE cultured on Synthemax®II-SC are similar to hESC-RPE derived on Matrigel® and Synthemax®-R with respect to gene expression and function. Furthermore, hESC-RPE derived on Synthemax®II-SC retain RPE identity and function when seeded onto transplantable parylene-C scaffolds.

## **Materials and Methods**

### *hESC Culture*

Cultures of hESC lines H9 and H14 (WiCell Research Institute) were maintained on Matrigel® hESC-qualified matrix (Corning® #354277) in mTeSR™1 (STEMCELL Technologies, #05850). Stem cell colonies were manually passaged every 4-7 days: differentiated regions were removed followed by manual dissection of pluripotent colonies. To compare hESCs grown on Synthamax®II-SC Substrate to other commercially available substrates, hESCs were passaged onto tissue culture treated plates coated with Corning®Matrigel®, Corning® Synthamax®-R Surface (#3979, 3984, 3977XX1), and Synthamax®II-SC Substrate (Cat#3536-XX1, Lot#DEV45-10) and were serially passaged by manual dissection. Similar number and size of colonies were chosen for propagation on the 3 surfaces. hESCs between passages 40-49 were used for characterization. For differentiation into germ layers, hESCs on Synthamax®II-SC were differentiated for 10 days in DMEM/F12+GlutaMAX™I, 20% KnockOut Serum Replacement, 1x non-essential amino acids, and 0.1mM β-mercaptoethanol (all reagents from Life Technologies).

### *Differentiation, Enrichment and Culture of RPE*

Pluripotent hESCs were spontaneously differentiated on the substrates of interest for 115 days in XVIVO™10 medium (Lonza #04-743Q) with Normocin (Invivogen #ant-nr-1). Pigmented cells were enriched by treatment with TrypLE Select (Gibco #12563-011), followed by manual removal of non-pigmented cells. Remaining RPE were dissociated with TrypLE Select for 5 min. at 37°C, passed through a 40µm nylon cell strainer and seeded on the substrates of interest at  $1.5 \times 10^5$  cells/cm<sup>2</sup>. RPE cultures were maintained in XVIVO™10 medium and passaged with TrypLE Select every 28 days for 3 months and

seeded at  $1.0 \times 10^5$  cells/cm<sup>2</sup> onto Matrigel®, Synthemax®-R, and Synthemax®II-SC Substrate (Cat#3536-XX1, Lot#28512016, 14413006, 22413018). Cells at passage 2 day 28 were used for characterization. The “Matrigel”, “Synthemax-R” and “Synthemax-II” designations describe the condition of hESCs propagated, differentiated, enriched and passaged as RPE solely on the Matrigel®, Synthemax®-R, and Synthemax®II-SC substrates, respectively. “Mg-SR” denotes the condition of undifferentiated hESCs grown and differentiated on Matrigel®, then enriched and grown as RPE on Synthemax®-R as described previously<sup>17,37</sup>.

#### *Fetal Human RPE (fRPE) Culture*

Fetal human RPE were a kind gift of Dean Bok (University of California Los Angeles) and Lincoln Johnson (Center for the Study of Macular Degeneration, UC Santa Barbara). fRPE were maintained in Miller medium<sup>38</sup>:  $\alpha$ -Modification MEM media (Sigma M4526) supplemented with non-essential amino acids (Gibco #11140-050), GlutaMax-I (Life Technologies 35050), N1 supplement (Sigma N6530), 1mL of THT per 500mL of media (0.0065 $\mu$ g/mL triiodothyronine, Sigma T5516; 10 $\mu$ g/mL hydrocortisone, Sigma H0396; 125mg/mL taurine, Sigma T0625) and heat-inactivated fetal bovine serum (15% for seeding fRPE, 5% for fRPE maintenance) (Atlas Biologicals F-0500A).

#### *Synthemax®II-SC Substrate Vessel Coating*

Tissue culture vessels were coated with Synthemax®II-SC according to the manufacturer’s recommendations. Briefly, Synthemax®II-SC powder was resuspended to 1mg/mL in HyClone HyPure Cell Culture Grade Water (AWK21536) and stored at 4°C for 1 month or further diluted 1:40 (0.025mg/mL) to coat tissue culture vessels (Corning

CellBIND<sup>®</sup> Surface, #3335; Costar<sup>®</sup> cell culture plates and flasks, #3516, 3603, 430641, 431082), Millicell-HA inserts (Millipore, PIHA01250), and Thermo Lab-Tek Permanox Chamber Slides (#177445) at 5µg/cm<sup>2</sup> for 2 hours at room temperature. Remaining Synthemax<sup>®</sup>II-SC solution was then aspirated and the air-dried vessels were used immediately or stored at 4°C for up to 3 months.

### *Immunocytochemistry*

Cells were rinsed with warm DPBS (Gibco #14190-144) and fixed with 4.0% paraformaldehyde (Electron Microscopy Sciences #15710) in 0.1M sodium cacodylate buffer (Electron Microscopy Sciences #11652) for 5 minutes at 4°C. Fixed cells were blocked with 1% BSA (Gibco #15260), 1% goat serum (Sigma #G9023) and 0.1% Triton-X (Roche 11332481001) in PBS for 1 hour at 4°C. Primary antibodies diluted in block solution were applied overnight at 4°C (msαOct4, 1:100 Santa Cruz sc-5279; msαTra1-81, 1:100 Millipore MAB4381; rbαSall4, 1:800 Abcam ab29112; msαTra1-60, 1:100 Millipore MAB4360, msαHMB45 (PMEL17), 1:100 Dako M0634; msαBestrophin, 1:100 Abcam ab2182; msαZO-1, 1:100 Life Technologies 339100; rbαOtx2, 1:4000 Millipore 9566). Cells were rinsed 3 times with PBS and secondary antibodies were diluted 1:300 in block solution and applied for 30 minutes at 4°C (Alexa Fluor<sup>®</sup> 546 gtα rb A11035; Alexa Fluor<sup>®</sup> 488 gt-αms IgG, IgM A10680; and Alexa Fluor<sup>®</sup> 488 gt-αms IgM A21042; Life Technologies). Cells were incubated with Hoechst nuclear stain (8µg/mL, Sigma 33258) for 5 minutes at room temperature in the dark and rinsed 3x with PBS. Slides were mounted with Pro-Long<sup>®</sup> Gold Antifade Reagent (Life Technologies #P36930) and imaged with QCapture Pro software on Olympus IX71 or BX51 fluorescence microscopes.

### *Quantitative Polymerase Chain Reaction*

For RNA collection, whole wells of hESCs ready for passage were harvested from each substrate; differentiated regions were not removed prior to harvest. RNA was harvested using the RNeasy Plus kit (QIAGEN #74136) and converted to cDNA (iScript cDNA Synthesis kit, Bio-Rad #170-8891). For hESC-RPE,  $1.5 \times 10^5$  cells were collected at passage 2 day 28 and processed with the Cells-to-Ct kit (Ambion #4399002). Real-time qPCR was completed with TaqMan Gene Expression Assays (Life Technologies #4351372, Supplemental Table 1) in TaqMan Gene Expression Master Mix (Life Technologies #4369016) using a Bio-Rad CFX96™ Real-Time System. Data was analyzed with the Bio-Rad CFX Manager software.

### *Flow Cytometry*

Whole wells of hESCs ready for passage were harvested from each substrate; differentiated regions were not removed prior to harvest. hESCs were dissociated by 5-13 minute incubations in TrypLE Select at 37°C and diluted 1:5 in fresh medium. For hESC-RPE,  $1 \times 10^6$  cells were collected at passage 2 day 28. For fixation, cells were centrifuged at 1500rpm for 3 minutes, washed in 0.5% BSA Fraction V (Gibco #15260-037) in PBS, and fixed in 4% paraformaldehyde in PBS for 20 minutes at room temperature in the dark. Cells were pelleted at 2300rpm for 3 minutes and permeabilized with 0.2% Triton-X (Roche 11332481001), 0.1% BSA Fraction V in PBS for 3 minutes at room temperature. Fixed cells were stored at 4°C in 0.5% BSA until stained.

Cells were stained with primary antibodies diluted in 3% BSA and PBS for 30 minutes at 4°C (hESCs) or room temperature (RPE) (PE-Oct4 IgG, 1:5 BD Pharm 560186; PE-Isotype IgG Control, 1:5 BD Pharm 559320; PE-SSEA4 IgG<sub>3</sub>, 0.1µg/ml R&D Systems FAB1435P; Mouse IgG<sub>3</sub>-RPE Clone B10, 0.1µg/ml Southern Biotech; HMB45 (PMEL17),

0.1 µg/ml Dako M0634; Mouse IgG1 isotype control, Dako X0931). Samples were stained with a secondary antibody for 30 minutes at room temperature (AlexaFluor® 488, Life Technologies A21202). Cells were rinsed with 0.5% BSA and data was collected on a BD Accuri®C6 Flow Cytometer with 10,000 gated events per sample. Gates were set to exclude 99.0% of the population stained with the isotype control of the primary antibody. Data was analyzed with FCS Express (De Novo Software).

### *Karyotype*

Cells were seeded in a T-25 flask (Corning #430168) that was coated with Matrigel® or Synthemax®II-SC Substrate and shipped in log-phase overnight to Cell Line Genetics Inc. for G-band karyotyping.

### *Pigment Quantification*

ImageJ (<http://imagej.nih.gov/ij/>) was used to quantify pigmented area in the differentiated hESC cultures. Briefly, photographs of the differentiated hESC-RPE plates were converted to 8-bit images. Scale was set to 500 pixels:17.3 mm for a 6-well plate. The well area was selected, contrast enhanced (20%, Normalize, Equalize histogram), background subtracted (15%, Light Background, disabled smoothing), converted to binary, and analyzed for particle size (size: 0.02-10mm<sup>2</sup>).

### *PEDF ELISA*

To compare secretion of pigment epithelium-derived factor (PEDF), hESC-RPE derived on different substrates were seeded onto transwell Millicell-HA inserts (Millipore, PIHA01250) coated with 2.63 µg/cm<sup>2</sup> human vitronectin (BD BioSciences 354238) or



Synthemax®II-SC. Cells were maintained in 400µL XVIVO™10 within the insert and 600µL in the well. Apical and basal supernatants were collected on passage 2 day 30, 72 hours post-medium change, snap-frozen in liquid nitrogen and stored at -80°C. Supernatants from hESC-RPE on parylene-C membranes were collected 30 days after thaw/seed, 24 hours post medium change. Supernatants were diluted 1:5000; concentration of PEDF was determined with the PEDF ELISA kit (Bioproducts MD #PED613-Human) according to the manufacturer's instructions. Optical density was measured at 450 nm.

#### *Rod Outer Segment (ROS) Phagocytosis*

The ROS phagocytosis assay was performed as previously described<sup>39</sup>. Briefly, hESC-RPE, human fRPE and ARPE19 cells were seeded in quadruplicate onto gelatin, Synthemax®II-SC or human vitronectin-coated 96 well plates at  $1 \times 10^5$  cells/cm<sup>2</sup> and maintained in Miller medium. Rod outer segments were isolated from fresh bovine retinas, labeled with fluorescein isothiocyanate (FluoReporter FITC Protein Labeling kit, Life Technologies #F6434) and resuspended in 2.5% sucrose in Miller medium. Four weeks after plating, confluent cells were incubated with  $1 \times 10^6$  labeled ROS, with or without 62.5µg/ml of the anti-αvβ5 function blocking antibody (Abcam #ab24694) or the isotype control (Abcam #ab18447) for 5 hours at 37°C in 5% CO<sub>2</sub>. Unbound ROS were removed with six rinses of warm 2.5% sucrose in PBS and extracellular fluorescence was quenched with 0.4% trypan blue (Corning #25-900Cl) for 20 minutes at 37°C. Trypan blue was replaced with 40µL of PBS-sucrose and internalized fluorescence was imaged with an Olympus IX71. ImageJ software was used to calculate the internalized fluorescence intensity by pixel densitometry. Fluorescent signals from each condition were normalized to the ARPE19 signal.

### *hESC-RPE on Parylene-C*

Mesh-supported submicron parylene-C membranes were manufactured as described previously<sup>16</sup>. These scaffolds were coated with human vitronectin in a 48 well plate; hESC-RPE derived on Synthemax®II-SC or by the Mg-SR method were thawed and seeded on the membrane at  $1.5 \times 10^5$  cells/well and grown for 30 days in XVIVO™10 medium without antibiotics.

## ***A. Novel Substrate Supports Human Embryonic Stem Cells***

### **Results**

#### **Synthemax®II-SC Supports Long Term Culture of H9 and H14 hESCs**

Matrigel® is one of the most widely used cell-free substrates for hESC culture<sup>18,40</sup>. Therefore, morphology and gene expression of hESCs cultured on Synthemax®II-SC were compared to hESCs on Matrigel®. Comparisons were also made to hESCs maintained on Synthemax®-R to determine if Synthemax®II-SC is an acceptable alternative ACF substrate.

Overall, hESC colonies cultured on Synthemax®II-SC exhibited morphology similar to hESCs grown on Matrigel®, characterized by a homogenous layer of small, tightly packed cells and a distinct colony border. Colonies on Synthemax®II-SC generally appeared larger than those grown on Synthemax®-R but were more compact than those grown on Matrigel® (Fig. 5A; supplemental Fig. 1). To investigate the percent of cells expressing pluripotency markers Oct4 and SSEA4, flow cytometry was carried out on cultures at passages 1, 3, 5, and 9 (Fig. 5B; supplemental Fig. 2A). While hESC cultures on Matrigel® showed consistent expression of both pluripotency markers, a decrease in

expression of Oct4 was observed on both xeno-free surfaces at some passages. Additional markers of undifferentiated cells were examined by qPCR and immunocytochemistry. By passage 7, hESCs on Synthemax®II-SC and Matrigel® expressed similar levels of pluripotency-associated mRNAs (Fig. 5 C; supplemental Fig. 2B) and had similar colony morphologies. Throughout all passages, hESCs on Synthemax®II-SC and Matrigel® expressed the pluripotent surface antigens SSEA4, Tra1-60 and Tra1-81 along with nuclear hESC transcription factors Oct4 and Sall4 (Fig. 5 B,F; supplemental Fig. 2 A,B).

To determine if long-term cultures of H9 and H14 hESCs on Synthemax®II-SC maintain a normal karyotype, these lines were subcultured for 23 and 16 passages, respectively. Each line maintained a normal human karyotype (Fig. 5D; supplemental Fig. 2D). The differentiation potential of hESCs grown on Synthemax®II-SC was investigated by culturing cells in a differentiation medium for 10 days. These differentiated cells expressed markers from the 3 germ layers at higher levels than the undifferentiated cultures. Markers of ectoderm (Microtubule associated protein 2, MAP2)<sup>35</sup>, mesoderm (T-Box Protein 6, Tbx6)<sup>36</sup>, and endoderm ( $\alpha$ -feto protein, AFP)<sup>41,42</sup> were detected (Fig. 5E; supplemental Fig. 2C).

Taken together, these data demonstrate that Synthemax®II-SC is a suitable, ACF substrate for the maintenance of hESCs that express canonical pluripotency markers and can differentiate into all three germ layers.

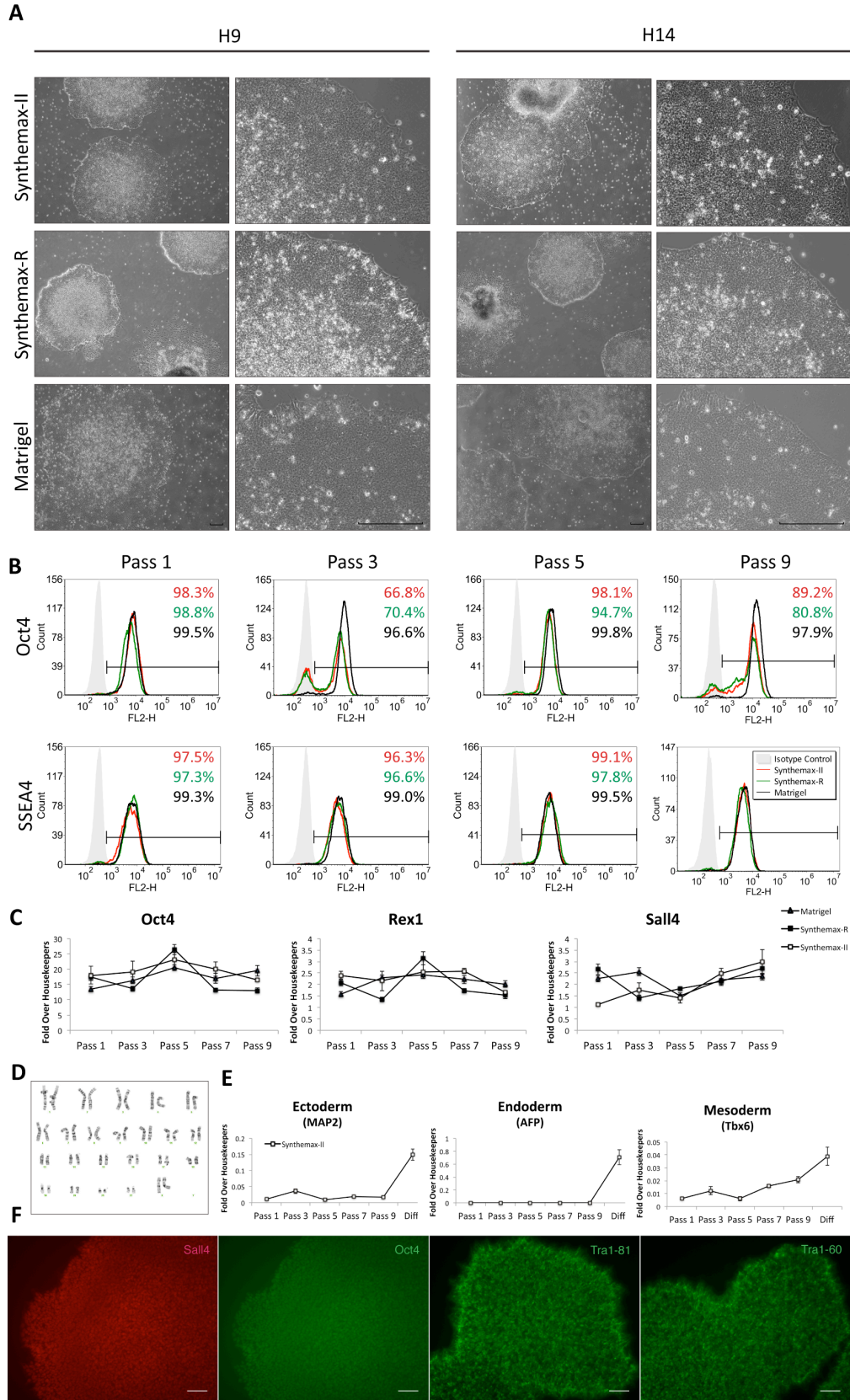


**Figure 5.** Characterization of hESCs cultured on Synthemax®II-SC, Synthemax®-R and Matrigel®. **(A)** Representative phase contrast micrographs of H9 and H14 hESC colony morphology after 9 passages on the indicated substrate. Scale bars = 200µm. **(B)** Representative flow cytometry histograms for pluripotency markers Oct4 and SSEA4 in H9 cultures grown on the indicated substrate at passages 1, 3, 5 and 9. **(C)** Relative mRNA expression of pluripotency genes in H9 cultures grown on Synthemax®II-SC, Synthemax®-R and Matrigel® at passages 1, 3, 5 and 9 as detected by qPCR. **(D)** Normal karyotype of H9 hESCs maintained on Synthemax®II-SC for 23 passages. **(E)** Relative mRNA expression of germ layer markers for H9 hESCs grown and differentiated on Synthemax®II-SC as detected by qPCR. **(F)** H9 hESCs on Synthemax®II-SC stained for nuclear pluripotency transcription factors Oct4 and Sall4, and surface markers Tra1-81 and Tra1-60. Scale bar = 80µm.

---

## ***B. Xeno-Free Spontaneous hESC Differentiation into Functional RPE***

### **Synthemax®II-SC permits RPE differentiation from hESCs**

Since Synthemax®II-SC was found to support the defined culture of hESCs, we next investigated whether this substrate also permitted efficient, xeno-free differentiation of hESCs into RPE. H9 and H14 hESC lines adapted to Matrigel®, Synthemax®-R, and Synthemax®II-SC were spontaneously differentiated into RPE by changing the growth medium to XVIVO™10, a xeno-free formulation lacking bFGF (Fig. 6). During this process, pigmented foci appeared after 4 weeks and continued to enlarge over the next few months. At 115 days post-differentiation, the area of pigmentation on each substrate was quantified (Fig. 6). Unexpectedly, Synthemax®II-SC yielded significantly more pigmented area than Synthemax®-R ( $p < 0.01$ ). However, there was no difference in the amount of pigmented area produced on Matrigel® and Synthemax®II-SC. This suggests that Synthemax®II-SC is an acceptable replacement for Matrigel® in the xeno-free production of clinical-grade RPE from hESCs.

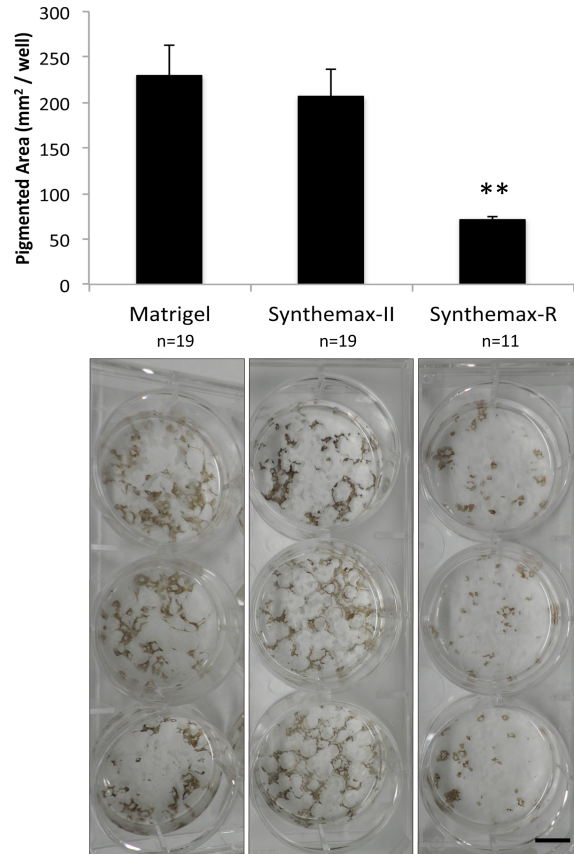


**Figure 6.** Spontaneous differentiation of hESC-RPE on Matrigel® and Synthemax®II-SC yield significantly more pigmented area than hESC-RPE on Synthemax®-R. Top: Pigmented area in individual wells was calculated with ImageJ software after 115 days of differentiation. Error bars denote standard deviation; \*\*  $p < 0.01$ , ttest. Below: Three representative wells from a 6 well plate of differentiated hESC-RPE seeded on each substrate are shown. Scale bar = 1cm.

### RPE cultured on Synthemax®II-SC maintain RPE identity

Pigmented regions produced by spontaneous differentiation (Fig. 6) were manually isolated from non-pigmented cells in a process termed “enrichment.” Protocols have been developed whereby hESCs are differentiated to RPE on Matrigel® and then enriched onto Synthemax®-R (Mg-SR method)<sup>16,17,44</sup>. To investigate if Synthemax®II-SC can entirely replace Matrigel® for the growth of hESCs and their differentiation into RPE, we compared cultures maintained solely on Synthemax®II-SC to those produced using the Mg-SR

method. Synthemax®II-SC hESC-RPE were also compared to cells produced solely on Synthemax®-R or Matrigel®.

After 30 days in culture, the hESC-RPE produced on Synthemax®II-SC and Synthemax®-R qualitatively appeared darker than those produced on Matrigel® or by the Mg-SR method (Fig. 7A; supplemental Fig. 3A). Interestingly, H9 hESC-RPE derived on Synthemax®II-SC expressed pigmentation markers to a similar extent as Mg-SR but expressed significantly more tyrosinase (Tyr) mRNA than RPE on Synthemax®-R at passage 2 day 28 (Fig. 7C). H14-derived RPE did not exhibit this difference. No significant difference was found in the expression of other pigmentation-related proteins PMEL17 and tyrosinase related protein-1 (Typr1) in either line of hESC-RPE. All lines displayed the typical cobblestone morphology of cultured RPE. A few lacunae, were observed in a minority of hESC-RPE cultures on Synthemax®II-SC, which may be related to the efficiency of enrichment and non-RPE paracrine signaling effects on tight junctions in the monolayer<sup>45</sup> or uneven coating of the substrate (supplemental Fig. 4).

The purity of the RPE population and efficiency of enrichment were measured at passage 2 day 28 by assessing the percentage of cells that express PMEL17, an essential structural protein for melanogenesis<sup>46,47</sup>. All cultures were over 95% positive for the protein PMEL17 and localization was confirmed by immunocytochemistry (Fig. 7B,E; supplemental Fig. 3B,C). There was no significant difference in the expression of RPE65 and RLBP1 transcripts, which are involved in the visual cycle<sup>6,48</sup> nor the RPE chloride channel, bestrophin-1 (BEST1) (Fig. 7C; supplemental Fig. 5A). Furthermore, RPE produced on Synthemax®II-SC expressed RPE marker proteins with proper localization. The RPE master transcription factor Otx2<sup>49,50</sup> was visualized in the nucleus and Zonula



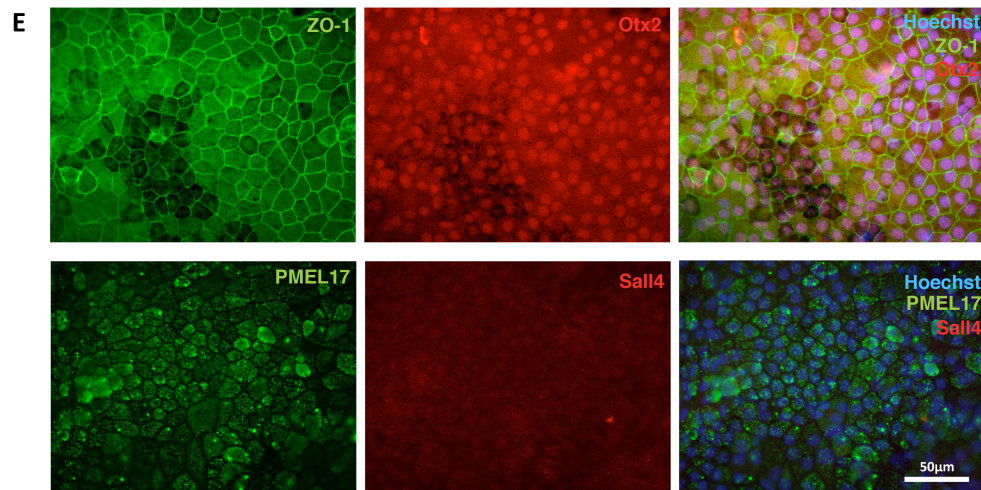
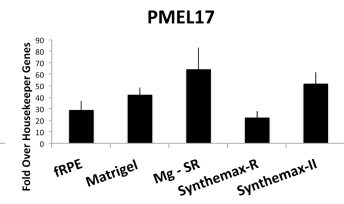
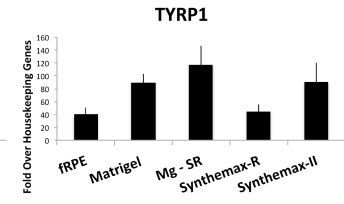
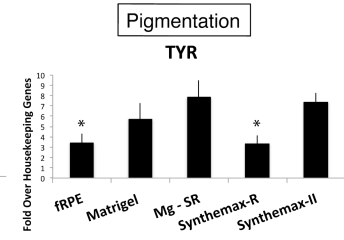
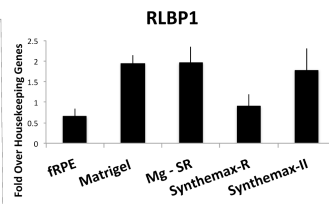
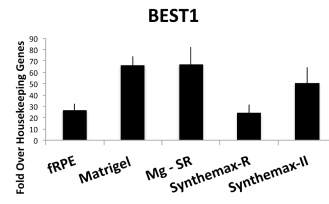
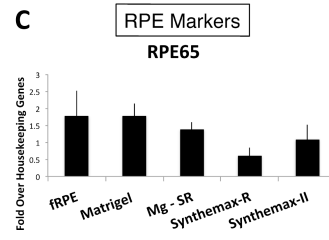
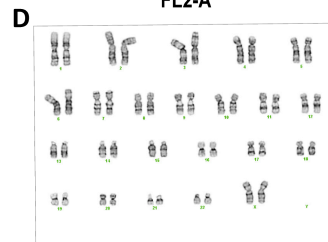
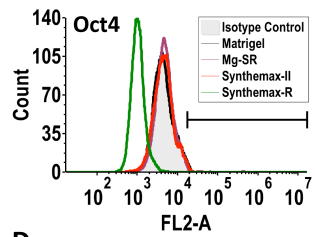
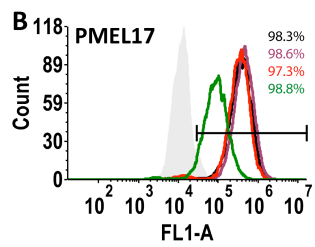
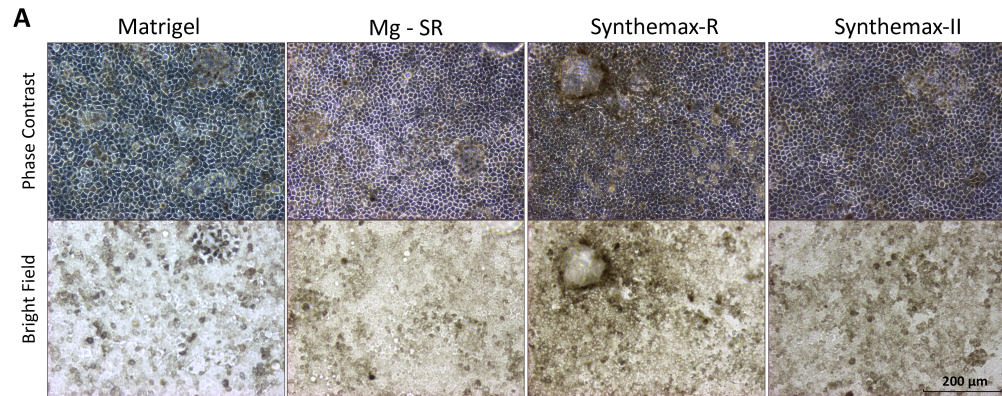




**Figure 7.** Characterization of hESC-RPE derived on Synthemax®II-SC. **(A)** Phase contrast and bright field images show the typical pigmentation and cobblestone morphology of H9 hESC-RPE cultured on different surfaces are shown. Mg-SR denotes the condition of culturing and differentiating hESCs on Matrigel® then enriching and propagating the hESC-RPE on Synthemax®-R. Scale bar = 200µm. **(B)** Representative flow cytometry histograms are shown for the premelanosome pigmentation marker PMEL17 and the pluripotency marker Oct4 (not detected) in H9-RPE at pass 2, day 28 on the indicated substrate. **(C)** Expression of RPE marker genes in H9 hESC-RPE on the indicated substrates. Fetal RPE (fRPE) served as a positive control.  $n=3$ , \*  $p < 0.05$ , ttest. **(D)** Normal karyotype of H9 hESC-RPE after spontaneous differentiation, enrichment and 3 passages on Synthemax®II-SC. **(E)** Epifluorescent images are shown of H9 hESC-RPE derived on Synthemax®II-SC stained for the tight junction marker, ZO-1, RPE markers Otx2 and PMEL17, and the pluripotency marker Sall4 (not detected). Nuclei were detected using Hoechst (blue, merged right panels). Scale bar = 50µm.

---

Occludens-1 (ZO-1)<sup>6</sup> immunoreactivity was observed at cell junctions, consistent with localization to tight junctions (Fig. 7E).

One of the primary concerns regarding stem cell-derived therapies involves the potential of introducing tumorigenic, undifferentiated stem cells into patients<sup>51</sup>. Therefore, expression of the pluripotency markers Oct4, Rex1 and Sall4 were assessed for all lines of H9 and H14 hESC-RPE. All lines tested negative for these embryonic stem cell markers (Fig 7B; supplemental Figs. 3B,C; 5B,C). Also, the proliferative marker mKi67 could not be detected in any of the hESC-RPE derived under different conditions, which suggested that the cells are quiescent and have exited the cell cycle (supplemental Fig. 5B,C). Furthermore, H9 and H14 hESCs that were grown, differentiated, enriched and maintained as RPE for 3 passages on Synthemax®II-SC retain a normal human karyotype (Fig. 7D; supplemental Fig. 3D). These data demonstrate that hESC-RPE maintained in xeno-free conditions on Synthemax®II-SC retain an identity similar to RPE derived using the Mg-SR method.

## **RPE Derived on Synthemax®II-SC are Functional**

One of the primary functions of RPE in the retina is to internalize the shed photoreceptor outer segments by phagocytosis<sup>6,52,53</sup>. The phagocytic function of hESC-RPE derived on Synthemax®II-SC was compared to RPE generated on the other substrates. hESC-RPE on Synthemax®II-SC internalized FITC-labeled rod outer segments (ROS) at levels similar to the other hESC-RPE (Fig. 8A; supplemental Fig. 3E). In the first steps of ROS phagocytosis, integrin  $\alpha\text{v}\beta 5$  physically binds the ROS which activates focal adhesion kinase (FAK) to stimulate receptor tyrosine kinase Mer (MerTK) to initiate ROS engulfment<sup>52</sup>. To test if phagocytosis occurred via this pathway, function blocking antibodies to integrin  $\alpha\text{v}\beta 5$  or an isotype control antibody were added with the ROS. Inhibiting  $\alpha\text{v}\beta 5$  significantly reduced the amount of internalized ROS compared to the isotype control, indicating hESC-RPE derived on Synthemax®II-SC perform phagocytosis similarly to hESC-RPE derived on Matrigel®, Synthemax®-R or Mg-SR ( $p < 0.01$ ) (Fig. 8A; supplemental Fig. 3E). Since vitronectin-coated scaffolds are being developed as cellular therapies for AMD<sup>16</sup>, phagocytic function of hESC-RPE derived on Synthemax®II-SC was analyzed on human vitronectin-coated plastic. hESC-RPE derived under defined, xeno-free culture conditions using Synthemax®II-SC were capable of ROS phagocytic function when seeded on vitronectin-coated surfaces and Synthemax®II-SC ( $p < 0.01$ ) (Fig. 8B; supplemental Fig. 3F).

In addition to phagocytosis, RPE are known to secrete growth factors that support the health of the neural retina and its structural integrity<sup>6</sup>. Among these, is the apically secreted pigment epithelium-derived factor (PEDF), which protects photoreceptors from ischemia and light damage<sup>54,55</sup>. hESC-RPE derived on Synthemax®II-SC secrete significantly more PEDF on their apical side compared to the basolateral surface when seeded on either xeno-free human vitronectin or Synthemax®II-SC ( $p < 0.01$ ) (Fig. 8C).

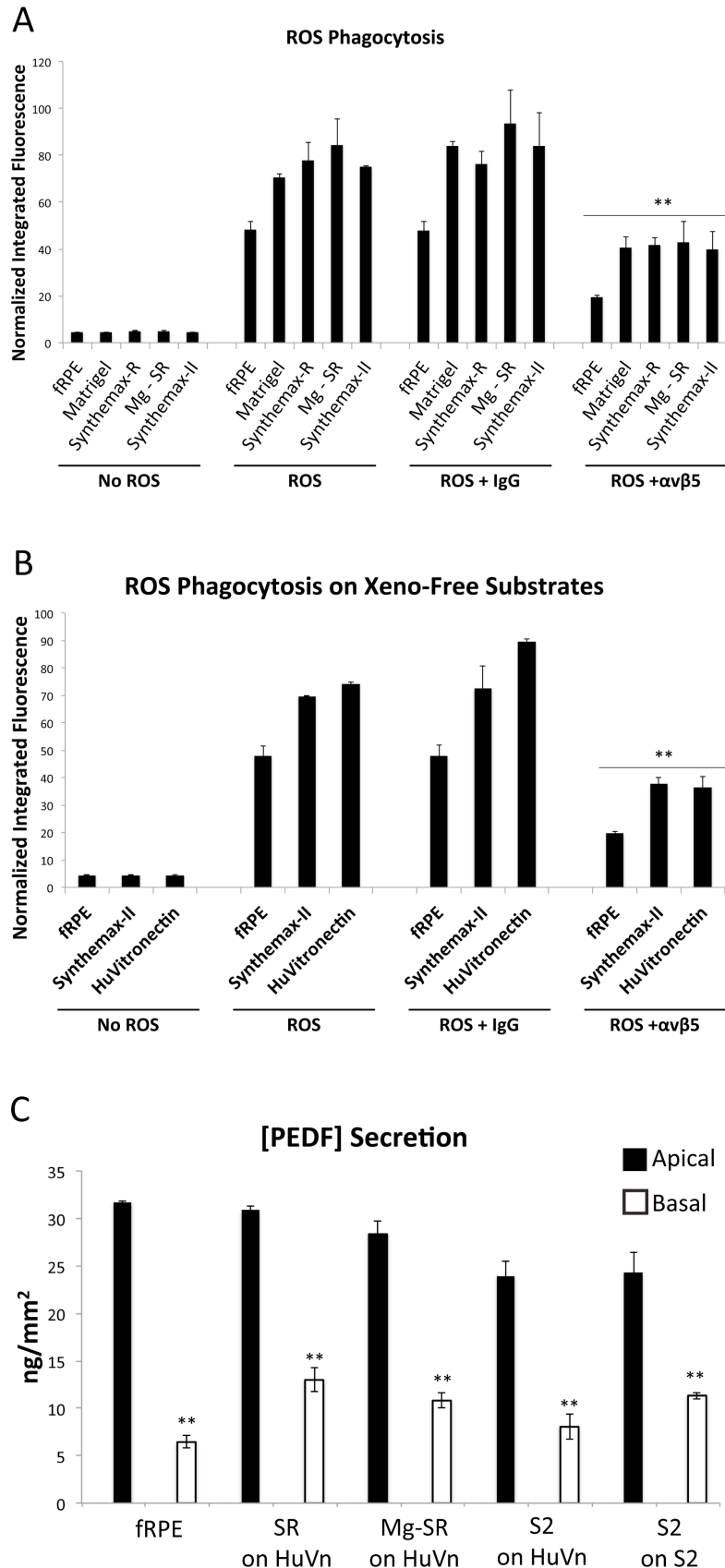


**Figure 8:** Functional characterization of H9 hESC-RPE derived on Synthemax®II-SC.

(A) Phagocytosis of rod outer segments (ROS) by H9 hESC-RPE derived on Matrigel®, Synthemax®-R, Synthemax®II-SC or Mg-SR (hESCs grown and differentiated on Matrigel® then enriched as hESC-RPE on Synthemax®-R). A function-blocking antibody against  $\alpha v \beta 5$  integrin, which is necessary for phagocytosis by RPE, significantly decreased internalization of ROS in all hESC-RPE when compared to the IgG isotype control,  $** p < 0.01$ , ttest. Fetal RPE (fRPE) served as a positive control.

(B) Phagocytosis of ROS by H9 hESC-RPE derived on Synthemax®II-SC after seeding on the defined substrates Synthemax®II-SC and human vitronectin. Phagocytic activity was significantly decreased with the function-blocking  $\alpha v \beta 5$  antibody when compared to the IgG isotype control,  $** p < 0.01$ , ttest.

(C) Significant apical secretion of pigment epithelial-derived factor (PEDF) by H9 hESC-RPE after seeding on surfaces coated with Synthemax®II-SC or human vitronectin,  $** p < 0.01$ , ttest.

(SR, S2, Mg-SR = hESC-RPE derived on Synthemax®-R, Synthemax®II-SC or Mg-SR, respectively; HuVn, human vitronectin; S2, Synthemax®II-SC).

Taken together, these data demonstrate that hESC-RPE derived under xeno-free conditions on the synthetic Synthemax®II-SC surface perform phagocytosis and apically secrete PEDF when seeded on defined substrates.

### **H9 hESC-RPE Derived on Synthemax®II-SC Maintain RPE Identity and Function on Parylene-C Scaffolds**

Vitronectin-coated mesh-supported submicron parylene-C membranes have been developed as transplantable scaffolds to deliver hESC-RPE produced by the Mg-SR method into AMD patients<sup>16,17,44</sup>. To determine if Synthemax®II-SC can be used as a xeno-free alternative to the Mg-SR method to produce hESC-RPE, cells from these two conditions were cultured for 30 days on vitronectin-coated parylene-C scaffolds. No difference in initial attachment was observed, and hESC-RPE derived under both conditions grew to confluent monolayers with cobblestone morphology (Fig. 9A). Once again, darker pigmentation was observed in the hESC-RPE cultures grown on Synthemax®II-SC (Fig. 9A,B). However, there was no significant difference in expression levels of genes associated with pigmentation as measured by qPCR (Fig. 9C). The mRNA encoding the melanocyte-specific Mitf-4 isoform (Mitf-M) was not detected, while variant 2 (Mitf-H), which is expressed during RPE development along with isoforms 1 and 7 (Mitf-A, -D), was observed (Fig. 9C)<sup>56</sup>. hESC-RPE derived under these two conditions expressed similar levels of RPE marker genes, RPE65, Best1 and RLPBP1. The Synthemax®II-SC hESC-RPE secreted slightly less PEDF than hESC-RPE derived using the Mg-SR method (16 vs. 19.6 ng/mm<sup>2</sup>) (Fig. 9D). Taken together, these data show that Synthemax®II-SC is a viable alternative to Matrigel® for the xeno-free derivation and culture of hESC-RPE on parylene-C scaffolds.

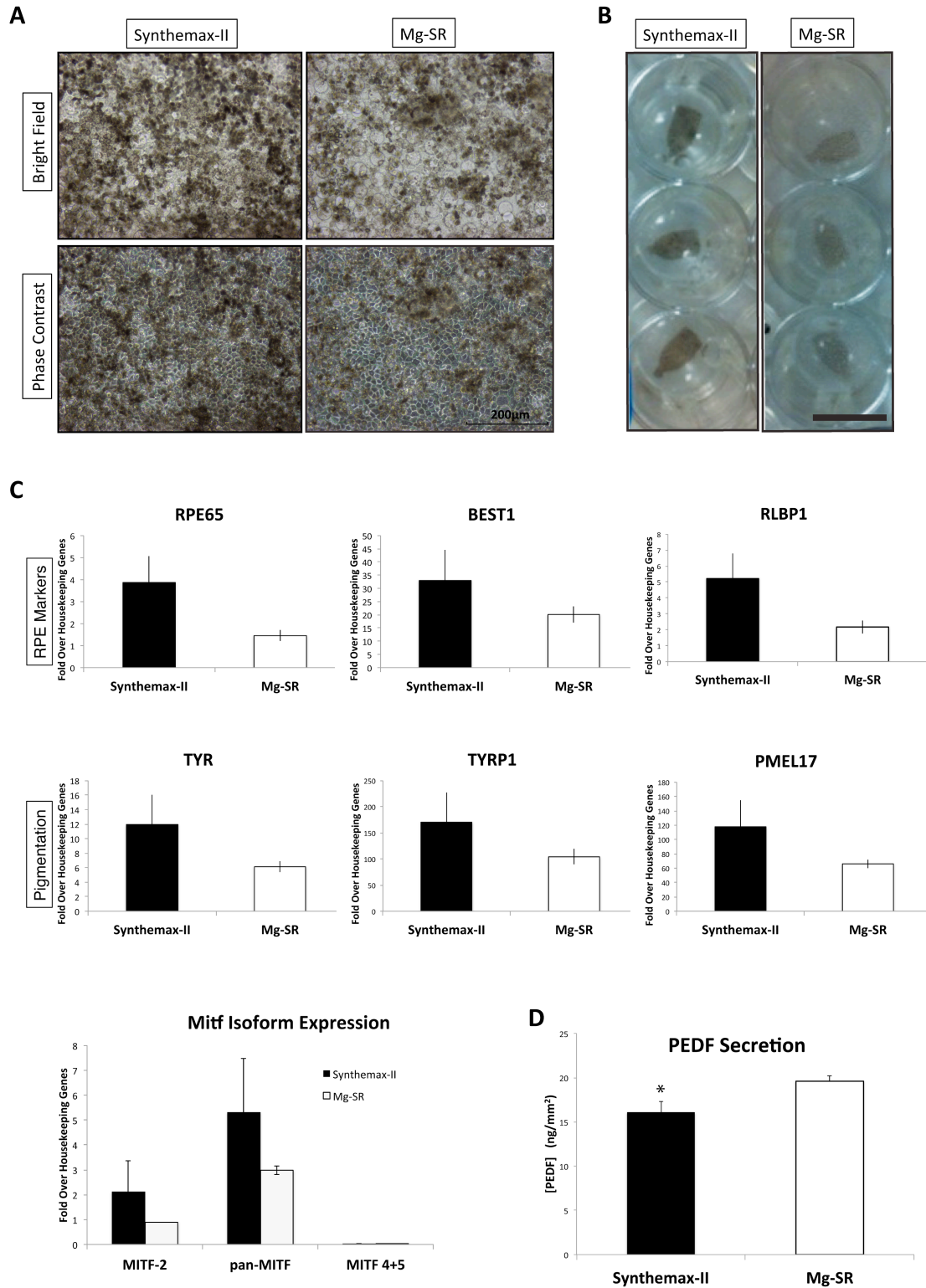


**Figure 9:** Characterization of H9 hESC-RPE derived on Synthemax®II-SC vs. Mg-SR seeded onto parylene-C scaffolds **(A)** Bright field and phase contrast images of H9 hESC-RPE cells grown for 30 days on parylene-C scaffolds. hESC-RPE were derived on Synthemax®II-SC or by the Mg-SR method (hESCs grown and differentiated on Matrigel® then enriched as hESC-RPE on Synthemax®-R). Ultrathin regions of the membrane appear as an array of circles in the micrographs. Scale bar = 200µm. **(B)** Bright field images of three representative parylene-C scaffolds seeded with hESC-RPE in a 24 well plate, n=8, Scale bar = 1cm. Note darker pigmentation in the RPE derived on Synthemax®II-SC. **(C)** Expression of RPE and pigmentation markers after 30 days on parylene-C scaffolds as detected by qPCR. n=3 **(D)** Quantification of PEDF protein secreted by hESC-RPE derived on Synthemax®II-SC or by the Mg-SR method after 30 days on parylene-C scaffolds. n=6, error is SEM, \*  $p < 0.05$ , ttest.

---

## Discussion

The advent of employing pluripotent stem cell-derived therapies to treat human diseases necessitates Good Manufacturing Practices and preferably, defined culture conditions that do not employ xenogeneic products<sup>19</sup>. However, some of the current methods to produce hESC-RPE use Matrigel®, a mixture of ECM proteins harvested from the Engelbreth-Holm-Swarm mouse sarcoma<sup>16,17,44</sup>. Co-culturing therapeutic cells with xenogeneic derivatives may inadvertently introduce non-human viruses that could potentially inoculate the patient post-transplantation. Synthemax®II-SC is a novel, ACF, GMP-compliant copolymer containing an RGD peptide. To date, it has been shown to support the growth of pluripotent human iPSCs as well as the large scale production of human mesenchymal stem cells<sup>35,36</sup>. Here, we present the first characterization of hESC cultures and the xeno-free derivation of RPE using Synthemax®II-SC. Furthermore, we have shown that hESC-RPE maintained on Synthemax®II-SC are similar to RPE derived by the Mg-SR method when seeded onto transplantable parylene-C scaffolds. These data show that Matrigel® can be entirely eliminated from the production of hESC-RPE and replaced with Synthemax®II-SC.

Qualitatively, hESC colonies were easier to passage on Synthemax®II-SC than Synthemax®-R because colonies on the latter substrate remained small and developed compact, differentiated centers, rendering the efficient passaging of undifferentiated cells difficult (supplemental Fig. 1). The observed restriction in colony size may be due to the slightly higher density of peptide on the Synthemax®-R Surface (8-12 pmole/mm<sup>2</sup>) compared to the recommended coating density for Synthemax®II-SC (5-10 pmole/mm<sup>2</sup>)<sup>25</sup>. Consistent with this observation, a previous study showed that human iPSC colonies on Synthemax®-R were more compact than the Matrigel® controls<sup>30</sup>. However, it is not uncommon to observe varying sizes of hESC colonies on various feeder-free substrates as demonstrated by a comparison of Matrigel®, CELLstart™, and vitronectin conducted by Yoon *et al.*<sup>40</sup>.

Introducing hESCs to new culture conditions has been shown to illicit various fluctuations in morphology and an increase in differentiation while the cells adapt to the new environment<sup>58,59</sup>. Previous studies have reported that hESCs undergo an adaption period once transferred to various feeder free substrates<sup>60,61</sup>. H9 and H14 hESCs transitioning to Synthemax®II-SC at passages 2 and 4, respectively, manifested dense differentiated areas harboring small regions devoid of cells within several colonies (supplemental Fig. 1A,C). This extent of differentiation was not observed in other passages. However, it is known that healthy hESC cultures will experience a slight degree of differentiation in every passage, and some differentiation is expected<sup>62</sup>. In this regard, hESCs on Matrigel® consistently demonstrated the least amount of differentiated morphology throughout 9 passages. Since the original cultures for these experiments were adapted to Matrigel®, the minimal differentiation observed in these cells is expected compared to the hESCs transitioning to a new substrate. hESCs on Synthemax®II-SC appeared slightly more differentiated than cells

on Matrigel® but were routinely less than Synthamax®-R (supplemental Fig. 1). After seven passages, hESCs on Synthamax®II-SC appeared very similar to those on Matrigel®. Therefore, only hESCs that had been cultured for seven or more passages on a given substrate were used for spontaneous differentiation into RPE. To demonstrate pluripotency, hESCs maintained on Synthamax®II-SC and allowed to differentiate expressed markers of the three germ layers at higher levels than the undifferentiated hESCs (Fig. 5E; supplemental Fig 2C). Microtubule associated protein 2 (MAP2) is expressed in neural ectoderm, and T-Box Protein 6 (Tbx6) is necessary for mesoderm development<sup>63,64</sup>. Post-implantation embryos synthesize  $\alpha$ -feto protein (AFP) in the visceral endoderm of the developing yolk sac and later in the fetal liver<sup>41,42</sup>.

Flow cytometric analysis of hESCs at passages 1, 3, 5 and 9 revealed stable expression of the pluripotency-associated surface antigen SSEA4<sup>65</sup> on all 3 substrates and a small subpopulation of cells negative for Oct4 on the synthetic surfaces (Fig. 5B; supplemental Fig. 2A). A previous study demonstrated that hESCs beginning to differentiate into an early neural lineage maintained high levels of SSEA4 expression while Oct4 was progressively down-regulated<sup>66</sup>. The differentiated morphology seen in the cultures on the Synthamax® surfaces could likely account for the small population of cells negative for Oct4 by flow cytometry (Fig. 5B). Despite the slightly smaller population positive for Oct4, we conclude that Synthamax®II-SC is a suitable, defined substrate for the maintenance of hESCs.

It is interesting that hESC-RPE on both the Synthamax®II-SC and Synthamax®-R display darker pigmentation than the other conditions. RPE pigmentation performs a myriad of essential roles for vision such as protecting against harmful short-wavelength light, participating as an antioxidant to reduce oxidative damage, and even contributing to proper



retinal structure during development<sup>6,67</sup>. The macula is also reported to contain a higher concentration of pigment granules than the peripheral retina<sup>68</sup>. However, the hESC-RPE derived on Synthemax®II-SC express significantly higher tyrosinase (Tyr) mRNA than those on Synthemax®-R (Fig 7A,C). The discrepancy between the Synthemax® cultures could be due to differential rates of RPE maturation on the various substrates. During embryonic development of the optic cup, activation of the tyrosinase promoter initiates RPE maturation and melanogenesis<sup>49,67</sup>. RPE then begin to produce melanosomes, which are specialized organelles for melanin synthesis. Tyrosinase, a heavily post-translationally modified enzyme, catalyzes the rate limiting step of melanin synthesis in developing melanosomes<sup>47,67,69</sup>. Pigment production in the RPE occurs during embryonic development however, and no melanogenesis nor melanosome assembly is thought to occur after gestation<sup>69</sup>. RPE manifesting darker pigmentation may be more mature and could thus be starting to reduce the expression of melanogenesis genes while the proteins persist. Differential expression of gene transcripts and proteins for tyrosinase have been previously been reported<sup>70</sup>. RPE pigmentation can vary considerably *in vivo*, however, and does not necessarily reflect on other functional capacities<sup>12</sup>.

hESC-RPE derived under xeno-free conditions with Synthemax®II-SC demonstrated polarized secretory function and the ability of ROS phagocytosis. Regarding the secretory function of hESC-RPE, polarized secretion of PEDF also testifies to the maturity of the cells. Also, detecting significantly more PEDF on the apical side of the monolayer testifies to the integrity of the tight junctions that separate the apical and basolateral environments. hESC-RPE derived on Synthemax®II-SC secreted slightly less PEDF when seeded on parylene-C scaffolds compared to hESC-RPE derived using the Mg-SR method (Fig. 9). However, H9 hESC-RPE on parylene-C have been observed to secrete a range of apical

PEDF concentrations between 11-20 ng/mm<sup>2</sup> of protein (in preparation). hESC-RPE derived under xeno-free conditions with Synthamax®II-SC functioned similarly to those derived on Matrigel® and Synthamax®-R in their ability to phagocytose ROS and this function was significantly reduced in the presence of the function blocking antibody to  $\alpha v \beta 5$  integrin. ROS phagocytosis by H14-derived RPE on all substrates was significantly less than that of H9-derived RPE, but was similar to the positive control, fRPE (supplemental figure 3).

In summary, we have found that Matrigel® can be replaced by the GMP-compliant substrate Synthamax®II-SC for the culture of hESCs and the production of hESC-RPE. hESCs cultured on Synthamax®II-SC express pluripotency markers and are capable of differentiation into cells expressing markers from the three germ layers. The yield of pigmented cells on Synthamax®II-SC after spontaneous differentiation of hESCs is significantly more than the yield on an alternative ACF substrate, Synthamax®-R. hESC-RPE derived on Synthamax®II-SC express RPE markers, internalize ROS by phagocytosis, and secrete apical PEDF similarly to hESC-RPE derived on Matrigel®. Taken together, this work validates the use of a novel, ACF substrate for the xeno-free production of hESC-RPE that can translate to stem cell-based therapies for AMD.

## **Conclusions**

hESC-derived therapies are expected to be a powerful tool in regenerative medicine, which requires defined, xeno-free culture conditions as the field moves forward. Here, we demonstrate that a novel synthetic substrate, Synthamax®II-SC, supports pluripotent hESC cultures and promotes their efficient differentiation into functional RPE.

## Acknowledgements:

We would like to thank the staff of the Center for Stem Cell Biology and Engineering as well as the Laboratory for Stem Cell Biology and Engineering. This work was supported by the Richard & Katherine Gee Breaux Fellowship in Vision Research, the Garland Initiative for Vision, financial support from Fight for Sight is gratefully acknowledged, a Grant-In-Aid of Research from Sigma Xi The Scientific Research Society, Wynn-Gund Translational Research Acceleration Program, the UCSB Institute for Collaborative Biotechnologies through grant W911NF-09-0001 from the U.S. Army Research Office, and the California Institute for Regenerative Medicine grants DR1-01444, CL1-00521, TG2-01151 and FA1-00616 (DOC). BOP was a fellow of the California Institute for Regenerative Medicine. The content of the information does not necessarily reflect the position or the policy of the Government, and no official endorsement should be inferred.

## References

1. Rein DB, Zhang P, Wirth KE, et al. The economic burden of major adult visual disorders in the United States. *Arch Ophthalmol*. 2006;124(12):1754–1760. doi:10.1001/archophth.124.12.1754.
2. MBiostat WLW, MD XS, BSc XL, et al. Global prevalence of age-related macular degeneration and disease burden projection for 2020 and 2040: a systematic review and meta-analysis. *The Lancet Global Health*. 2014;2(2):e106–e116. doi:10.1016/S2214-109X(13)70145-1.
3. Khandhadia S, Cherry J, Lotery AJ. Age-related macular degeneration. *Adv Exp Med Biol*. 2012;724:15–36. doi:10.1007/978-1-4614-0653-2\_2.
4. Young RW, Bok D. Participation of the retinal pigment epithelium in the rod outer segment renewal process. *J Cell Biol*. 1969;42(2):392–403.
5. Miller SS, Edelman JL. Active ion transport pathways in the bovine retinal pigment epithelium. *J Physiol (Lond)*. 1990;424:283–300.
6. Strauss O. The Retinal Pigment Epithelium in Visual Function. *Physiological Reviews*. 2005;85(3):845–881. doi:10.1152/physrev.00021.2004.
7. Carr A-JF, Smart MJK, Ramsden CM, Powner MB, da Cruz L, Coffey PJ. Development of human embryonic stem cell therapies for age-related macular degeneration. *Trends in Neurosciences*. 2013;36(7):385–395. doi:10.1016/j.tins.2013.03.006.
8. Hageman GS, Gehrs K, Johnson LV, Anderson D. Age-related macular degeneration (AMD). *Webvision: The Organization of the Retina and Visual System [Internet]* Salt Lake City, UT: University of Utah Health Sciences Center. 1995.
9. Schwartz SD, Hubschman J-P, Heilwell G, et al. Embryonic stem cell trials for macular degeneration: a preliminary report. *The Lancet*. 2012;379(9817):713–720.
10. Sipp D. Pilot clinical study into iPS cell therapy for eye disease starts in Japan | RIKEN. *rikenjp*. 2013. Available at: [http://www.riken.jp/en/pr/press/2013/20130730\\_1/](http://www.riken.jp/en/pr/press/2013/20130730_1/). Accessed July 14, 2014.
11. Kamao H, Mandai M, Okamoto S, et al. Characterization of Human Induced Pluripotent Stem Cell-Derived Retinal Pigment Epithelium Cell Sheets Aiming for Clinical Application. *Stem Cell Reports*. 2014;2(2):205–218. doi:10.1016/j.stemcr.2013.12.007.
12. Lu B, Malcuit C, Wang S, et al. Long-Term Safety and Function of RPE from Human Embryonic Stem Cells in Preclinical Models of Macular Degeneration. *Stem Cells*. 2009;27(9):2126–2135. doi:10.1002/stem.149.
13. Carr A-J, Vugler AA, Hikita ST, et al. Protective Effects of Human iPS-Derived Retinal Pigment Epithelium Cell Transplantation in the Retinal Dystrophic Rat. Koch K-W, ed. *PLoS ONE*. 2009;4(12):e8152. doi:10.1371/journal.pone.0008152.s004.
14. Binder S. Scaffolds for retinal pigment epithelium (RPE) replacement therapy. *British Journal of Ophthalmology*. 2011;95(4):441–442. doi:10.1136/bjo.2009.171926.
15. Hynes SR, Lavik EB. A tissue-engineered approach towards retinal repair: Scaffolds for cell transplantation to the subretinal space. *Graefes Arch Clin Exp Ophthalmol*. 2010;248(6):763–778. doi:10.1007/s00417-009-1263-7.
16. Lu B, Zhu D, Hinton D, Humayun MS, Tai Y-C. Mesh-supported submicron parylene-C membranes for culturing retinal pigment epithelial cells. *Biomed Microdevices*. 2012;14(4):659–667. doi:10.1007/s10544-012-9645-8.

17. Hu Y, Liu L, Lu B, et al. A Novel Approach for Subretinal Implantation of Ultrathin Substrates Containing Stem Cell-Derived Retinal Pigment Epithelium Monolayer. *Ophthalmic Res.* 2012;48(4):186–191. doi:10.1159/000338749.
18. Xu C, Inokuma MS, Denham J, et al. Feeder-free growth of undifferentiated human embryonic stem cells. *Nature Biotechnology.* 2001;19(10):971–974. doi:10.1038/nbt1001-971.
19. O'Connor MD. The 3R principle: advancing clinical application of human pluripotent stem cells. *Stem Cell Res Ther.* 2013;4(2):21. doi:10.1186/scrt169.
20. Vukicevic S, Kleinman HK, Luyten FP, Roberts AB, Roche NS, Reddi AH. Identification of multiple active growth factors in basement membrane Matrigel suggests caution in interpretation of cellular activity related to extracellular matrix components. *Exp Cell Res.* 1992;202(1):1–8.
21. McGuire PG, Seeds NW. The interaction of plasminogen activator with a reconstituted basement membrane matrix and extracellular macromolecules produced by cultured epithelial cells. *Journal of cellular biochemistry.* 1989;40(2):215–227.
22. Nakagawa M, Taniguchi Y, Senda S, et al. A novel efficient feeder-free culture system for the derivation of human induced pluripotent stem cells. *Sci Rep.* 2014;4. doi:10.1038/srep03594.
23. Vaajasaari H, Ilmarinen T, Juuti-Uusitalo K, et al. Toward the defined and xeno-free differentiation of functional human pluripotent stem cell-derived retinal pigment epithelial cells. *Mol Vis.* 2011;17:558–575.
24. Sorkio A, Hongisto H, Kaarniranta K, Uusitalo H, Juuti-Uusitalo K, Skottman H. Structure and Barrier Properties of Human Embryonic Stem Cell-Derived Retinal Pigment Epithelial Cells Are Affected by Extracellular Matrix Protein Coating. *Tissue Engineering Part A.* 2014;140120073644000. doi:10.1089/ten.tea.2013.0049.
25. Melkounian Z, Weber JL, Weber DM, et al. nbt.1629(2). *Nature Biotechnology.* 2010;28(6):606–610. doi:10.1038/nbt.1629.
26. Tucker BA, Anfinson KR, Mullins RF, Stone EM, Young MJ. Use of a Synthetic Xeno-Free Culture Substrate for Induced Pluripotent Stem Cell Induction and Retinal Differentiation. *Stem Cells Translational Medicine.* 2013;2(1):16–24. doi:10.5966/sctm.2012-0040.
27. Goh PA, Caxaria S, Casper C, et al. A Systematic Evaluation of Integration Free Reprogramming Methods for Deriving Clinically Relevant Patient Specific Induced Pluripotent Stem (iPS) Cells. Wilber AC, ed. *PLoS ONE.* 2013;8(11):e81622. doi:10.1371/journal.pone.0081622.s002.
28. Lin P-Y, Hung S-H, Yang Y-C, et al. A Synthetic Peptide-Acrylate Surface for Production of Insulin-Producing Cells from Human Embryonic Stem Cells. *Stem Cells and Development.* 2014;23(4):372–379. doi:10.1089/scd.2013.0253.
29. Li Y, Gautam A, Yang J, et al. Differentiation of Oligodendrocyte Progenitor Cells from Human Embryonic Stem Cells on Vitronectin-Derived Synthetic Peptide Acrylate Surface. *Stem Cells and Development.* 2013;22(10):1497–1505. doi:10.1089/scd.2012.0508.
30. Jin S, Yao H, Weber JL, Melkounian ZK, Ye K. A Synthetic, Xeno-Free Peptide Surface for Expansion and Directed Differentiation of Human Induced Pluripotent Stem Cells. Awad HA, ed. *PLoS ONE.* 2012;7(11):e50880. doi:10.1371/journal.pone.0050880.g005.
31. Maruotti J, Wahlin K, Gorrell D, Bhutto I, Luttj G, Zack DJ. A Simple and Scalable Process for the Differentiation of Retinal Pigment Epithelium From Human Pluripotent Stem Cells. *Stem Cells Translational Medicine.* 2013;2(5):341–354. doi:10.5966/sctm.2012-0106.
32. Baranov P, Regatieri C, Melo G, Clissold H, Young M. Synthetic Peptide-Acrylate Surface for Self-Renewal of Human Retinal Progenitor Cells. *Tissue Engineering Part C: Methods.* 2013;19(4):265–270. doi:10.1089/ten.tec.2012.0217.
33. Hayman EG, Pierschbacher MD, Ohgren Y, Ruoslahti E. Serum spreading factor (vitronectin) is present at the cell surface and in tissues. *Proc Natl Acad Sci USA.* 1983;80(13):4003–4007.
34. Ruoslahti E. RGD and other recognition sequences for integrins. *Annu Rev Cell Dev Biol.* 1996;12:697–715. doi:10.1146/annurev.cellbio.12.1.697.
35. Hervy M, Weber JL, Pecheul M, et al. Long Term Expansion of Bone Marrow-Derived hMSCs on Novel Synthetic Microcarriers in Xeno-Free, Defined Conditions. Pant AB, ed. *PLoS ONE.* 2014;9(3):e92120. doi:10.1371/journal.pone.0092120.g005.
36. Kelly J, Zhou J, Henry D, Dolley-Sonneville P, Weber J, Melkounian Z. Feeder-Free Expansion of Human Induced Pluripotent Stem Cells (hiPSC) on Corning Synthemax-II SC Substrate Coated Surface in Defined Medium. *SnAPPShots.* 2012. Available at: [http://www.corning.com/lifesciences/surfaces/en/synthemax/technical\\_resources.aspx?linkidentifier=id&itemid=47257&menutitle=posters](http://www.corning.com/lifesciences/surfaces/en/synthemax/technical_resources.aspx?linkidentifier=id&itemid=47257&menutitle=posters).
37. Buchholz DE, Hikita ST, Rowland TJ, et al. Derivation of functional retinal pigmented epithelium from induced

- pluripotent stem cells. *Stem Cells*. 2009;27(10):2427–2434. doi:10.1002/stem.189.
38. Maminishkis A, Miller SS. Experimental Models for Study of Retinal Pigment Epithelial Physiology and Pathophysiology. *JoVE*. 2010;(45). doi:10.3791/2032.
  39. Buchholz DE, Pennington BO, Croze RH, Hinman CR, Coffey PJ, Clegg DO. Rapid and Efficient Directed Differentiation of Human Pluripotent Stem Cells Into Retinal Pigmented Epithelium. *Stem Cells Translational Medicine*. 2013;2(5):384–393. doi:10.5966/sctm.2012-0163.
  40. Yoon T-M, Chang B, Kim H-T, Jee J-H, Kim D-W, Hwang D-Y. Human Embryonic Stem Cells (hESCs) Cultured Under Distinctive Feeder-Free Culture Conditions Display Global Gene Expression Patterns Similar to hESCs from Feeder-Dependent Culture Conditions. *Stem Cell Rev and Rep*. 2010;6(3):425–437. doi:10.1007/s12015-010-9158-x.
  41. Kwon GS, Fraser ST, Eakin GS, et al. Tg(Afp-GFP) expression marks primitive and definitive endoderm lineages during mouse development. *Dev Dyn*. 2006;235(9):2549–2558. doi:10.1002/dvdy.20843.
  42. Dziadek M, Adamson E. Localization and synthesis of alphafoetoprotein in post-implantation mouse embryos. *J Embryol Exp Morphol*. 1978;43:289–313.
  43. Idelson M, Alper R, Obolensky A, et al. Directed Differentiation of Human Embryonic Stem Cells into Functional Retinal Pigment Epithelium Cells. *Stem Cell*. 2009;5(4):396–408. doi:10.1016/j.stem.2009.07.002.
  44. Diniz B, Thomas P, Thomas B, et al. Subretinal implantation of retinal pigment epithelial cells derived from human embryonic stem cells: improved survival when implanted as a monolayer. *Investigative Ophthalmology & Visual Science*. 2013;54(7):5087–5096. doi:10.1167/iovs.12-11239.
  45. Lagunoff D, Rickard A. Mast Cell Granule Heparin Proteoglycan Induces Lacunae in Confluent Endothelial Cell Monolayers. *The American Journal of Pathology*. 2010;154(5):1591–1600. doi:10.1016/S0002-9440(10)65412-0.
  46. Kobayashi T, Urabe K, Orlow SJ, et al. The Pmel 17/silver locus protein. Characterization and investigation of its melanogenic function. *Journal of Biological Chemistry*. 1994;269(46):29198–29205.
  47. Wasmeier C, Hume AN, Bolasco G, Seabra MC. Melanosomes at a glance. *Journal of Cell Science*. 2008;121(24):3995–3999. doi:10.1242/jcs.040667.
  48. Saari JC, Nawrot M, Kennedy BN, et al. Visual cycle impairment in cellular retinaldehyde binding protein (CRALBP) knockout mice results in delayed dark adaptation. *Neuron*. 2001;29(3):739–748.
  49. Clegg DO, Buchholz D, Hikita S, Rowland T, Hu Q, Johnson LV. Retinal pigment epithelial cells: development in vivo and derivation from human embryonic stem cells in vitro for treatment of age-related macular degeneration. 2008:1–24.
  50. Meyer JS, Shearer RL, Capowski EE, et al. Modeling early retinal development with human embryonic and induced pluripotent stem cells. *Proc Natl Acad Sci USA*. 2009;106(39):16698–16703. doi:10.1073/pnas.0905245106.
  51. Tung P-Y, Knoepfler PS. Epigenetic mechanisms of tumorigenicity manifesting in stem cells. *Oncogene*. 2014;0. doi:10.1038/onc.2014.172.
  52. Finnemann SC. Focal adhesion kinase signaling promotes phagocytosis of integrin-bound photoreceptors. *The EMBO journal*. 2003;22(16):4143–4154.
  53. D'Cruz PMP, Yasumura DD, Weir JJ, et al. Mutation of the receptor tyrosine kinase gene MERTK in the retinal dystrophic RCS rat. *Hum Mol Genet*. 2000;9(4):645–651.
  54. Cao W, Tombran-Tink J, Elias R, Sezate S, Mrazek D, McGinnis JF. In vivo protection of photoreceptors from light damage by pigment epithelium-derived factor. *Investigative Ophthalmology & Visual Science*. 2001;42(7):1646–1652.
  55. Ogata N, Wang L, Jo N, et al. Pigment epithelium derived factor as a neuroprotective agent against ischemic retinal injury. *Current eye research*. 2001;22(4):245–252.
  56. Bharti K, Liu W, Csermely T, Bertuzzi S, Arnheiter H. Alternative promoter use in eye development: the complex role and regulation of the transcription factor MITF. *Development*. 2008;135(6):1169–1178. doi:10.1242/dev.014142.
  57. Chambers SM, Fasano CA, Papapetrou EP, Tomishima M, Sadelain M, Studer L. Highly efficient neural conversion of human ES and iPS cells by dual inhibition of SMAD signaling. *Nature Biotechnology*. 2009;27(3):275–280. doi:10.1038/nbt.1529.
  58. Bigdeli N, Andersson M, Strehl R, et al. Adaptation of human embryonic stem cells to feeder-free and matrix-free culture conditions directly on plastic surfaces. *Journal of Biotechnology*. 2008;133(1):146–153. doi:10.1016/j.jbiotec.2007.08.045.
  59. Stover AE, Schwartz PH. Adaptation of human pluripotent stem cells to feeder-free conditions in chemically defined medium with enzymatic single-cell passaging. *Methods Mol Biol*. 2011;767:137–146. doi:10.1007/978-1-61779-201-4\_10.

60. Tompkins JD, Hall C, Chen VC-Y, et al. Epigenetic stability, adaptability, and reversibility in human embryonic stem cells. *Proc Natl Acad Sci USA*. 2012;109(31):12544–12549. doi:10.1073/pnas.1209620109/-/DCSupplemental/st01.doc.
61. Ramos-Mejia V, Bueno C, Roldan M, et al. The Adaptation of Human Embryonic Stem Cells to Different Feeder-Free Culture Conditions Is Accompanied by a Mitochondrial Response. *Stem Cells and Development*. 2012;21(7):1145–1155. doi:10.1089/scd.2011.0248.
62. Perkel J. Tricks For Human Embryonic Stem Cells | The Scientist Magazine®. *The Scientist.com*. 2005. Available at: <http://www.the-scientist.com/?articles.view/articleNo/16566/title/Tricks-For-Human-Embryonic-Stem-Cells/>. Accessed July 16, 2014.
63. Yan CYI, Vieceli FM, Turri JAO, Hayashi MAF, Kanno TY. *Gene Expression in Embryonic Neural Development and Stem Cell Differentiation*. 2012.
64. Chapman DL, Papaioannou VE. Three neural tubes in mouse embryos with mutations in the T-box gene Tbx6. *Nature*. 1998;391(6668):695–697.
65. Adewumi O, Aflatoonian B, Ahrlund-Richter L, et al. Characterization of human embryonic stem cell lines by the International Stem Cell Initiative. *Nature Biotechnology*. 2007;25(7):803–816. doi:10.1038/nbt1318.
66. Noisa P, Ramasamy TS, Lamont FR, et al. Identification and Characterisation of the Early Differentiating Cells in Neural Differentiation of Human Embryonic Stem Cells. Ng HH, ed. *PLoS ONE*. 2012;7(5):e37129. doi:10.1371/journal.pone.0037129.s003.
67. Jeffery G. The retinal pigment epithelium as a developmental regulator of the neural retina. *Eye (Lond)*. 1998;12:499–503.
68. Boulton M, Dayhaw-Barker P. The role of the retinal pigment epithelium: topographical variation and ageing changes. *Eye (Lond)*. 2001;15(Pt 3):384–389. doi:10.1038/eye.2001.141.
69. Sarna T. New trends in photobiology: Properties and function of the ocular melanin—a photobiophysical view. *Journal of Photochemistry and Photobiology B: Biology*. 1992;12(3):215–258.
70. Hashimoto Y, Ito Y, Kato T, Motokawa T, Katagiri T, Itoh M. Expression profiles of melanogenesis-related genes and proteins in acquired melanocytic nevus. *Journal of cutaneous pathology*. 2006;33(3):207–215.

### **III. Rapid and Efficient Derivation of RPE from hESCS**

#### ***A. Development of a Directed Differentiation Protocol***

Britney Pennington co-authored the following chapter entitled “Rapid and Efficient Directed Differentiation of Human Pluripotent Stem Cells Into Retinal Pigmented Epithelium” with Dr. David E. Buchholz. Dr. Buchholz wrote the text and Britney Pennington contributed work to optimize the timeline of factor application, to investigate a potential mechanism of PARP-1 inhibition mediated by nicotinamide to expedite the derivation of hESC-RPE, and the data required for Fig. 10B, D; Fig. 11D; Fig. 12A, B, C; Fig. 14A.

This manuscript has been published by Alphamed Press in *Stem Cells Translational Medicine* 2013, 2:384-393 doi: 10.5966/sctm.2012-0163.

#### **Rapid and Efficient Directed Differentiation of Human Pluripotent Stem Cells Into Retinal Pigmented Epithelium**

David E. Buchholz, Britney O. Pennington, Roxanne H. Croze, Cassidy R. Hinman, Peter J. Coffey and Dennis O. Clegg

#### **Abstract**

Controlling the differentiation of human pluripotent stem cells is the goal of many laboratories, both to study normal human development and to generate cells for transplantation. One important cell type under investigation is the retinal pigmented epithelium (RPE). Age-related macular degeneration (AMD), the leading cause of blindness in the Western world, is caused by dysfunction and death of the RPE. Currently, RPE derived from human embryonic stem cells are in clinical trials for the treatment of AMD. Although protocols to generate RPE from human pluripotent stem cells have become more efficient since the first report in 2004, they are still time-consuming and relatively inefficient. We have found that the addition of defined factors at specific times leads to conversion of approximately 80% of the cells to an RPE phenotype in only 14 days. This protocol should be useful for rapidly generating RPE for transplantation as well as for studying RPE development *in vitro*.

## Introduction

Age-related macular degeneration (AMD) is the leading cause of blindness in the aging population of the Western world [1]. AMD presents in two forms, wet and dry, caused by dysfunction and death of the retinal pigmented epithelium (RPE) through mechanisms still being resolved [2]. The wet form, characterized by neovascularization, can be effectively treated with monthly injections of antiangiogenic drugs such as Lucentis® (Genentech, South San Francisco, CA, [http:// www.gene.com](http://www.gene.com)). Although effective, there is substantial cost and inconvenience associated with monthly injections into the back of the eye [3]. The dry form of AMD is characterized by drusenoid aggregates under the basal side of the RPE at early stages, which progresses to geographic atrophy with marked loss of RPE and photoreceptors. Currently there is no effective treatment for the dry form of AMD, which accounts for 80%–90% of AMD cases.

Because the etiology of AMD is still under investigation, one focus of therapy has been on replacing diseased RPE through transplantation [4]. The feasibility of this approach has been demonstrated by autologous replacement of RPE in the macula, the central portion of the retina responsible for high acuity vision, via macular translocation or relocation of peripheral RPE to the macula [5–7]. Although somewhat effective, these surgeries are long and complicated. The derivation of RPE from pluripotent cells and their efficacy in preclinical models of retinal degeneration have led to the design of simpler transplantation strategies that are much faster and cost-effective. Two methods of transplantation predominate: a subretinal bolus injection of single cells and subretinal insertion of a patch of RPE grown in its native monolayer form [8, 9]. Currently, clinical trials are under way using RPE derived from human embryonic stem cells (hESCs) using the bolus injection approach, with clinical trials using the patch soon to follow.



The translation of pluripotent stem cell-derived RPE has moved rapidly toward the clinic, and researchers in the lab have also been working to increase both the speed and efficiency of RPE derivation. Initial work on human pluripotent stem cell RPE began when it was observed that hESCs allowed to “spontaneously” differentiate would give rise to a low percentage of RPE, easily identifiable by pigmentation; this work was later recapitulated with induced pluripotent stem cells [10 –12]. This is the paradigm currently being used to generate RPE for the clinic. Although reliable, it is extremely inefficient and time-consuming, with an efficiency of ~1% after 1–2 months in culture (although this varies between lines). RPE are typically not harvested until after 2–3 months in culture, to give pigmented foci time to expand. A major breakthrough in the directed differentiation of pluripotent stem cells to RPE came in 2010 when the addition of nicotinamide and Activin-A was shown to increase the efficiency of RPE generation to 33% after 6 weeks as determined by the number of pigmented cells [13]. The highest reported efficiency of RPE generation was obtained by exposing pluripotent cells to basic fibroblast growth factor (bFGF), Noggin, retinoic acid, and Shh. An efficiency of ~60% *Mitf*<sup>+</sup> cells after 60 days of differentiation was reported [14].

Interestingly, a report in 2006 showed that neural retinal progenitors could be generated with ~80% efficiency after 21 days of differentiation through the application of a handful of factors (insulin-like growth factor 1 [IGF1], Noggin, Dkk1, and bFGF) [15]. Because RPE and the neural retina arise from a common progenitor pool [16], we sought to determine whether this protocol could be altered to direct pluripotent stem cells to RPE with a similar efficiency. Through the combined use of the retinal inducing factors (IGF1, Noggin, Dkk1, and bFGF) and other factors (nicotinamide, Activin A, SU5402, and vasoactive intestinal peptide [VIP]) added at appropriate times, we have found that pluripotent stem cells could

be directed to RPE with an efficiency of ~80% based on Pmel17 expression. Importantly, these cells could be isolated as early as 14 days following the onset of differentiation. This protocol should be useful for quickly generating quantities of RPE for transplantation as well as for the study of RPE development.

## **Materials and Methods**

### *Pluripotent Stem Cell Culture*

The human embryonic stem cell line H9 (WiCell Research Institute, Madison, WI, <http://www.wicell.org>) was maintained in Dulbecco's Modified Eagle's Medium: Nutrient Mixture F-12 (DMEM/F12) containing 2mM GlutaMAX-I, 20% knockout serum replacement, 0.1mM Modified Eagle's Medium Non-Essential Amino Acids (MEM NEAA), 0.1mM  $\beta$ -mercaptoethanol (Invitrogen, Carlsbad, CA, <http://www.invitrogen.com>) and 4 ng/ml bFGF (Peprotech, Rocky Hill, NJ, <http://www.peprotech.com>) on a mitomycin C (Sigma-Aldrich, St. Louis, MO, <http://www.sigmaaldrich.com>)-treated mouse embryonic fibroblast feeder layer. H9s for flow cytometry were grown on growth factor-reduced Matrigel (BD Biosciences, San Diego, CA, <http://www.bdbiosciences.com>) in mTESR1 (StemCell Technologies, Vancouver, BC, Canada, <http://www.stemcell.com>) medium. The human embryonic stem cell line UCSF4 (NIH registry no. 0044, University of California, San Francisco) was maintained on growth factor-reduced Matrigel (BD Biosciences) in mTESR1 medium (StemCell Technologies). The induced pluripotent stem cell line iPS(IMR90)-4 (IMR904) (kind gift of J. Thomson, University of Wisconsin and University of California, Santa Barbara) was maintained in DMEM/F12 containing 2 mM GlutaMAX-I, 20% knockout serum replacement, 0.1 mM MEM NEAA, 0.1 mM  $\beta$ -mercaptoethanol (Invitrogen) and 100 ng/ml recombinant zebrafish bFGF (gift of J. Thomson) on a mitomycinC (Sigma-Aldrich)-treated mouse embryonic fibroblast feeders.

### *Differentiation Into Retinal Pigmented Epithelium*

Pluripotent stem cells were passaged directly onto Matrigel (BD Biosciences) in DMEM/F12 with 1x B27, 1x N2, and 1x NEAA (Invitrogen). From days 0 to 2, 50 ng/ml Noggin, 10 ng/ml Dkk1, and 10 ng/ml IGF1 (R&D Systems Inc., Minneapolis, MN, <http://www.rndsystems.com>) and in some experiments 10 mM nicotinamide or 5 mM 3-aminobenzamide (Sigma-Aldrich) were added to the base medium. From days 2 to 4, 10 ng/ml Noggin, 10 ng/ml Dkk1, 10 ng/ml IGF1, and 5 ng/ml bFGF and in some experiments 10 mM nicotinamide or 5 mM 3-aminobenzamide were added to the base medium. From days 4 to 6, 10 ng/ml Dkk1 and 10 ng/ml IGF1 and in some experiments 100 ng/ml Activin A (R&D Systems) were added to the base medium. From days 6 to 14, 100 ng/ml Activin A, 10  $\mu$ M SU5402 (EMD Millipore, Darmstadt, Germany, <http://www.emdmillipore.com>), and 1  $\mu$ M VIP (Sigma-Aldrich) were added to the base medium. Control experiments were also performed in base media alone (DMEM/F12, B27, N2, and NEAA).

The cells were mechanically enriched by scraping away cells with non-RPE morphology. Subsequently, the remaining RPE were digested using TrypLE Express (Invitrogen) for ~5 minutes at 37°C. The cells were passed through a 30- $\mu$ m single-cell strainer and seeded onto Matrigel-coated tissue culture plastic, Transwell membranes (Corning Enterprises, Corning, NY, <http://www.corning.com>), or CC2-treated chambered slides. Enriched cells were cultured in DMEM-high glucose with 1% fetal bovine serum (FBS), GlutaMAX, and sodium pyruvate (Invitrogen) for 30 days [17].

Hs27 and cultured fetal human RPE (kind gift of D. Bok) were cultured on Matrigel-coated Transwell membranes in DMEM-high glucose with 1% FBS, GlutaMAX, and sodium pyruvate (Invitrogen). MeWo cells were cultured in DMEM/F12 GlutaMAX1 (Invitrogen) with 10% fetal bovine serum (HyClone, Logan, UT, <http://www.hyclone.com>).

### *Quantitative Real-Time Polymerase Chain Reaction*

Total RNA was isolated using the RNeasy Plus Mini Kit (Qiagen, Hilden, Germany, <http://www.qiagen.com>). cDNA was synthesized from 1 µg of RNA using the iScript cDNA Synthesis Kit (Bio-Rad, Hercules, CA, <http://www.bio-rad.com>). Primer pairs were designed to create a 75–200-base pair product (Beacon Design 4.0; Premier Biosoft International, Palo Alto, CA, <http://www.premierbiosoft.com>). Quantitative real-time polymerase chain reaction (PCR) was carried out on a Bio-Rad MyIQ Single Color Real-Time PCR Detection System using the SYBR Green method [18]. Triplicate 20-µl reactions were run in a 96-well plate with half of the cDNA synthesis reaction used per plate. Primer specificity was confirmed by melting temperature analysis, gel electrophoresis, and direct sequencing (Iowa State DNA Facility, Ames, IA). The data were normalized to the geometric mean of the “housekeeping” genes: glyceraldehyde phosphate dehydrogenase (*GAPDH*), hydroxymethylbilane synthase (*HMBS*), and glucose phosphate isomerase (*GPI*) [19].

### *Immunocytochemistry*

The cells were grown on Matrigel-coated 12-well tissue culture plates (days 0 –14) or enriched onto Matrigel-coated chambered slides and cultured for 1 month. For fixation, the plates and slides were washed with phosphate-buffered saline (PBS), fixed with 4% paraformaldehyde in 0.1 M sodium cacodylate buffer, pH 7.4, for 15 minutes at 4°C, and stored in PBS at 4°C until labeling. The slides were washed with PBS, blocked with PBS containing 5% BSA and 0.1% NP40 in PBS for 1 hour at 4°C, treated with ice-cold 90% methanol for 5 minutes, and incubated with primary anti- bodies overnight at 4°C. The slides were incubated with an appropriate Alexa Fluor (Invitrogen)-conjugated secondary antibody (1:300) for 30 minutes at 4°C, stained with Hoechst (2 µg/ml) (Invitrogen) for 5 minutes at room temperature, washed with PBS, and then imaged at room temperature using

an Olympus IX71 fluorescence microscope or an Olympus Fluoview FV10i confocal microscope (Olympus, Center Valley, PA, <http://www.olympusamerica.com>).

### *Flow Cytometry*

The samples were fixed in 4% paraformaldehyde in PBS (Electron Microscopy Sciences, Hatfield, PA, <http://www.emsdiasum.com/microscopy>) and permeabilized with 0.2% Triton X-100 (Roche, Indianapolis, IN, <http://www.roche.com>). The samples were labeled with primary or isotype control antibodies for 30 minutes at 4°C. Primary and isotype control antibodies that were not conjugated to fluorophores were labeled with fluorophore-conjugated secondary antibodies for 30 minutes at 4°C. The labeled samples were run on an Accuri C6 flow cytometer with CFlow collection software (BD Biosciences). Data analysis was performed on FCS Express 4 Flow Research Edition (De Novo Software, Thornhill, ON, Canada, <http://www.denovosoftware.com>). The positive percentage was based on a background level set at 1% positive expression in samples labeled with isotype control antibodies.

### *Rod Outer Segment Phagocytosis*

Rod outer segment (ROS) phagocytosis assays were performed as previously described [20]. Bovine eyes were obtained fresh from Sierra Medical Inc. (Whittier, CA, <http://www.sierra-medical.com>); ROSs were purified from retinal extracts and fluorescently labeled using the FluoReporter FITC Protein Labeling Kit (Invitrogen). The cells were seeded in quadruplicate on gelatin-coated wells in a 96-well plate at a concentration of 25,000–50,000 cells per well and allowed to grow to confluence for 4 weeks. The cells were then challenged with  $1 \times 10^6$  fluorescein isothiocyanate-labeled ROSs per well with or without 50  $\mu$ g/ml anti- $\alpha$ v $\beta$ 5 (ab24694; Abcam, Cambridge, U.K., <http://www.abcam.com>)

or 50  $\mu$ g/ml IgG1 control (ab9404; Abcam) for 5 hours at 37°C in 5% CO<sub>2</sub>. The wells were then vigorously washed five times with warm PBS to remove unbound ROSs. To determine the level of ROS internalization, an equal volume of 0.4% trypan blue was added to the PBS for 10 minutes to quench extracellular fluorescence. Trypan blue was aspirated, and 40  $\mu$ l of PBS was added to the well to prevent the cells from drying out. The internalized ROSs were then documented in fluorescence photomicrographs. Fluorescence intensity was quantified by pixel densitometry using ImageJ software (National Institutes of Health, Bethesda, MD) for photomicrograph analysis. Photomicrographs from three wells for each condition were averaged within each assay. Separate experiments were normalized to the positive control ARPE-19 cell line, which was assayed in each experiment.

## **Results**

### **Nicotinamide Speeds Up Early Eye Field Differentiation**

Because nicotinamide had previously been shown to increase differentiation of RPE from pluripotent stem cells [13], we tested whether nicotinamide would influence differentiation at early stages of eye field development. In this first segment of differentiation, cell clumps are mechanically dissected from pluripotent stem cell colonies and seeded on Matrigel in the presence of IGF1, Noggin, and DKK1. On day 2, bFGF is added. The addition of nicotinamide to IGF1, Noggin, Dkk1, and bFGF significantly decreased expression of the pluripotency genes Oct4 and Nanog on day 4 compared with controls (Fig. 10A, 10B). Expression of early neural/early eye field markers Lhx2 and Rax increased in the presence of nicotinamide on day 4 compared with controls; however, the increase in Rax was not significant (Fig. 10B). Interestingly, Pax6(-5a) expression was similar between nicotinamide and control conditions (Fig. 10B). Cells in the presence of nicotinamide rapidly adopted a radial/rosette morphology compared with control cells, which still

contained a large percentage of cells with undifferentiated morphology (Fig. 10C). Control cells expanded more rapidly than cells in nicotinamide.

Nicotinamide can have many effects on cultured cells, including inhibition of poly(ADP-ribose) polymerase (PARP), which can protect cells from oxidative stress [13, 21]. To examine the mechanism of nicotinamide induced differentiation, we tested the ability of 3-aminobenzamide, an inhibitor of PARP, to recapitulate the effects of nicotinamide. 3-Aminobenzamide reduced levels of Oct4 and Nanog compared with controls on day 4, but not as much as nicotinamide (Fig. 10B). Similarly, 3-aminobenzamide significantly increased levels of Lhx2 and Rax compared with controls on day 4, but not as much as nicotinamide (Fig. 10B). Overall, 3-aminobenzamide was able to partially recapitulate the effects of nicotinamide.

#### **Activin A, SU5402, and VIP Direct Early Eye Field Cells to an RPE Fate**

Following the acquisition of early eye field markers by day 4 (Fig. 10B), we sought to direct the cell to RPE instead of neural retina. With this in mind, we phased out the addition of nicotinamide (added days 0 – 4), Noggin (added days 0 – 4), bFGF (added days 2–4), IGF1 (added days 0–6), and Dkk1 (added days 0–6) and tested the effect of Activin A, SU5402, and VIP on RPE specification.

The addition of Activin A on days 4–10 had little effect on gene expression of *Mitf*, a marker of the optic vesicle and of RPE. Expression of *Rax*, a marker of the early eye field and neural retina, was significantly decreased (Fig. 10D). Addition of SU5402 on days 6 –10 had little effect on expression of either *Mitf* or *Rax*; however, in combination with Activin A, expression of *Rax* was further decreased (Fig. 10D). VIP has been previously shown to speed up maturation of cultured primary RPE by increasing intra- cellular cAMP and activating pp60(c-src) [22]. Addition of VIP on days 6–10 significantly increased



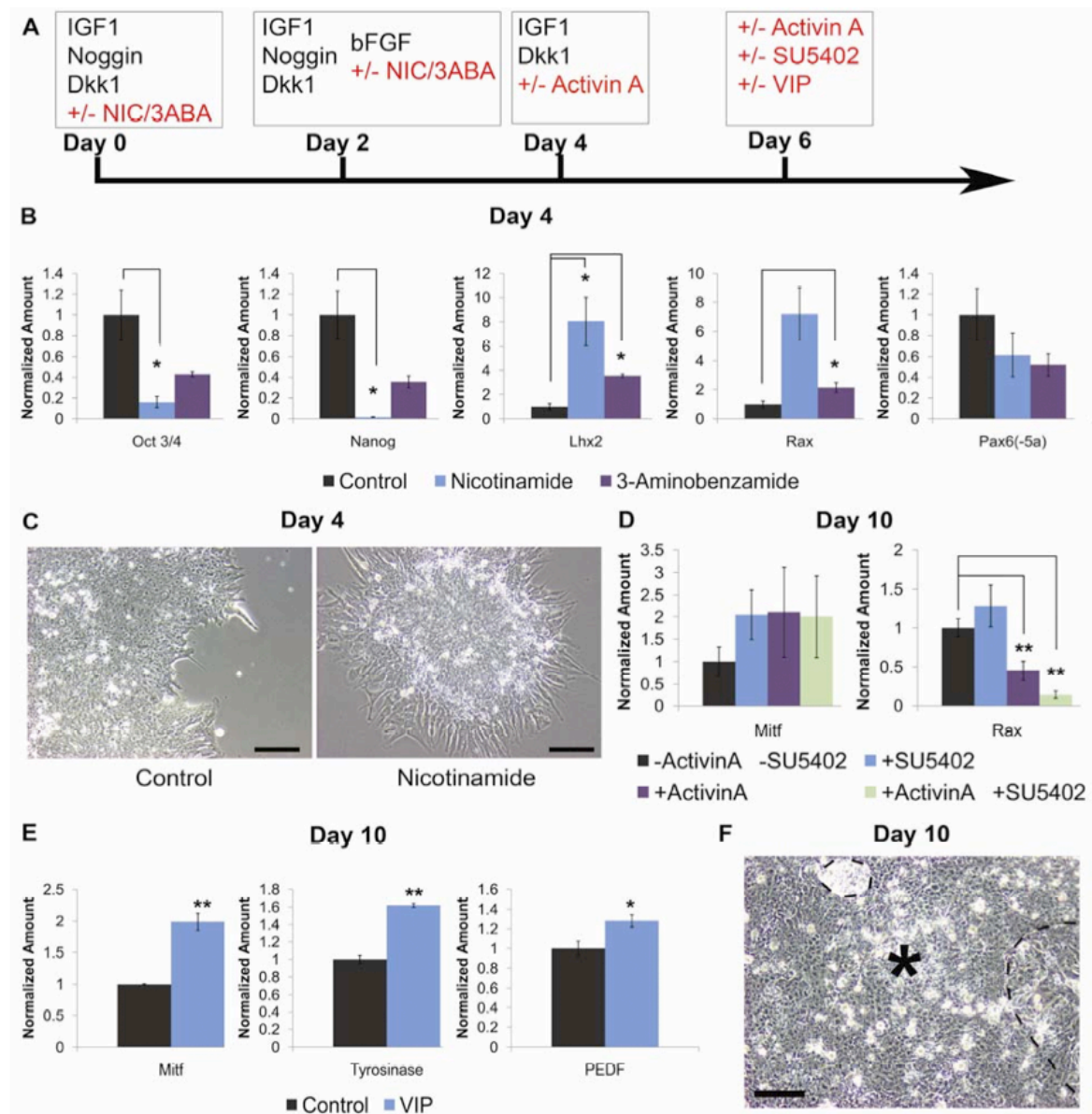


**Figure 10.** Defined factors rapidly direct pluripotent cells toward an early eye field and retinal pigmented epithelium fate. **(A):** Timing of factor addition. The factors in red were under investigation. **(B):** The effect of nicotinamide and 3-aminobenzamide on pluripotency and early eye field gene expression. mRNA levels were quantified by polymerase chain reaction (qPCR) and normalized to the control condition (IGF1, Noggin, DKK1, and bFGF at the times shown in [A]). The error bars represent the standard error of the mean. \*,  $p < .1$ . **(C):** The effect of nicotinamide on cell morphology. Phase contrast images are shown. Scale bars = 200  $\mu$ m. **(D):** The effect of Activin A and SU5402 alone and in combination on Mitf and Rax gene expression. mRNA levels were quantified by qPCR and normalized to the control condition (IGF1, Noggin, DKK1, bFGF, and nicotinamide at the times shown in [A]). The error bars represent the standard error of the mean. **(E):** The effect of VIP on retinal pigmented epithelium gene expression. mRNA levels were quantified by qPCR and normalized to the control condition (IGF1, Noggin, DKK1, bFGF, nicotinamide, Activin A, and SU5402 at the times shown in [A]). The error bars represent the standard error of the mean. \*\*,  $p \leq .05$ . **(F):** Morphology at day 10 following the addition of IGF1, Noggin, DKK1, bFGF, nicotinamide, Activin A, SU5402, and VIP at the times shown in (A). The asterisk marks an area with cobblestone morphology. Scale bar = 200  $\mu$ m. Abbreviations: bFGF, basic fibroblast growth factor; IGF, insulin-like growth factor; VIP, vasoactive intestinal peptide.



expression of RPE marker genes *Mitf*, tyrosinase, and PEDF (Fig. 10E). Consistent with the roles of *Mitf* and tyrosinase in pigment synthesis, pigmentation was increased in cultures containing VIP between days 10 and 14 (data not shown). By day 10, sheets of cells with cobblestone morphology and distinct borders were visible (Fig. 10F; supplemental Fig. 6A, 6B).

### **Differentiation to RPE Is Highly Efficient**

Following 4 more days in culture with Activin A, SU5402, and VIP, the borders of cobblestone sheets became more defined, and some cells began to pigment (Fig. 11A; supplemental Fig. 6A, 6B). Immunocytochemistry for the melanosomal protein *Pmel17* (upon which melanin pigment is deposited) exclusively labeled these pigmenting sheets of cells (Fig. 11A). Quantitative polymerase chain reaction (qPCR) analysis showed that compared with cells differentiated in B27/N2 containing basal medium only (no factor differentiation), cells that had been exposed to RPE differentiation factors (nicotinamide, IGF1, DKK1, Noggin, bFGF, Activin A, SU5402, and VIP) had significantly increased levels of the RPE marker genes *Mitf*, Tyrosinase, *Tyrp2*, PEDF, *BEST1*, and *Pmel17* (Fig. 11B). Additional immunocytochemistry revealed *Mitf* expression exclusively in pigmenting sheets of cells, whereas *Lhx2* and *ZO1* could be found in both pigmenting sheets and non-RPE cells (Fig. 11C). Interestingly, in addition to *Lhx2*, some non-RPE cells expressed *Oct4* (Fig. 12B). When isolated and replated in pluripotent stem cell conditions, these cells did not form colonies with typical undifferentiated stem cell morphology, and many appeared to differentiate into neurons (supplemental Fig. 6C).

To determine the efficiency of differentiation, we performed flow cytometry using the *Pmel17* antibody, which is highly sensitive and which labels only pigmenting sheets of

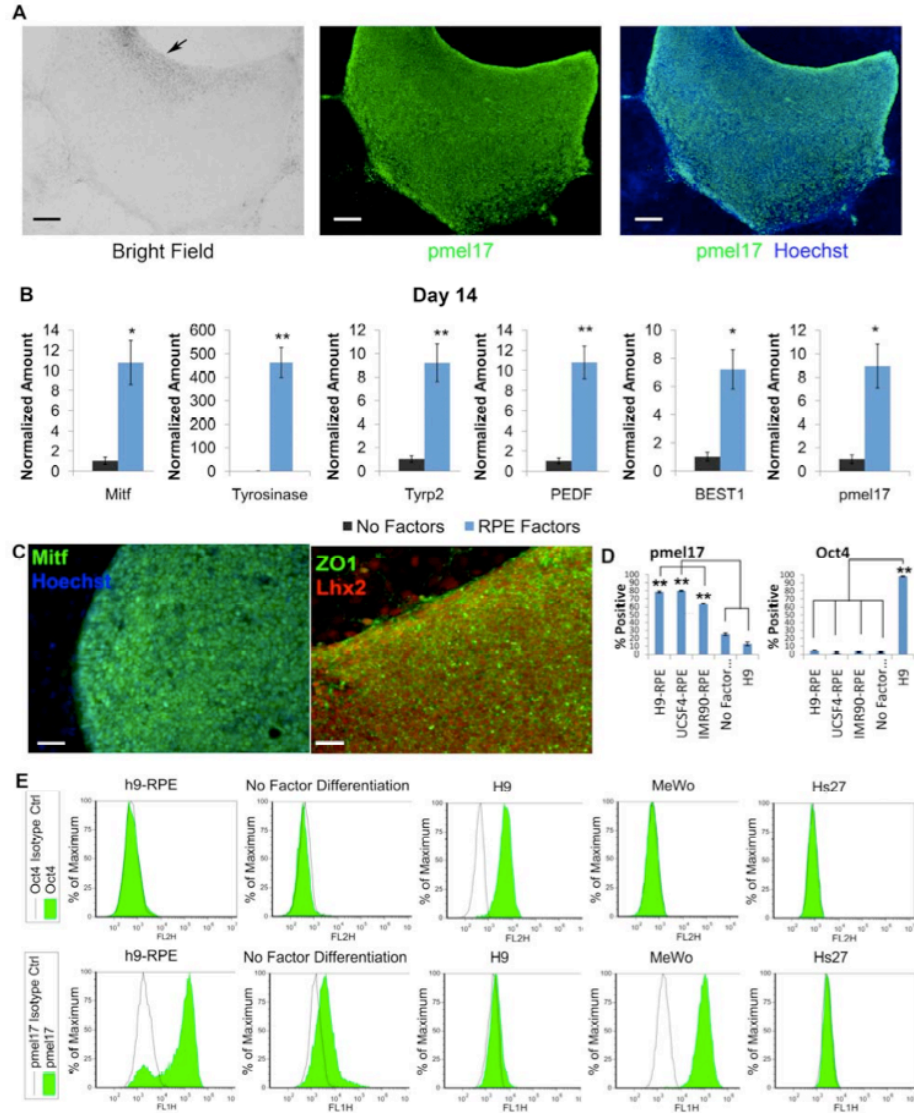


**Figure 11.** Sheets of RPE progenitors are efficiently generated and begin to pigment by day 14 of differentiation. **(A):** Bright field and immunofluorescence images of a sheet of RPE at day 14. The arrow points to pigmented cells. Scale bars = 500  $\mu$ m. **(B):** RPE gene expression following differentiation in insulin-like growth factor 1, Noggin, DKK1, basic fibroblast growth factor, nicotinamide, Activin A, SU5402, and vasoactive intestinal peptide compared with differentiation in basal medium alone. mRNA levels were quantified by quantitative polymerase chain reaction and normalized to the no factor condition (differentiated in B27/N2 DMEM/F12 medium). The error bars represent the standard error of the mean. \*,  $p \leq .1$ ; \*\*,  $p \leq .05$ . **(C):** Immunofluorescence images of RPE sheets at day 14. Scale bar = 100  $\mu$ m. **(D):** Quantification of Pmel17 and Oct4 immunoreactivity by flow cytometry after 14 days differentiation of H9, UCSF4, and IMR90, compared with undifferentiated H9. The error bars represent the standard error of the mean. \*\*,  $p \leq .05$ . **(E):** Representative flow cytometry histograms for Pmel17 and Oct4 at day 14 (H9-RPE, H9 no factor differentiation), undifferentiated H9 cells, MeWo cells (positive control for Pmel17), and Hs27 cells (negative control for both Pmel17 and Oct4). Abbreviations: Ctrl, control; RPE, retinal pigmented epithelium.

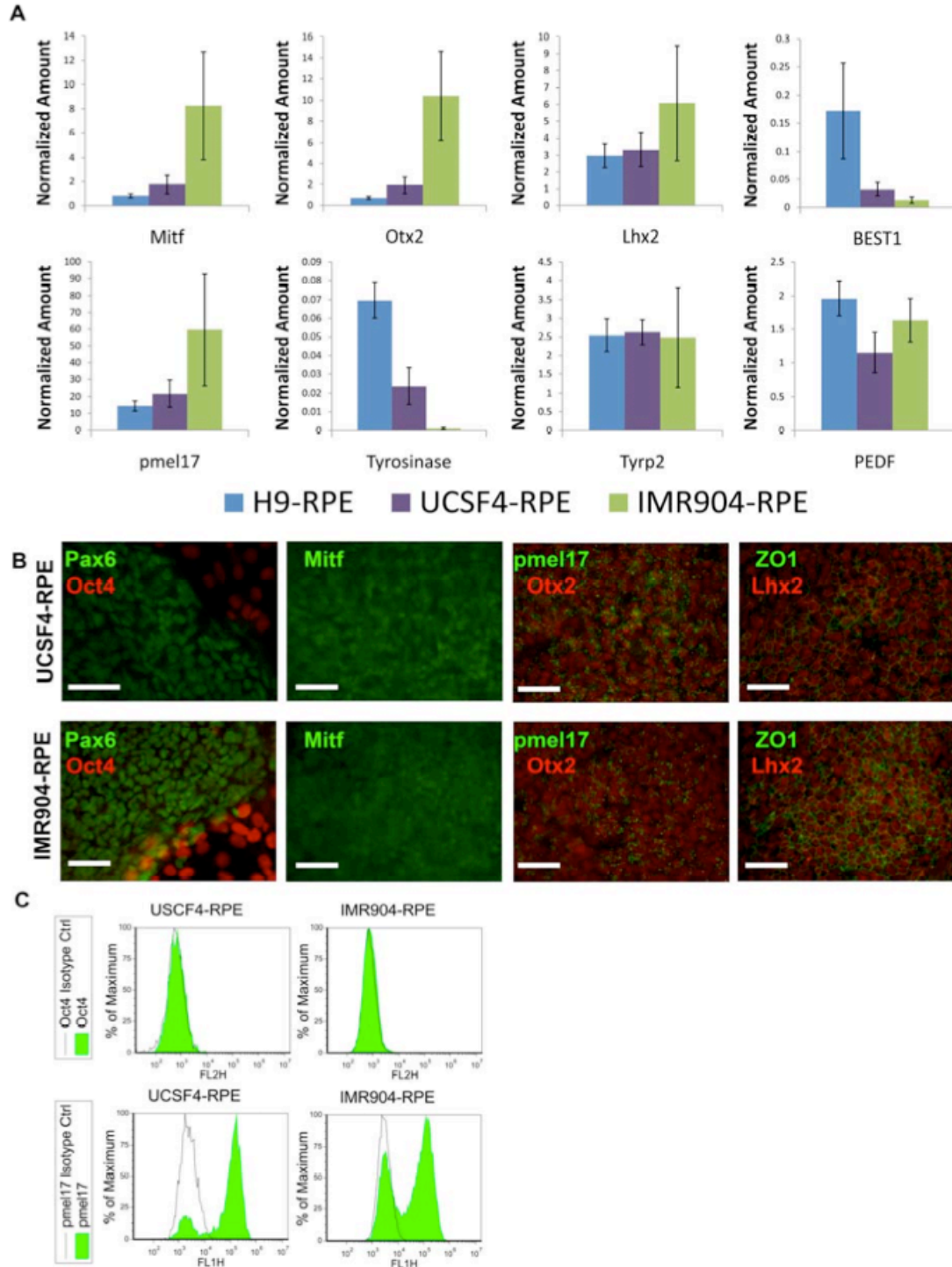


**Figure 12.** Gene expression, protein expression and flow cytometry histograms for cells differentiated from additional pluripotent cells lines on day 14. (A) qPCR analysis of RPE marker genes at day 14. Expression is normalized to expression of a panel of housekeeping genes; error bars represent standard error of the mean. (B) Immunofluorescence images of RPE and pluripotency markers. Scale bars = 50µm. (C) Representative Oct4 and pmel17 flow cytometry histograms.

cells by immunocytochemistry. We also examined the loss of the pluripotency marker Oct4 by flow cytometry. We found that H9 cells could be differentiated into Pmel17<sup>+</sup> cells by day 14 with an average efficiency of 78.5% ( $\pm 1.2\%$ ,  $n = 6$ , H9-RPE) (Fig. 11D). This was highly significant when compared with either undifferentiated H9 cells ( $12.8\% \pm 2.4\%$ ,  $n = 3$ , H9) or cells differentiated in basal medium alone ( $25.2\% \pm 1.6\%$ ,  $n = 3$ , no factor differentiation) (Fig. 11D). We tested the differentiation protocol on two additional pluripotent stem cell lines: the embryonic stem cell line UCSF4 and the induced pluripotent stem cell line IMR904. The UCSF4 line yielded Pmel17<sup>+</sup> cells with an efficiency similar to H9 cells ( $79.8\% \pm 0.88\%$ ,  $n = 3$ , UCSF4-RPE), whereas the IMR904 line was slightly less efficient ( $63\% \pm 0.88\%$ ,  $n = 3$ , IMR904-RPE) (Fig. 11D). The percentage of Oct4<sup>+</sup> cells was less than 5% in all conditions except undifferentiated H9 cells ( $98.1\% \pm 0.6\%$ ,  $n = 3$ , H9) (Fig. 11D).

Examination of representative flow cytometry histograms reveals population expression levels of Pmel17 and Oct4 protein on day 14. We compared H9-RPE cells differentiated in basal media (no factor differentiation), undifferentiated H9 cells, the melanocyte cell line MeWo (a positive control for Pmel17), and the fibroblast line Hs27 (a negative control for both Oct4 and Pmel17). Interestingly, undifferentiated H9 cells appeared to express low levels of Pmel17 (Fig. 11E). This is consistent with findings in our own lab and others that undifferentiated stem cells express low levels of this transcript [11, 23]. A high level of Pmel17 protein expression was only seen in H9-RPE cells and the positive control MeWo cells (melanocytes) (Fig. 11E).

Interestingly, cells left in culture past day 14 with Activin A, SU5402, and VIP led to death of non-RPE cells (supplemental Fig. 6A, 6B). This suggests that the culture conditions are both directive and selective for RPE. Because one of our goals was to determine the earliest time we could generate homogeneous cultures of RPE, we focused on day 14 as the

end point of directed differentiation.

### **Protein and mRNA Time Courses Reveal Stages of RPE Development**

To better understand the nature of our differentiation protocol, we analyzed both protein and mRNA expression of a panel of genes over 14 days of differentiation. As expected, pluripotency gene and protein expression (Oct4 and Nanog) decreased rapidly over the first 4 days (Fig. 13A, 13B). Interestingly, Oct4 and Nanog expression increased slightly between days 4 and 6, during which time Activin A was added to the protocol (Fig. 13B). Early neural and eye field markers (Lhx2, Pax6(-5a), Pax6(-5a), and Rax) were expressed as early as day 2, with expression increasing throughout the 14-day time period with the exception of Rax (Fig. 13A, 13B). Rax expression was transient, increasing from days 2– 6 and then rapidly decreasing between days 6 and 8 (Fig. 13B). At day 6, IGF1 and DKK1 were removed from the protocol, whereas SU5402 and VIP were added, which could account for the decrease in Rax expression. RPE marker genes were expressed slightly later in two phases, between days 4 and 6 (Mitf, PEDF, and BEST1) and between days 6 and 8 (Pmel17, Tyrosinase, and Tyrp2) (Fig. 13A, 13B). Interestingly, Otx2 mRNA and protein were expressed at relatively consistent levels throughout differentiation.

### **Differentiated Cells Can Be Enriched on Day 14 to Homogenous Cultures of Functional RPE**

To generate more homogenous populations of RPE, readily visible sheets on day 14 were mechanically isolated, dissociated into single cells, and replated in an RPE medium [17] on Matrigel-coated tissue culture plastic, chambered slides, or Transwell inserts. Surprisingly, RPE enriched on day 14 were sensitive to single-cell dissociation in the media tested, leading to cell death or senescence (supplemental Fig. 6D). Because the Rho-associated protein kinase (ROCK) inhibitor Y27632 has been previously shown to support single-cell dissociation of epithelial cells [24 –26], including pluripotent stem cells [27], we



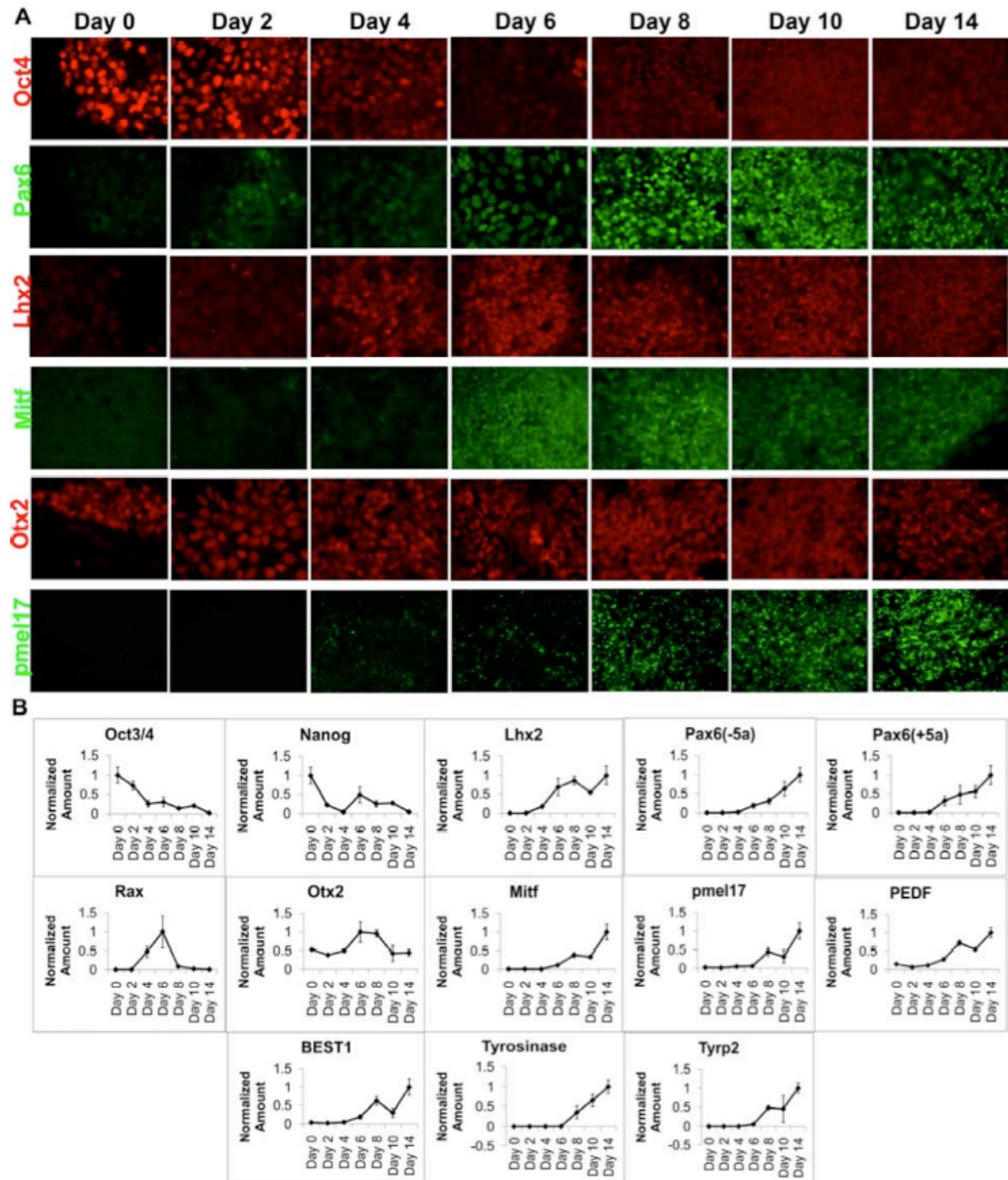


**Figure 13.** Differentiating cells rapidly acquire early eye field and retinal pigmented epithelium (RPE) marker expression. **(A):** Immunofluorescence images of pluripotency (Oct4), early eye field (Pax6, Lhx2, and Otx2), and RPE (Pax6, Lhx2, Mitf, Otx2, and Pmel17) proteins during days 0 –14 of differentiation. Scale bars = 100  $\mu$ m. **(B):** Quantitative polymerase chain reaction analysis of pluripotency (Oct4 and Nanog), early eye field (Lhx2, Pax6(-5a), Pax6(+5a), Rax, and Otx2), and RPE (Lhx2, Pax6(-5a), Pax6(+5a), Otx2, Mitf, Pmel17, PEDF, BEST1, Tyrosinase, and Tyrp2) gene expression. Expression is normalized to the maximum level of expression over the time period. The error bars represent the standard error of the mean.

tested the ability of this small molecule to rescue dissociated RPE. The addition of Y27632 at 10  $\mu$ M for the first 3 days after passage facilitated RPE survival and maturation (Fig. 14; supplemental Fig. 6D).

After enriching RPE at day 14, we allowed the cells to redifferentiate for 30 days and then analyzed gene and protein expression and phagocytosis of rod outer segments. To analyze gene expression, hESC-RPE, cultured fetal human RPE (fRPE), and Hs27 fibroblasts were cultured on Transwell inserts for 30 days. qPCR analysis showed similar levels of expression of all RPE marker genes between hESC-RPE and fRPE (Fig. 14A). We used Hs27 cells as a negative control for RPE-specific genes; however, we detected some *Mitf*, *PEDF*, and *BEST1* expression in Hs27. Compared with undifferentiated H9 cells, expression of *Oct4* was ~1,000-fold lower in all other cell lines (Fig. 14A).

Immunocytochemistry of cells enriched at day 14 and grown on chambered slides for 30 days showed homogenous populations of RPE based on *Mitf*, *Otx2*, *Lhx2*, *ZO1*, and *Pmel17* expression (Fig. 14B). Expression of *BEST1* and *RPE65*, markers of more mature RPE, was heterogeneous, indicating varying levels of maturity in these cultures (Fig. 14B). Integrin  $\alpha$ v was localized apically compared with *Otx2* nuclear expression, showing proper polarized protein trafficking in these cells (Fig. 14B, inset in Integrin  $\alpha$ v/*Otx2* panel). Although some *Oct4*<sup>+</sup> cells were present at day 14 of initial differentiation, no *Oct4*<sup>+</sup> cells were observed following enrichment and 30 days of culture (Fig. 14B).

To determine whether our hESC-RPE were functional, we tested their ability to carry out phagocytosis of fluorescently labeled ROSs. Compared with the negative control Hs27 cells, hESC-RPE internalized significantly more ROSs (Fig. 14C). This internalization was blocked by an antibody against integrin  $\alpha$ v $\beta$ 5, showing that both hESC-RPE and fRPE use the same receptor for ROS phagocytosis. hESC-RPE ROS phagocytosis was even greater

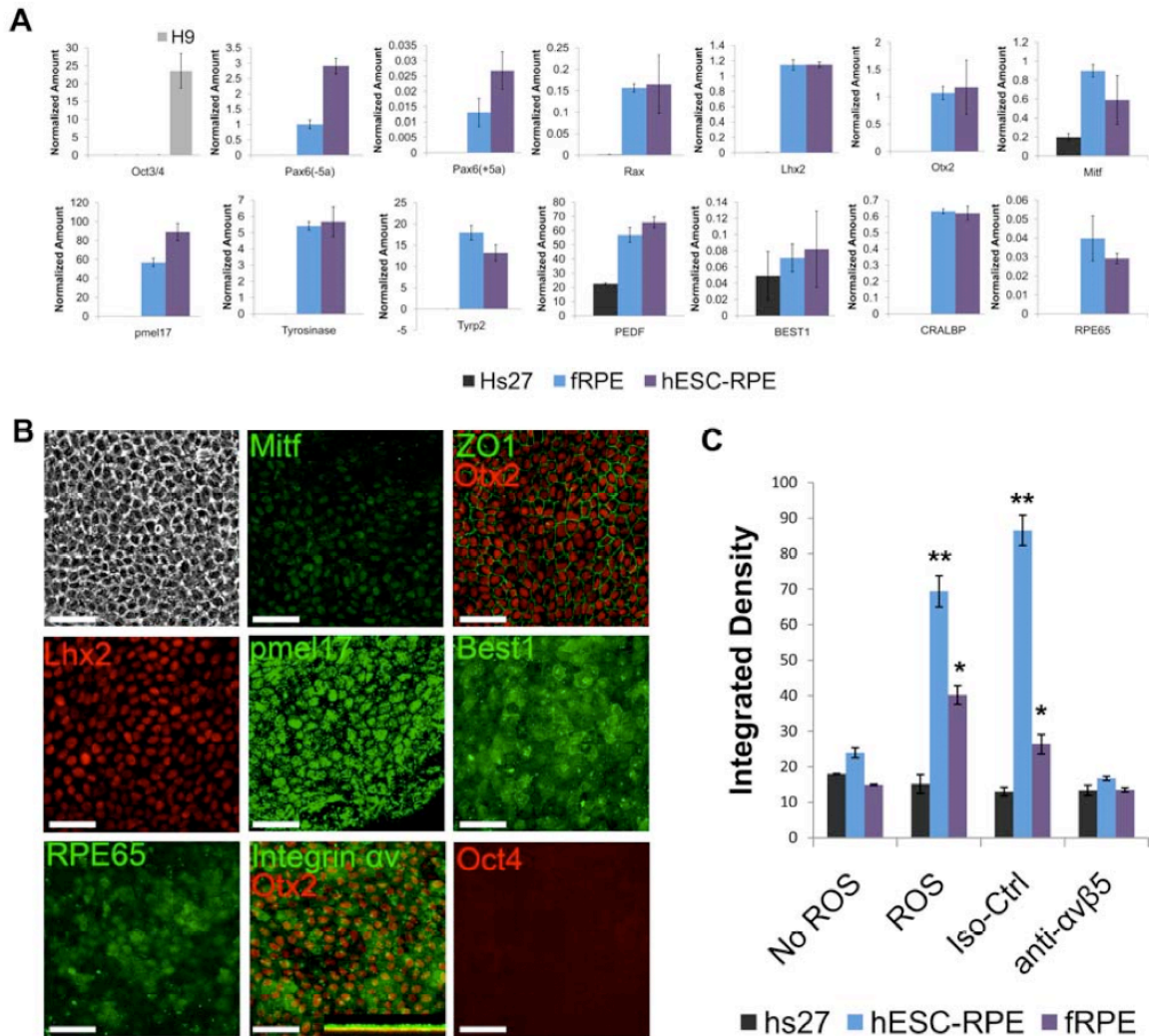


**Figure 14.** Analysis of RPE enriched on day 14 and grown for 30 days in culture. **(A):** Quantitative polymerase chain reaction analysis comparing gene expression levels in hESC-RPE to cultured fetal human RPE as a positive control and Hs27 cells as a negative control. Undifferentiated H9 cells are included as a positive control for Oct4 expression in the first panel. Expression is normalized to a panel of housekeeping genes. The error bars represent the standard error of the mean. **(B):** Bright field and immunofluorescent labeling of RPE and pluripotency markers. The inset in the Integrin  $\alpha$ v/Otx2 panel shows the confocal z-stack cross-section. Scale bars = 50  $\mu$ m. **(C):** Internalization of fluorescently labeled ROSs quantified by integrated pixel density analysis of fluorescent images. The error bars represent the standard error of the mean. \*,  $p \leq .05$ ; \*\*,  $p \leq .01$  versus respective Hs27 control and corresponding anti- $\alpha$ v $\beta$ 5 condition. Abbreviations: anti- $\alpha$ v $\beta$ 5, function blocking integrin  $\alpha$ v $\beta$ 5 antibody; fRPE, fetal human retinal pigmented epithelium; hESC, human embryonic stem cell; Iso-Ctrl, isotype control antibody; RPE, retinal pigmented epithelium; ROS, rod outer segment.



than that of fRPE, although both RPE lines internalized significantly more ROSs than Hs27 cells.

## **Discussion**

The challenge of efficiently directing pluripotent stem cells into a specific lineage has progressed rapidly since the derivation of human embryonic stem cells 15 years ago [28, 29]. Development of efficient protocols to generate RPE, which are the second hESC derivative used in clinical trials, has been progressing since initial reports of spontaneous differentiation 8 years ago [10, 13, 14, 30]. Here we report a protocol that is both fast and efficient. By drawing upon knowledge from developmental biology and other stem cell studies, we have optimized timing of factor addition to generate RPE within 14 days.

Nicotinamide has previously been used to differentiate pluripotent stem cells into RPE [13]. It was shown that nicotinamide had an antiapoptotic effect following 2 weeks of differentiation, in line with other studies showing neural protection by nicotinamide. Based on previous research, it was suggested that this action could be through inhibition of poly(ADP-ribose) polymerase-1 (PARP1), which was found to regulate cell death upon hESC neural induction [21]. In our experiments, the addition of nicotinamide to retinal inducing factors IGF1, DKK1, Noggin, and bFGF [15] decreased expression of pluripotency genes while concomitantly increasing neural/early eye field genes by day 4. Because it is known that the IGF1, DKK1, Noggin, and bFGF protocol induces expression of Lhx2, Rax, and Pax6 [15], these gene expression changes suggest that the addition of nicotinamide speeds up differentiation. Interestingly, not all neural/early eye field genes were affected by nicotinamide. Although Lhx2 and Rax expression increased with nicotinamide addition on day 4, Pax6 expression was slightly lower, although this change was not significant. This suggests that nicotinamide may not have an effect on Pax6 and may act on a factor

downstream. Further studies are needed to elucidate the effect of nicotinamide-expedited differentiation on the entire early eye field transcription factor network (Pax6, Lhx2, Rax, Six3, Six6, and Tll [31]). We also saw fewer cells in nicotinamide conditions, which could result from either cell death or a decrease in proliferation. A decrease in proliferation has previously been reported upon exposure of hESCs to nicotinamide [32]. Although these results suggest a role for nicotinamide outside of cell survival, we wondered whether PARP1 inhibition was still involved. To test the role of PARP1 inhibition in our nicotinamide induced differentiation, we tested the ability of another PARP1 inhibitor, 3-aminobenzamide, to induce differentiation. We found that 3-aminobenzamide could partially recapitulate the effects seen with nicotinamide. Although the exact mechanism of nicotinamide-induced neuronal differentiation remains to be elucidated, it is clear that nicotinamide can potentiate differentiation, and this potentiation appears to act at least partially through PARP inhibition. Neuroprotective/antiapoptotic effects of PARP inhibition may also play a role. We find that nicotinamide is a useful tool to speed up initial neural differentiation and could potentially be applied to other neural differentiation protocols.

The addition of Activin A and the FGFR1 inhibitor SU5402 led to only slight increases in RPE genes, whereas the early eye field/ neural retina marker Rax was significantly downregulated by day 10. We attribute the former to the potent retinal inducing properties of IGF1 [15, 33], whereas the latter confirms the roles of Activin A and FGF signaling in the optic vesicle to optic cup stages of eye development. This is seen in both animal and hESC models where Activin signaling and FGF inhibition direct the progenitor cells toward RPE (Rax<sup>-</sup>) instead of neural retina (Rax<sup>+</sup>) [13,16,30]. The addition of VIP significantly increases expression of Mitf, Tyrosinase, and PEDF, in agreement with results found in primary cultures of RPE [22]. Although we continued to use VIP for these experiments and indeed

saw an increase in pigmentation at earlier time points, the use of VIP at 1  $\mu$ M can be quite expensive. For practical purposes, VIP can be left out of the protocol.

By day 14 of differentiation, sheets of RPE can clearly be seen with defined borders that express several RPE marker genes and proteins. By this time cells have begun to pigment. Interestingly, the speed of pigmentation appears to be inversely correlated with the efficiency of RPE differentiation or size of the RPE sheet (data not shown). Small sheets (<500  $\mu$ m) tended to pigment faster than large sheets (>5 mm). This suggests that signals coming from non-RPE cells may have a positive effect on pigmentation. Future studies will be necessary to determine what those signals may be.

Generation of RPE from both H9 and UCSF4 embryonic stem cell lines was highly efficient, averaging close to 80% based on Pmel17 immunoreactivity. This method induced efficient differentiation of RPE in the UCSF4 cell line, which is resistant to RPE differentiation using the spontaneous method (data not shown). The efficiency of RPE generation from IMR904 induced pluripotent stem (iPS) cells was somewhat less efficient at 60%. The cause of this difference in efficiency is unclear, although it could be due to incomplete silencing of the reprogramming transgenes. It will be interesting to see whether the efficiency is consistently lower in iPS cells compared with embryonic stem cells, although we do not suspect this to be the case.

Cells that did not express Pmel17 on day 14 of differentiation expressed Oct4 and Lhx2. When isolated on day 14 and placed back in embryonic stem cell conditions, these cells did not form colonies that resembled embryonic stem cell morphology, and many appeared to differentiate into neurons. We suspect that these cells may be stuck in a partially differentiated state. If differentiating cultures were kept longer than 14 days, these non-RPE cells began to die. We therefore consider the Activin A-, SU5402-, and VIP-supplemented

medium to both direct differentiation and select for RPE over non-RPE cells, leading to virtually homogenous populations of RPE after 3 weeks.

Analysis of gene and protein expression throughout the 14-day differentiation period revealed several interesting trends. First, as expected, early neural and eye field genes were expressed first, followed by later markers of the optic vesicle and RPE [16]. Interestingly, although gene expression followed the known developmental sequence, transition from early eye field to optic vesicle and RPE was quite rapid. This suggests that during normal development, the ability of a cell to respond to developmental cues can precede those signals by a significant amount of time, perhaps to allow time for tissue growth. Between days 4 and 6, a slight increase in Oct4 and Nanog gene expression was observed. We believe this is likely because of the addition of Activin A on day 4 because Activin A signaling has been shown to maintain pluripotency [34–36]. Consistent with recent observations in Rax-GFP pluripotent stem cells undergoing ocular morphogenesis [37, 38], we saw transient expression of Rax between days 2 and 8. This would appear to correspond with expression in the early eye field followed by down-regulation in the RPE. Interestingly, Otx2, which has been shown to be repressed by Rax specifically in the early eye field of *Xenopus* [31], maintained a fairly consistent level of both mRNA and protein expression over the 14-day time course. In fact, Otx2 mRNA expression increased when Rax mRNA expression was at its highest. These observations, along with results from other hESC retinal differentiation protocols [30], suggest that Otx2 is expressed in the early eye field of humans. Alternatively, there are two known protein isoforms of Otx2 in humans and several different transcripts, which may be alternatively regulated. Our experiments do not differentiate between these isoforms. There is also the possibility that maintained Otx2 expression throughout ocular differentiation may be an artifact of cell culture and may not be found *in vivo*.

Because morphologically distinct sheets of RPE became visible between days 10 and 14, we tried to isolate cells at these early time points. Initial attempts were unsuccessful; however, with the addition of the ROCK inhibitor Y27632 over the first few days of culture, RPE could be enriched at both of these time points and would mature into functional RPE when replated. The borders of RPE sheets at day 10 were harder to distinguish, which made enrichment to homogenous populations difficult; therefore we focused on enrichment at day 14. Tight junctions among non-RPE cells made them easy to remove as sheets by dragging a pipette tip along borders with RPE.

ROCK inhibition has been used successfully to maintain survival of hESCs dissociated into single cells as well as to enhance proliferation of certain epithelial cell types [24 –27]. The mechanism of ROCK inhibition has been worked out in hESCs, where ROCK mediates E-cadherin cell adhesion sensing [39]. The mechanism of ROCK inhibition in proliferation of other epithelial cell types, including in our own system, remains to be elucidated. Primary RPE cultures, when dissociated into single cells over several passages, lose their ability to redifferentiate into mature RPE and become fibroblastic in morphology. This may be a wound response for an epithelium that does not normally exist as single cells and may be similar to the effect we see following single-cell dissociation on day 14 of differentiation. Additionally, our selection of basal medium may not be optimal for proliferating cultures of RPE enriched at day 14. We are currently testing novel medium compositions, some of which support single-cell growth even in the absence of ROCK inhibitor. Although the mechanism is not known, enrichment of RPE cells on day 14 in the presence of ROCK inhibitor can generate homogenous populations that express RPE marker genes at similar levels to cultured fetal human RPE, express proper RPE proteins, are polarized, and display integrin  $\alpha\beta5$ -dependent phagocytosis of rod outer segments.

## Conclusion

This protocol should be useful for studying human ocular differentiation within a shorter time period than *in vivo* development. Signals that specify melanogenesis in RPE are still under investigation. Our observation that cultures with more non-RPE cells led to faster RPE pigmentation suggests that these cells may secrete factors that activate melanogenesis. Analysis of the proteome of these non-RPE cells may lead to identification of melanogenic factors. This protocol will also be useful for rapidly generating banks of RPE for the treatment of age-related macular degeneration and other disorders of the RPE.

## Acknowledgements

We thank Sherry Hikita and Monte Radeke for their guidance and the University of California, Santa Barbara, Center for Stem Cell Biology and Engineering staff for support. This work was supported by Grants CL1-00521, DR1-01444, FA1-006161, and TG2-01151 from the California Institute for Regenerative Medicine (CIRM). B.O.P. was supported by a CIRM scholarship, and P.J.C. was supported by a CIRM Leadership Award. Further support was provided by the Institute for Collaborative Biotechnologies through Grant W911NF-09-0001 from the U.S. Army Research Office. The content of the information does not necessarily reflect the position or the policy of the government, and no official endorsement should be inferred.

## References

- 1 Khandhadia S, Cherry J, Lotery AJ. Age-related macular degeneration. *Adv Exp Med Biol* 2012;724:15–36.
- 2 Anderson DH, Radeke MJ, Gallo NB et al. The pivotal role of the complement system in aging and age-related macular degeneration: Hypothesis re-visited. *Prog Retin Eye Res* 2010;29:95–112.
- 3 Cruess AF, Berger A, Colleaux K et al. Canadian expert consensus: Optimal treatment of neovascular age-related macular degeneration. *Can J Ophthalmol* 2012;47:227–235.
- 4 Rowland TJ, Buchholz DE, Clegg DO. Pluripotent human stem cells for the treatment of retinal disease. *J Cell Physiol* 2012;227:457–466.
- 5 Chen FK, Uppal GS, MacLaren RE et al. Long-term visual and microperimetry outcomes following autologous retinal pigment epithelium choroid graft for neovascular age-related macular degeneration. *Clin Experiment Ophthalmol* 2009;37:275–285.
- 6 Chen FK, Patel PJ, Uppal GS et al. A comparison of macular translocation with patch graft in neovascular age-related macular degeneration. *Invest Ophthalmol Vis Sci* 2009;50:1848–1855.
- 7 Chen FK, Patel PJ, Uppal GS et al. Long-term outcomes following full macular translocation surgery in neovascular age-related macular degeneration. *Br J Ophthalmol* 2010;94:1337–1343.
- 8 Schwartz SD, Hubschman JP, Heilwell G et al. Embryonic stem cell trials for macular degeneration: A preliminary report. *Lancet* 2012; 379:713–720.
- 9 Hu Y, Liu L, Lu B et al. A novel approach for subretinal implantation of ultrathin substrates containing stem cell-derived retinal pigment epithelium monolayer. *Ophthalmic Res* 2012; 48:186–191.
- 10 Klimanskaya I, Hipp J, Rezai KA et al. Derivation and comparative assessment of retinal pigment epithelium from human embryonic stem cells using transcriptomics. *Cloning Stem Cells* 2004;6:217–245.
- 11 Buchholz DE, Hikita ST, Rowland TJ et al. Derivation of functional retinal pigmented epithelium from induced pluripotent stem cells. *STEM CELLS* 2009;27:2427–2434.
- 12 Carr AJ, Vugler AA, Hikita ST et al. Protective effects of human iPS-derived retinal pigment epithelium cell

- transplantation in the retinal dystrophic rat. PLoS One 2009;4:e8152.
- 13 Idelson M, Alper R, Obolensky A et al. Directed differentiation of human embryonic stem cells into functional retinal pigment epithelial cells. Cell Stem Cell 2009;5:396 – 408.
  - 14 Zahabi A, Shahbazi E, Ahmadi H et al. A new efficient protocol for directed differentiation of retinal pigmented epithelial cells from normal and retinal disease induced pluripotent stem cells. Stem Cells Dev 2012;21:2262–2272.
  - 15 Lamba DA, Karl MO, Ware CB et al. Efficient generation of retinal progenitor cells from human embryonic stem cells. Proc Natl Acad Sci USA 2006;103:12769 –12774.
  - 16 Martínez-Morales JR, Rodrigo I, Bovolenta P. Eye development: A view from the retinal pigmented epithelium. Bioessays 2004;26:766 – 777.
  - 17 Ahmado A, Carr AJ, Vugler AA et al. Induction of differentiation by pyruvate and DMEM in the human retinal pigment epithelial cell line ARPE-19. Invest Ophthalmol Vis Sci 2011;52:7148 –7159.
  - 18 Woo TH, Patel BK, Cinco M et al. Identification of *Leptospira biflexa* by real-time homogeneous detection of rapid cycle PCR product. J Microbiol Methods 1999;35:23–30.
  - 19 Radeke MJ, Peterson KE, Johnson LV et al. Disease susceptibility of the human macula: Differential gene transcription in the retinal pigmented epithelium/choroid. Exp Eye Res 2007;85:366 –380.
  - 20 Lin H, Clegg DO. Integrin  $\alpha$ v $\beta$ 5 participates in the binding of photoreceptor rod outer segments during phagocytosis by cultured human retinal pigment epithelium. Invest Ophthalmol Vis Sci 1998;39:1703–1712.
  - 21 Cimadamore F, Curchoe CL, Alderson N et al. Nicotinamide rescues human embryonic stem cell-derived neuroectoderm from parthanatic cell death. STEM CELLS 2009;27:1772–1781.
  - 22 Koh SM. VIP enhances the differentiation of retinal pigment epithelium in culture: From cAMP and pp60(c-src) to melanogenesis and development of fluid transport capacity. Prog Retin Eye Res 2000;19:669 – 688.
  - 23 Sperger JM, Chen X, Draper JS et al. Gene expression patterns in human embryonic stem cells and human pluripotent germ cell tumors. Proc Natl Acad Sci USA 2003;100:13350 –13355.
  - 24 Chapman S, Liu X, Meyers C et al. Human keratinocytes are efficiently immortalized by a Rho kinase inhibitor. J Clin Invest 2010;120: 2619 –2626.
  - 25 Liu X, Ory V, Chapman S et al. ROCK inhibitor and feeder cells induce the conditional reprogramming of epithelial cells. Am J Pathol 2012;180:599 – 607.
  - 26 Okumura N, Koizumi N, Ueno M et al. ROCK inhibitor converts corneal endothelial cells into a phenotype capable of regenerating in vivo endothelial tissue. Am J Pathol 2012; 181:268 –277.
  - 27 Watanabe K, Ueno M, Kamiya D et al. A ROCK inhibitor permits survival of dissociated human embryonic stem cells. Nat Biotechnol 2007;25:681– 686.
  - 28 Ben-David U, Kopper O, Benvenisty N. Expanding the boundaries of embryonic stem cells. Cell Stem Cell 2012;10:666 – 677.
  - 29 Thomson JA, Itskovitz-Eldor J, Shapiro SS et al. Embryonic stem cell lines derived from human blastocysts. Science 1998;282:1145–1147.
  - 30 Meyer JS, Shearer RL, Capowski EE et al. Modeling early retinal development with human embryonic and induced pluripotent stem cells. Proc Natl Acad Sci USA 2009;106:16698 –16703.
  - 31 Zuber ME, Gestri G, Viczian AS et al. Specification of the vertebrate eye by a network of eye field transcription factors. Development 2003;130:5155–5167.
  - 32 Vaca P, Berna G, Araujo R et al. Nicotinamide induces differentiation of embryonic stem cells into insulin-secreting cells. Exp Cell Res 2008;314:969 –974.
  - 33 Pera EM, Wessely O, Li SY et al. Neural and head induction by insulin-like growth factor signals. Dev Cell 2001;1:655– 665.
  - 34 Beattie GM, Lopez AD, Bucay N et al. Activin A maintains pluripotency of human embryonic stem cells in the absence of feeder layers. STEM CELLS 2005;23:489 – 495.
  - 35 Xiao L, Yuan X, Sharkis SJ. Activin A maintains self-renewal and regulates fibroblast growth factor, Wnt, and bone morphogenic protein pathways in human embryonic stem cells. STEM CELLS 2006;24:1476 –1486.
  - 36 Vallier L, Alexander M, Pedersen RA. Activin/nodal and FGF pathways cooperate to maintain pluripotency of human embryonic stem cells. J Cell Sci 2005;118:4495– 4509.
  - 37 Eiraku M, Takata N, Ishibashi H et al. Self-organizing optic-cup morphogenesis in three-dimensional culture. Nature 2011;472:51–56.
  - 38 Nakano T, Ando S, Takata N et al. Self-formation of optic cups and storable stratified neural retina from human ESCs. Cell Stem Cell 2012;10:771–785.
  - 39 Ohgushi M, Sasai Y. Lonely death dance of human pluripotent stem cells: ROCKing between metastable cell states. Trends Cell Biol 2011;21:274 –282.

## ***B. Xeno-Free Adaptation of Rapid and Efficient Directed Differentiation***

**Britney O. Pennington**

### **Abstract**

Age-related macular degeneration (AMD) is the leading cause of blindness in people over 65 years of age, and it is caused by the dysfunction of the retinal pigmented epithelium (RPE). Transplantable therapies consisting of human embryonic stem cell derived-RPE (hESC-RPE) are currently under development. However, production of hESC-RPE can be very time intensive, therefore several directed differentiation protocols have been established. The most rapid protocol to date generates hESC-RPE in 14 days (D14 protocol) but utilizes animal derivatives throughout the process. In order to generate hESC-RPE for cellular therapies, defined reagents compliant with good manufacturing practices (GMP) must be used. This chapter describes the preliminary work to qualify xeno-free substitutes for the components of the D14 protocol. These data demonstrate that Matrigel<sup>®</sup> can be replaced with the synthetic substrate Synthemax<sup>®</sup>II-SC and that the defined small molecule DMH1, a specific BMP inhibitor, can replace recombinant mouse Noggin during the D14 protocol. This chapter also presents results of a pilot study employing dual-Smad inhibition with DMH1 and SB431542 that effectively replaces the recombinant growth factors msNoggin, Dkk-1, IGF-1 and bFGF to generate a cell population expressing PMEL17, a pigmented cell marker, in 14 days. Further research is needed to confirm the RPE identity of these cells and to identify defined alternatives to the remaining two growth factors in the D14 protocol. A rapid and efficient xeno-free protocol for generating hESC-RPE would contribute a tremendous advantage to the cost-effective production of cellular therapies for AMD.



## Introduction

Age-related macular degeneration (AMD) is a debilitating blinding disease affecting the elderly and is caused by the dysfunction and death of the retinal pigmented epithelium (RPE). Although therapies utilizing human embryonic stem cell-derived RPE (hESC-RPE) are under development, the production of the therapeutic cells can be exceedingly time intensive. Spontaneous differentiation of hESCs into RPE requires several months and the efficiency can vary greatly. Therefore, many directed differentiation protocols that accelerate the rate of differentiation and increase final yield of RPE have been explored [1-4]. We have recently developed the most rapid protocol to date, one that promotes RPE cell differentiation from stem cells in just 14 days. Up to 80% of these cells expressing PMEL17, a protein necessary for the deposition of melanin granules in the melanosomes of pigmented cells [5, 6]. However, this “D14” protocol utilizes animal-derived products and recombinant proteins. These components represent a challenge to develop these cells as therapies due to the risk of exposure to non-human immunogens, which may affect patients post-transplantation. In order to convert the D14 protocol into a xeno-free procedure, synthetic, animal-derived component-free (ACF) replacements must be found for each constituent.

The D14 protocol utilizes Matrigel<sup>®</sup>, a substrate rich in extracellular matrix proteins derived from the Engelbreth-Holm-Swarm murine sarcoma [7]. Synthemax<sup>®</sup>II-SC Substrate, is a novel, ACF peptide-copolymer that we have demonstrated to support hESC differentiation into functional RPE (Pennington et al. *submitted*). hESC-RPE differentiated on Synthemax<sup>®</sup>II-SC were similar to those on Matrigel<sup>®</sup> in gene expression and function. This suggests that Synthemax<sup>®</sup>II-SC may also be a viable alternative to Matrigel<sup>®</sup> for directed differentiation under xeno-free conditions.

The original D14 protocol employs recombinant mouse Noggin (msNoggin), as well as other recombinant human proteins. Full-length recombinant proteins are prone to batch-to-batch variation and can raise production costs [8, 9], which may hinder large-scale production of therapeutic hESC-RPE. Therefore, synthetic small molecule replacements for the original D14 growth factors must be investigated. The original D14 protocol emulates two distinct differentiation steps: the first establishes neural induction and the second establishes RPE identity. A primary aim was to identify a small molecule alternative as a replacement for msNoggin in the neural induction step.

Noggin protein is a secreted homodimer [10] that has a high binding affinity for BMP2 and BMP4 and can inhibit the bone morphogenetic protein (BMP) branch of the TGF $\beta$  superfamily signaling pathway, which consists of BMPs, growth/differentiation factors (GDF) and anti-Müllerian hormones (AMH) [11]. Soluble BMP dimers associate with Type I receptor dimers via hydrophobic interactions [12]. The ligand-receptor complex recruits Type II receptor dimers which become constitutively active and phosphorylate the Type I receptor [13]. Both receptor types are serine/threonine kinases; upon activation, the Type I receptor phosphorylates a receptor-regulated Smad, which promotes Smad association with co-Smad4. The Smad heterocomplex translocates into the nucleus to regulate the expression of genes that modulate growth and differentiation [12-14]. Noggin binds and prevents BMP4 from associating with its receptor, and this inhibition is necessary for neural induction [11].

Synthetic small molecule alternatives to noggin could antagonize any component in the pathway. BMP4 associates with Type I activin receptor-like kinase (ALK)-3 to phosphorylate downstream Smads1/5/8 [15]. Small molecule antagonists to BMP-specific ALKs have been developed. The first small molecule inhibitor was identified through a

phenotypic screen of small molecules that promoted dorsalization in zebrafish embryos. Compound C, a known inhibitor of AMPK, was renamed Dorsomorphin as it stimulated dorsalization during zebrafish development by inhibiting ALK2, ALK3 and ALK6 [16]. Its derivative, LDN-193189 has increased effectiveness in inhibiting the BMP receptors [14]. However, these two small compounds also have high inhibitory activity against many off-target proteins such as VEGF, AMPK and FGF-R than the desired ALKs [13]. To improve specificity, a structure-activity relationship study in zebrafish using analogues of dorsomorphin was used to identify the small molecule DMH1, which is a highly specific inhibitor of ALK2 and ALK3 and can effectively inhibit the phosphorylation of Smads1/5/8 ( $IC_{50} < 0.2\mu M$ ) [17]. Therefore, DMH1 is a viable, xeno-free candidate to replace msNoggin during the D14 directed differentiation.

The BMP/GDF/AMH subfamily is not the only branch of the TGF $\beta$  pathway that can suppress neural differentiation however. The Nodal/Activin/TGF $\beta$  subfamily has also been implicated in impeding development of the neuroectoderm while promoting the mesoderm and endoderm lineages [18]. For example, Nodal knockout mice have enhanced neuralization [19] and Activin-A promotes hESCs to differentiate into definitive endoderm [20]. Furthermore, Nodal and Activin-A can also sustain the pluripotent state of hESCs [21, 22]. Therefore, in order to encourage hESC differentiation towards an anterior neuroectoderm lineage, signaling by the Nodal/Activin/TGF $\beta$  subfamily should also be targeted. This branch of soluble ligands first binds to Type II receptors which recruit the Type I receptors (ALK4, ALK5, and ALK7) to mediate intracellular signaling by Smad2/3 phosphorylation [12, 13]. SB431542 is a small molecule that competitively binds to the ATP-binding site on ALK4/5/7 and acts as a highly specific inhibitor with an  $IC_{50} < 0.2\mu M$

for each receptor [23]. In the presence of other compounds, SB431542 can augment the neural differentiation of hESCs but is insufficient to do so alone [24].

A more effective approach to promote neural induction is to simultaneously antagonize both the Nodal/Activin/TGF $\beta$  and the BMP/GDF/AMH branches of the TGF $\beta$  superfamily, known as dual-Smad inhibition and was first explored in 2009 [24]. Accomplishing dual-Smad inhibition with Noggin and SB431542 directs hESCs and iPSCs to differentiate into neural precursor populations with rosette morphologies that are positive for Pax6, an early neural marker essential for ocular development, and these cells can further be directed into dopaminergic neurons and motoneurons [24, 25]. Performing dual-Smad inhibition with LDN-193189 and SB431542 has been shown to promote differentiation of human pluripotent stem cells into nociceptors of the peripheral nervous system [26], but LDN-193189 has also been shown to have numerous off-target effects [13]. Combining the BMP-specific inhibitor DMH1 and SB431542 during differentiation of hiPSCs recapitulated the decrease in Oct4 and Nanog expression and an increase in Pax6 transcripts observed in cells exposed to Noggin and SB431542. Furthermore, the neural precursors produced solely by the two small molecules were competent to further differentiate into dopaminergic neurons [27]. This study by Neely et al. demonstrated that dual-Smad inhibition by DMH1 and SB431542 is sufficient to induce a neural population during differentiation of pluripotent stem cells. This indicates that DMH1 and SB431542 may be viable alternatives to recombinant growth factors during the neural induction step of the D14 directed differentiation protocol.

The ultimate goal of these studies is to replace all of the original D14 growth factors with small molecules. This chapter describes the initial steps taken to optimize a xeno-free D14 protocol and presents data showing that Synthemax<sup>®</sup> II-SC can replace Matrigel<sup>®</sup> and

that the xeno-free small molecules DMH1 and SB431542 can replace msNoggin, Dkk1, IGF1, and bFGF to accomplish neural induction in the D14 protocol to yield cells positive for PMEL17 in two weeks.

## **Materials and Methods**

### *hESC culture*

H9 hESCs at passages 62-64 (on Synthemax<sup>®</sup>II-SC for 25-27 passages) were grown on Synthemax<sup>®</sup>II-SC coated vessels (5  $\mu\text{g}/\text{cm}^2$ ) (Corning #3536-XX1) in mTeSR<sup>™</sup>1 stem cell medium (STEMCELL Technologies, #05850) and passaged by manual dissection for hESC maintenance.

### *Synthemax<sup>®</sup>II-SC Substrate Vessel Coating*

Tissue culture vessels were coated with Synthemax<sup>®</sup>II-SC according to the manufacturer's recommendations for routine hESC culture. Briefly, Synthemax<sup>®</sup>II-SC powder was resuspended to 1 mg/mL in HyClone HyPure Cell Culture Grade Water (AWK21536) and stored at 4°C for 1 month or further diluted 1:40 (0.025 mg/mL). Tissue culture vessels for hESC culture were coated at a density of 5  $\mu\text{g}/\text{cm}^2$ , and 12 well tissue culture plates for differentiation were coated at a density of 2.6  $\mu\text{g}/\text{cm}^2$  for 2 hours at room temperature. Synthemax<sup>®</sup>II-SC solution was aspirated and the air-dried vessels were used immediately or stored at 4°C for up to 3 months.

### *Directed Differentiation*

Differentiation of hESCs into RPE was accomplished with modifications to the original D14 protocol previously described [28]. Briefly, hESCs were rinsed 3 times and passaged by EDTA dissociation with Versene Solution (Life Technologies, #15040-066) for 8 minutes at room temperature. Colonies were resuspended in retinal differentiation medium,

RDM (DMEM/F12+GlutaMAX™, #10565-018; N-2 Supplement, #17502-048; B-27 Supplement, #17504-044; NEAA, #11140-050; all reagents from Life Technologies) supplemented with 10ng/mL recombinant mouse noggin (#1967-NG), 10 ng/mL recombinant human IGF-1 (291-G1-200), 10 ng/mL recombinant human Dkk-1 (#5439-DK) and 10 mM nicotinamide and were seeded on tissue culture plates coated with 2.6 µg/cm<sup>2</sup> of Synthemax® II-SC. This “control” condition was further modified by replacing noggin with 0.5 µM DMH-1 (Tocris 4126) or by replacing all growth factors with DMH-1 and 10 µM SB431542 (Tocris 1614). For the control condition, 5ng/mL of bFGF was added on Day 2. For all conditions on Day 4, nicotinamide was removed from the media and 100ng/mL Activin-A (PeproTech #120-14E) was added. On Day 6, all RDM media was only supplemented with Activin-A, 1 µM VIP (Sigma V6130), and 10 µM SU5402 (EMD Millipore 572630-500UG) until Day 14.

### *Flow Cytometry*

On Day 14, wells were washed with warm DPBS, dissociated with TrypLE Select for 7 minutes at 37°C and diluted 1:5 in fresh RDM. Cells were pelleted at 1000 rpm for 3 minutes, rinsed in 0.5% BSA Fraction V (Gibco #15260-037) in PBS, and pellets were fixed in 4.0% paraformaldehyde (Electron Microscopy Sciences #15710) for 10 minutes at room temperature in the dark. Cells were pelleted at 2300 rpm for 3 minutes and permeabilized with 0.2% Triton-X (Roche 11332481001), 0.1% BSA Fraction V in PBS for 3 minutes at room temperature. Fixed cells were stored at 4°C in 0.5% BSA until staining.

Cells were stained with primary antibodies diluted with 3% BSA in PBS for 40 minutes at room temperature (HMB45 (PMEL17), 0.1 µg/ml Dako M0634; Mouse IgG1 isotype control, Dako X0931). Samples were stained with a secondary antibody for 30 minutes at room temperature (AlexaFluor® 488, Life Technologies A21202). Cells were

rinsed with 0.5% BSA in PBS and data were collected on a BD Accuri<sup>®</sup>C6 Flow Cytometer with 10,000 gated events per sample. Gates were set to exclude 99.0% of the population stained with the isotype control of the primary antibody. Data was analyzed with FCS Express (De Novo Software).

### *Quantitative Polymerase Chain Reaction*

On Day 14,  $1.5 \times 10^5$  cells were collected with TrypLE Select and processed with the Cells-to-Ct kit (Ambion #4399002). Real-time qPCR was completed with TaqMan Gene Expression Assays (Life Technologies #4351372) in TaqMan Gene Expression Master Mix (Life Technologies # 4369016) using a Bio-Rad CFX96<sup>™</sup>Real-Time System. Data were analyzed with the Bio-Rad CFX Manager software and expression was normalized to housekeeping genes.

## **Results**

### **A Decrease in the concentrations of msNoggin and Synthemax<sup>®</sup>II-SC is required to eliminate Matrigel<sup>®</sup> from the D14 Protocol.**

The first step in adapting the D14 protocol to a xeno-free procedure aimed to replace Matrigel<sup>®</sup> with the ACF peptide copolymer, Synthemax<sup>®</sup>II-SC. However, direct substitution of Synthemax<sup>®</sup>II-SC at its recommended concentration ( $5 \mu\text{g}/\text{cm}^2$ ) for Matrigel<sup>®</sup> resulted in a low yield of cells that expressed PMEL17 by day 14 (data not shown). Instead, three-dimensional aggregates developed during the directed differentiation phase. Neural rosette morphology appeared by day 4 of differentiation in these cultures (Fig. 15A). The original D14 differentiation protocol yields a monolayer of cells with the majority expressing PMEL17 by day 14. At day 14 on Synthemax<sup>®</sup>II-SC however, the most prevalent morphology was thick clusters of neural rosettes and only ~12% of the cells expressed PMEL17 (Fig. 15A, flow data not shown). Although RPE arise from the neural

ectoderm, the greater than normal neural differentiation exhibited by these cultures suggested that the inductive signals should be decreased.

Since noggin is a primary neural inducer [29], concentrations lower than the original 50 ng/mL were tested (0, 5, and 10 ng/mL). A slight increase in the number of regions containing cellular monolayers appeared by day 14 compared to the 50ng/mL noggin control cultures, but the majority of each condition still consisted of thick, three-dimensional aggregates with neural rosettes. We hypothesized that the concentration of substrate was too dense to allow sufficient cellular migration, which may have contributed to the formation of thick cellular clumps. Therefore, the original D14 protocol was conducted on dilutions of Synthemax®II-SC (2.6, 1.0 and 0.5  $\mu\text{g}/\text{cm}^2$ ) in the presence of 50ng/mL msNoggin. However, each condition still developed neural rosettes, despite the reduced substrate concentrations (data not shown).

Since individually diluting msNoggin or Synthemax®II-SC only yielded a very small population of cells positive for PMEL17, combined dilutions of msNoggin and Synthemax®II-SC were tested. The condition of 10 ng/mL msNoggin for the first four days of directed differentiation on tissue culture vessels coated with Synthemax®II-SC at a density of 2.6  $\mu\text{g}/\text{cm}^2$  yielded a cellular monolayer with defined regions of RPE sheets by day 14 (Fig. 15B). Half of the culture was positive for PMEL17 as detected by flow cytometry (Fig. 15B). When the initial seeding density was doubled, the majority of the culture produced by day 14 was a monolayer of RPE, and 80% of the cells were positive for PMEL17 (Fig. 15B). In summary, the simultaneous dilution of msNoggin and Synthemax®II-SC concentrations was required to eliminate Matrigel® from the D14 protocol. This demonstrates that a xeno-free substrate is compatible with the rapid derivation of hESC-RPE.



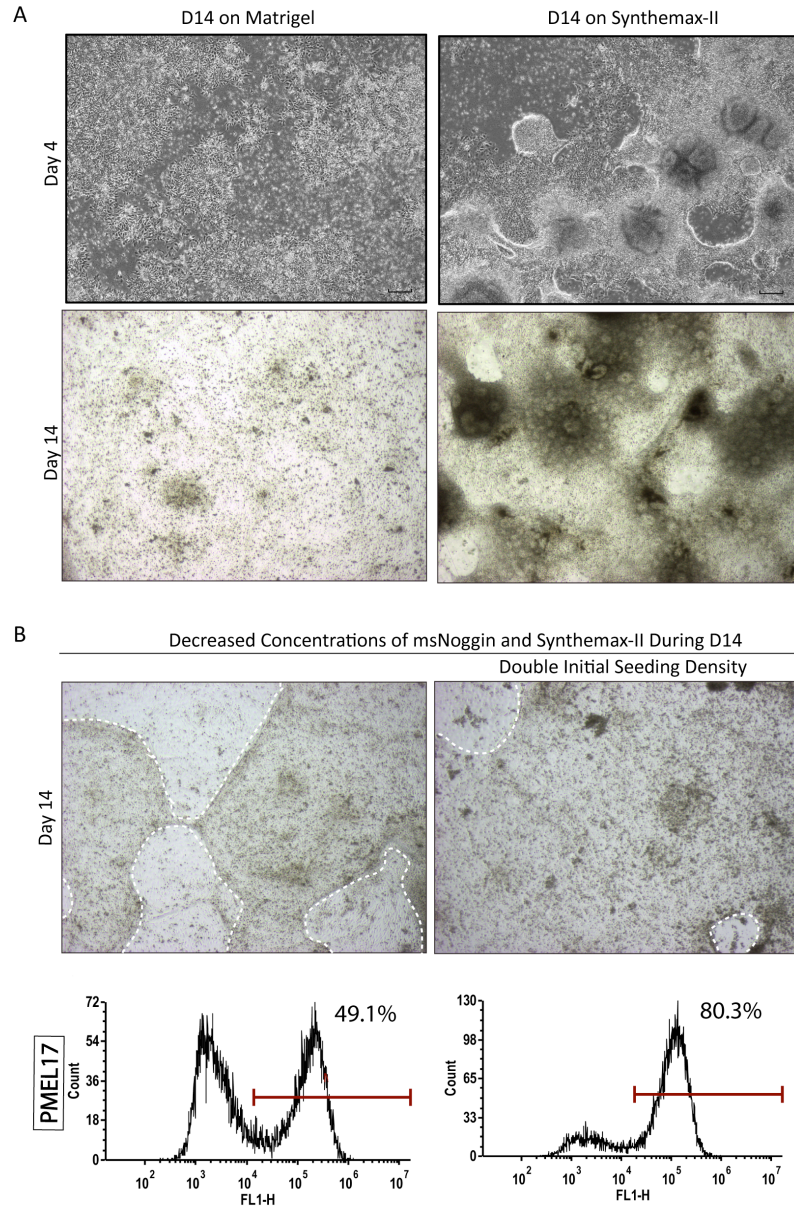


**Figure 15:** Altering concentrations of msNoggin and Synthemax<sup>®</sup> II-SC allows elimination of Matrigel<sup>®</sup> from the D14 protocol. (A) Replacing Matrigel<sup>®</sup> with Synthemax<sup>®</sup> II-SC in the original D14 protocol yields thick aggregates of cells that promote formation of neural rosettes. The original D14 protocol yields a monolayer of RPE cells after two weeks while thicker neural clusters are observed on Synthemax<sup>®</sup> II-SC. (B) Altering the concentration of the neural inducing growth factor, msNoggin, and decreasing the peptide density of Synthemax<sup>®</sup> II-SC markedly increases the yield of cells positive for PMEL17 by day 14. Top: Areas of lighter, non-RPE cells are outlined in the bright field images of cells differentiated for 14 days with 10ng/mL msNoggin on Synthemax<sup>®</sup> II-SC (2.6  $\mu\text{g}/\text{cm}^2$ ). Right: Doubling the initial seeding density prior to differentiation notably increased the yield of cells positive for PMEL17. Bottom: Flow cytometry histograms representing the yield of cells positive for PMEL17 in each condition after 14 days of directed differentiation with modified concentrations of msNoggin and Synthemax<sup>®</sup> II-SC. (A,B) Scale bar = 200 $\mu\text{m}$ .

## **Replacing animal-derived products in the D14 differentiation protocol with Xeno-Free alternatives**

The next goal was to eliminate recombinant msNoggin from the modified D14 protocol using Synthemax<sup>®</sup> II-SC. Noggin is a secreted protein that directly binds to the soluble BMP ligand to prevent its association with ALK3 to inhibit signaling. Previous studies have shown that DMH1, a synthetic small molecule, specifically inhibits ALK2 and ALK3 and mimics the effects of noggin [17, 27]. Replacing msNoggin with 0.5 $\mu$ M DMH1 recapitulated the formation of RPE sheets after 14 days of directed differentiation (Fig. 16A). Furthermore, 75% of the cells were positive for PMEL17 after replacing msNoggin with DMH1 (Fig. 16B). Cells generated by either msNoggin or DMH1 displayed similar gene expression levels for the pigmentation marker *Silv* (PMEL17), *Mitf* isoforms and somewhat reduced expression of the RPE chloride channel, *Best 1* (Fig. 17). Importantly, neither condition produced cells positive for *Mitf* isoform 4, which is indicative of melanocytes and not RPE.

The next goal aimed to eliminate the remaining recombinant growth factors during the neural induction step in the D14 protocol using dual-Smad inhibition. In the original D14 protocol, this step is accomplished within the first four days, resulting in neural morphology (Fig. 18A) and the expression of early eye field transcription factors *Otx2*, *Lhx2*, *Rax* and *Pax6* [28]. However, according to a previously published report, *Otx2* and *Pax6* expression does not become up-regulated by DMH1 and SB431542 until the fifth or seventh day, depending on the iPSC line [27]. Therefore, dual-Smad inhibitors were applied for either the first 4 or 6 days of the modified D14 protocol on Synthemax<sup>®</sup> II-SC. At day 4, hESCs undergoing neuralization by DMH1 and SB431542 manifested a different morphology than cells generated by the original D14 method (Fig. 18B). Cells exposed to

the small molecules until day 6 however, displayed the typical neural phenotype (Fig. 18C). After neural induction for either four or six days, Activin-A, vasoactive intestinal peptide (VIP) and SU5402, an FGF inhibitor, were added until day 14 to establish an RPE identity. Interestingly, ~80% of the cells in both conditions were positive for PMEL17. These preliminary findings suggest that dual-Smad inhibition by DMH1 and SB431542 may be a viable alternative to recombinant growth factors during the initial phase of the rapid D14 protocol.

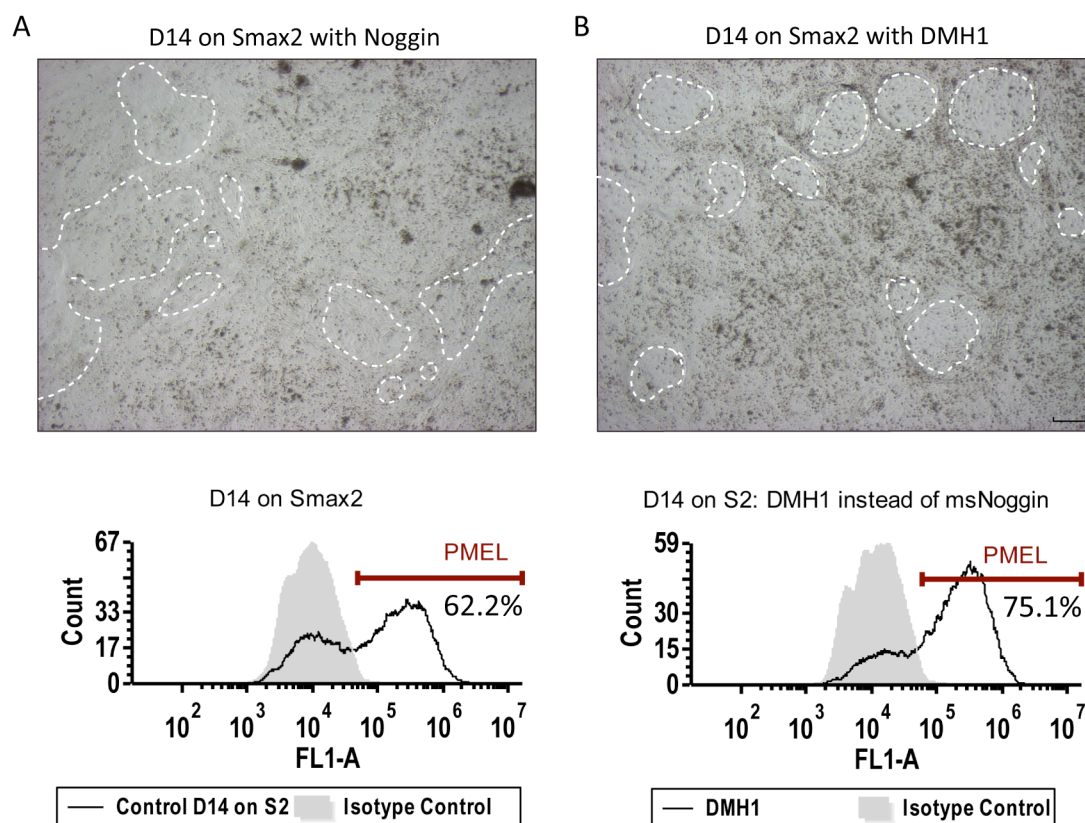


**Figure 16.** Replacing msNoggin with DMH1 during D14 yields cells positive for PMEL17. Top: Regions of non-RPE are encircled on bright field images after 14 days of differentiation on Synthamax® II-SC (Smax2) by using neural induction with (A) 10ng/mL msNoggin or (B) 0.5  $\mu$ M DMH1. Bottom: Flow cytometry histograms representing the percentage of cells positive for PMEL17 after differentiation on Synthamax® II-SC for 14

days with (A) msNoggin or (B) DMH1 during the first four days of directed differentiation. Scale bar = 200µm.

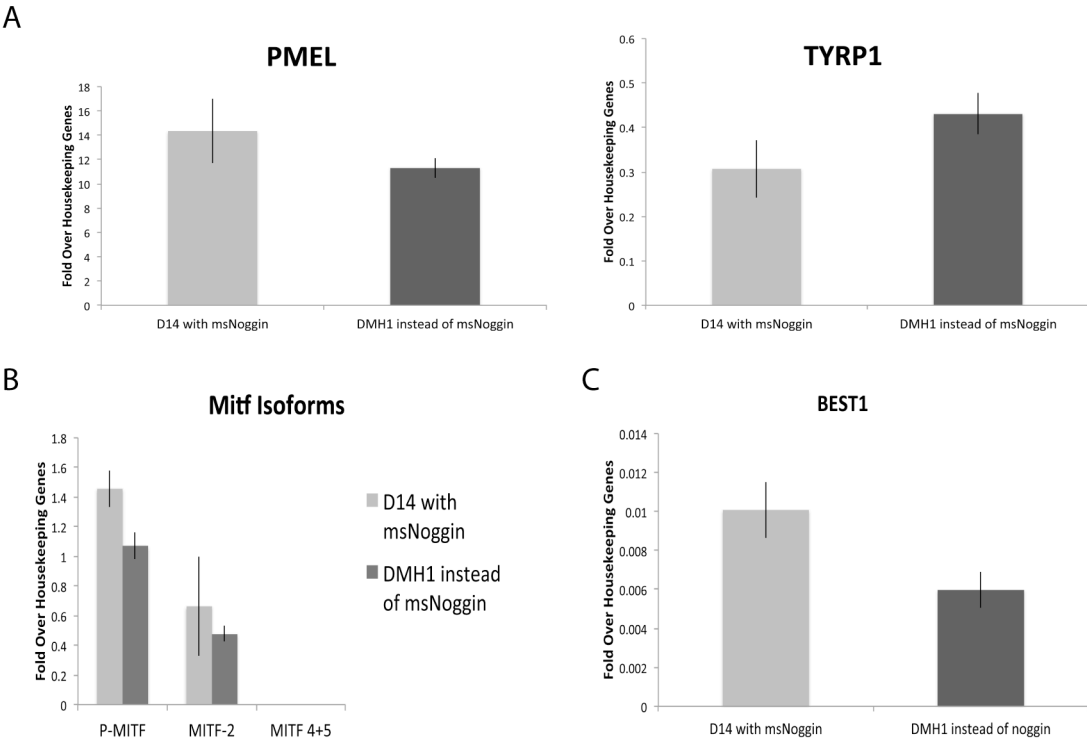


**Figure 17.** Replacing msNoggin with DMH1 in the D14 protocol yields cells with similar gene expression. At day 14, cells directly differentiated on Synthamax® II-SC with msNoggin or DMH1 have similar gene expression levels for (A) pigmentation markers, (B) Mitf isoforms, and (C) the RPE chloride channel Best1. (B) Note the absence of the melanocyte-specific Mitf isoform 4.

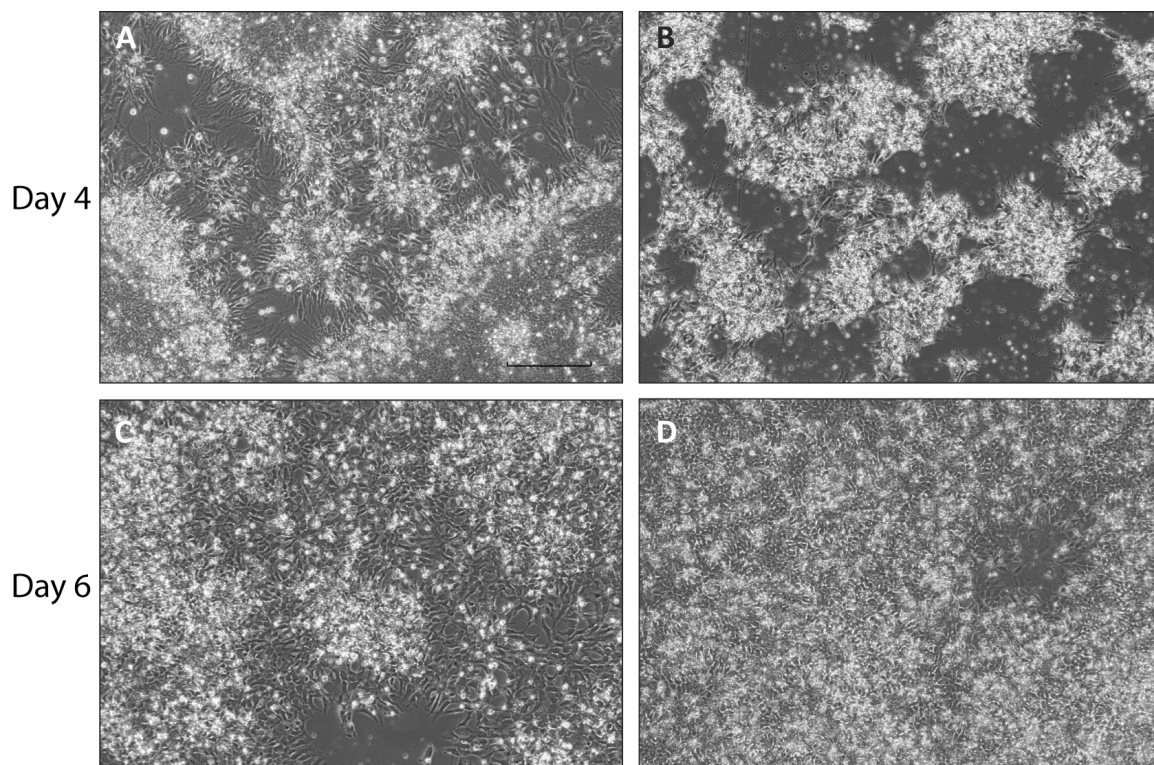


**Figure 18.** Achieving neural morphology with small molecules DMH1 and SB431542 instead of recombinant growth factors during directed differentiation. A) Cells at day 4 grown under the original D14 protocol with Matrigel®, recombinant growth factors and nicotinamide. Note the neural protrusions at the edges of the colonies. B) Day 4 of differentiation on Synthemax® II-SC with DMH1 and SB431542 just prior to addition of Activin-A. C) Day 6 of a prolonged neural differentiation step on Synthemax® II-SC with DMH1 and SB431542 just prior to addition of Activin-A. D) Cells from (B) at Day 6 after a 48-hour exposure to Activin-A. Scale bar = 200μm.

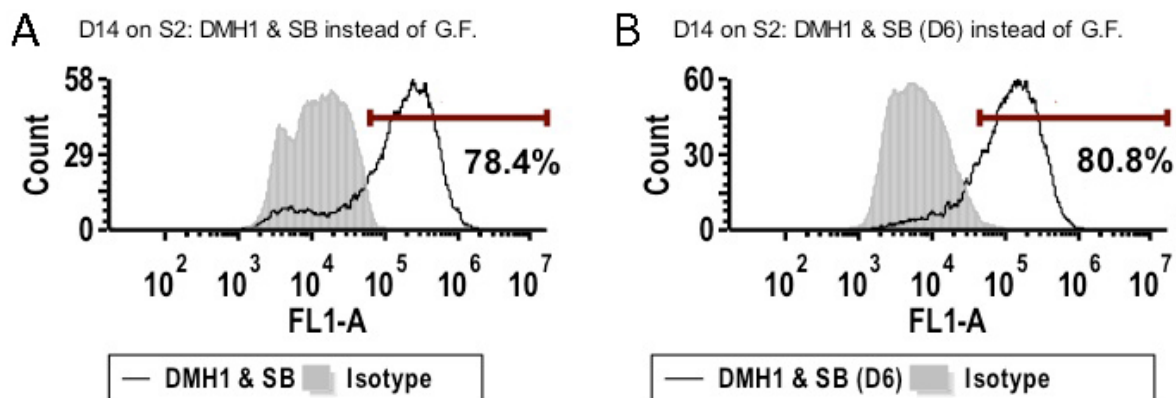


**Figure 19.** Dual-Smad inhibition with DMH1 and SB431542 produces a majority of cells positive for PMEL17 by day 14. Replacing recombinant growth factors with the small molecules DMH1 and SB431542 for the first (A) four days or (B) six days of directed differentiation yields a majority of cells that express the premelanosome marker PMEL17 (S2, Synthemax® II-SC; G.F., recombinant growth factors; SB, SB431542).

## Discussion

These studies describe promising xeno-free alternatives to the animal-derived substrates and recombinant proteins used for differentiation of stem cells into RPE [28]. Ideally, synthetic small molecules would replace all recombinant growth factors during the directed differentiation of GMP-grade hESC-RPE. The preliminary data suggest that DMH1 and SB431542 can effectively replace msNoggin, Dkk-1, IGF-1 and bFGF during the neural induction step to generate cells positive for PMEL17 by day 14. However, further characterization is required to determine the true identity of these PMEL-positive cells produced via small molecules and RPE gene expression and protein localization should be determined with additional characterization assays such as immunocytochemistry and qPCR.

Early neural development gives rise to two types of cells that could express PMEL17: RPE and neural crest-derived melanocytes, both of which can be generated via dual-Smad inhibition. However, previous studies achieved differentiation of stem cells into



neural crest cells only when using low initial seeding densities [24, 26, 30], while higher seeding densities yielded cells positive for Pax6 that were capable of differentiating into neurons of the central nervous system and RPE [24]. Perhaps this differential outcome can be explained by the extent of cell-cell interaction experienced by the cells. During neurulation of embryogenesis, the neural plate folds on itself to form the neural groove which continues to fold until the edges of the neural plate are juxtaposed and subsequently fuse and separate from the overlying ectoderm via preferential homotypic binding of N-cadherin, thus forming the neural tube [31]. The RPE arise from within the neural plate and form tight junctions and interact with adjacent cells [32]. In contrast, neural crest cells arise from the margins of the neural plate and are not incorporated within the neural tube. Instead, they detach from the neural plate, undergo epithelial to mesenchymal transition (EMT), migrate to several distinct destinations in the developing embryo, and give rise to multiple cell types such as melanocytes, sympathetic and parasympathetic neurons, carotid cells and many others [33, 34]. This may explain the propensity of cells *in vitro* to adopt a neural crest fate if there is opportunity to divide and migrate. However, the cell-density studies generating neural crest cells by dual-Smad inhibition used SB431542 in combination with Noggin or LDN-193189, not DMH1. Additional research is needed to determine if DMH1 and SB431542 can feasibly generate neural crest cells. It will be interesting to investigate whether a higher seeding density will facilitate the acquisition RPE identity.

The second half of the original D14 protocol employs the growth factors Activin-A and VIP to direct the neural precursors into RPE. VIP significantly enhances the expression of RPE markers, but its addition is not required for producing hESC-RPE within 14 days [28]. Further investigation is required to determine the necessity of VIP in the xeno-free adaptation of the D14.

The original D14 protocol uses the synergistic effects of nicotinamide and Activin-A to increase the yield of pigmented cells from differentiating hESCs. Activin-A was identified as a candidate compound from the extraocular mesenchyme in chicks that induces RPE fate [35], and nicotinamide significantly promotes hESC differentiation into pigmented RPE [3]. Activin-A has been since used for the directed differentiation of RPE from hESCs [3, 4, 36], but it may not be essential. Free-floating cultures of hESC aggregates differentiating in the presence of nicotinamide without Activin-A produced significantly more pigmented regions than cultures without either Activin-A or nicotinamide. Furthermore, monolayer cultures exposed to nicotinamide and Activin-A increased RPE yield, but not when Activin-A was applied alone [3]. Due to the paucity of commercial agonists to the TGF $\beta$  pathway, especially the Type I ALK4 receptor activated by Activin-A signaling, modulating the concentrations of nicotinamide and the duration of its exposure or employing GMP-grade human Activin-A may have to suffice in the xeno-free adaption of the D14 protocol.

The results shown here demonstrate a promising, preliminary step towards developing a xeno-free protocol for producing hESC-RPE in 14 days. Further investigation is needed to confirm the identity of these cells and to identify alternatives to the remaining recombinant growth factors. Only then will we achieve a true state of Xeno-Freedom. In the long term, these efforts will contribute to optimizing hESC-RPE production for use in cell therapies for AMD.

## References

1. Osakada F, Ikeda H, Sasai Y, Takahashi M (2009) Stepwise differentiation of pluripotent stem cells into retinal cells. *Nat Protoc* 4:811–824. doi: 10.1038/nprot.2009.51
2. Klimanskaya I, Hipp J, Rezai KA, et al. (2004) Derivation and comparative assessment of retinal pigment epithelium from human embryonic stem cells using transcriptomics. *Cloning Stem Cells* 6:217–245. doi: 10.1089/clo.2004.6.217
3. Idelson M, Alper R, Obolensky A, et al. (2009) Directed Differentiation of Human Embryonic Stem Cells into Functional Retinal Pigment Epithelium Cells. *Stem Cell* 5:396–408. doi: 10.1016/j.stem.2009.07.002
4. Zhu Y, Carido M, Meinhardt A, et al. (2013) Three-Dimensional Neuroepithelial Culture from Human Embryonic Stem Cells



- and Its Use for Quantitative Conversion to Retinal Pigment Epithelium. *PLoS ONE* 8:e54552. doi: 10.1371/journal.pone.0054552.s010
5. Buchholz DE, Hikita ST, Rowland TJ, et al. (2009) Derivation of functional retinal pigmented epithelium from induced pluripotent stem cells. *Stem Cells* 27:2427–2434. doi: 10.1002/stem.189
  6. Wasmeler C, Hume AN, Bolasco G, Seabra MC (2008) Melanosomes at a glance. *Journal of Cell Science* 121:3995–3999. doi: 10.1242/jcs.040667
  7. Xu C, Inokuma MS, Denham J, et al. (2001) Feeder-free growth of undifferentiated human embryonic stem cells. *Nature Biotechnology* 19:971–974. doi: 10.1038/nbt1001-971
  8. Braam SR, Zeinstra L, Litjens S, et al. (2008) Recombinant Vitronectin Is a Functionally Defined Substrate That Supports Human Embryonic Stem Cell Self-Renewal via  $\alpha$ V $\beta$ 5 Integrin. *Stem Cells* 26:2257–2265. doi: 10.1634/stemcells.2008-0291
  9. Melkounian Z, Weber JL, Weber DM, et al. (2010) nbt.1629(2). *Nature Biotechnology* 28:606–610. doi: 10.1038/nbt.1629
  10. Smith WC, Knecht AK, Wu M, Harland RM (1993) Secreted noggin protein mimics the Spemann organizer in dorsalizing *Xenopus* mesoderm. *Nature* 361:547–549. doi: 10.1038/361547a0
  11. Zimmerman LB, De Jesús-Escobar JM, Harland RM (1996) The Spemann organizer signal noggin binds and inactivates bone morphogenetic protein 4. *Cell* 86:599–606.
  12. Shi Y, Massagué J (2003) Mechanisms of TGF- $\beta$  Signaling from Cell Membrane to the Nucleus. *Cell* 113:685–700. doi: 10.1016/S0092-8674(03)00432-X
  13. Vogt J, Traynor R, Sapkota GP (2011) The specificities of small molecule inhibitors of the TGF $\beta$  and BMP pathways. *Cellular Signalling* 23:1831–1842. doi: 10.1016/j.cellsig.2011.06.019
  14. Cuny GD, Yu PB, Laha JK, et al. (2008) Structure–activity relationship study of bone morphogenetic protein (BMP) signaling inhibitors. 18:4388–4392. doi: 10.1016/j.bmcl.2008.06.052
  15. Aoki H, Fujii M, Imamura T, et al. (2001) Synergistic effects of different bone morphogenetic protein type I receptors on alkaline phosphatase induction. *Journal of Cell Science* 114:1483–1489.
  16. Yu PB, Hong CC, Sachidanandan C, et al. (2007) Dorsomorphin inhibits BMP signals required for embryogenesis and iron metabolism. *Nat Chem Biol* 4:33–41. doi: 10.1038/nchembio.2007.54
  17. Hao J, Ho JN, Lewis JA, et al. (2010) In Vivo Structure–Activity Relationship Study of Dorsomorphin Analogues Identifies Selective VEGF and BMP Inhibitors. 5:245–253. doi: 10.1021/cb9002865
  18. Smith JR, Vallier L, Lupo G, et al. (2008) Inhibition of Activin/Nodal signaling promotes specification of human embryonic stem cells into neuroectoderm. *Dev Biol* 313:107–117. doi: 10.1016/j.ydbio.2007.10.003
  19. Camus A, Perea-Gomez A, Moreau A, Collignon J (2006) Absence of Nodal signaling promotes precocious neural differentiation in the mouse embryo. *Dev Biol* 295:743–755. doi: 10.1016/j.ydbio.2006.03.047
  20. D'Amour KA, Agulnick AD, Eliazar S, et al. (2005) Efficient differentiation of human embryonic stem cells to definitive endoderm. *Nature Biotechnology* 23:1534–1541. doi: 10.1038/nbt1163
  21. Vallier L, Reynolds D, Pedersen RA (2004) Nodal inhibits differentiation of human embryonic stem cells along the neuroectodermal default pathway. *Dev Biol* 275:403–421. doi: 10.1016/j.ydbio.2004.08.031
  22. Xu R-H, Sampsell-Barron TL, Gu F, et al. (2008) NANOG Is a Direct Target of TGF $\beta$ /Activin-Mediated SMAD Signaling in Human ESCs. *Cell Stem Cell* 3:196–206. doi: 10.1016/j.stem.2008.07.001
  23. Inman GJ, Nicolás FJ, Callahan JF, et al. (2002) SB-431542 is a potent and specific inhibitor of transforming growth factor- $\beta$  superfamily type I activin receptor-like kinase (ALK) receptors ALK4, ALK5, and ALK7. *Mol Pharmacol* 62:65–74.
  24. Chambers SM, Fasano CA, Papapetrou EP, et al. (2009) Highly efficient neural conversion of human ES and iPS cells by dual inhibition of SMAD signaling. *Nature Biotechnology* 27:275–280. doi: 10.1038/nbt.1529
  25. Chow RL, Altmann CR, Lang RA, Hemmati-Brivanlou A (1999) Pax6 induces ectopic eyes in a vertebrate. *Development* 126:4213–4222.
  26. Qi Y, Mica Y, Lee G, et al. (2012) nbt.2249. *Nature Biotechnology* 30:715–720. doi: 10.1038/nbt.2249
  27. Neely MD, Litt MJ, Tidball AM, et al. (2012) DMH1, a Highly Selective Small Molecule BMP Inhibitor Promotes Neurogenesis of hiPSCs: Comparison of PAX6 and SOX1 Expression during Neural Induction. *ACS Chem Neurosci* 3:482–491. doi: 10.1021/cn300029t
  28. Buchholz DE, Pennington BO, Croze RH, et al. (2013) Rapid and Efficient Directed Differentiation of Human Pluripotent Stem Cells Into Retinal Pigmented Epithelium. *Stem Cells Translational Medicine* 2:384–393. doi: 10.5966/sctm.2012-0163
  29. Lamb TM, Knecht AK, Smith WC, et al. (1993) Neural induction by the secreted polypeptide noggin. *Science* 262:713–718.
  30. Kreitzer FR, Salomonis N, Sheehan A, et al. (2013) A robust method to derive functional neural crest cells from human pluripotent stem cells. *Am J Stem Cells* 2:119–131.
  31. Detrick RJ, Dickey D, Kintner CR (1990) The effects of N-cadherin misexpression on morphogenesis in *Xenopus* embryos. *Neuron* 4:493–506.
  32. Strauss O (2005) The Retinal Pigment Epithelium in Visual Function. *Physiological Reviews* 85:845–881. doi: 10.1152/physrev.00021.2004
  33. Dupin E, Sommer L (2012) Neural crest progenitors and stem cells: From early development to adulthood. *Dev Biol* 366:83–95. doi: 10.1016/j.ydbio.2012.02.035
  34. Planque N (2004) Microphthalmia Transcription Factor Induces Both Retinal Pigmented Epithelium and Neural Crest Melanocytes from Neuroretina Cells. *Journal of Biological Chemistry* 279:41911–41917. doi: 10.1074/jbc.M404964200
  35. Fuhrmann S, Levine EM, Reh TA (2000) Extraocular mesenchyme patterns the optic vesicle during early eye development in the embryonic chick. *Development* 127:4599–4609.
  36. Hongisto H (2012) Low level of activin A secreted by fibroblast feeder cells accelerates early stage differentiation of retinal pigment epithelial cells from human pluripotent stem cells. *SCD* 02:176–186. doi: 10.4236/scd.2012.24022

## IV. Development of Interactive Learning Exercises for Biochemistry

### Interactive Hangman Teaches Amino Acid Structures and Abbreviations

Britney O. Pennington<sup>§¶</sup>, Duane Sears<sup>¶</sup>, Dennis O. Clegg<sup>§¶</sup>

*From the §Center for Stem Cell Biology and Engineering, Neuroscience Research Institute, Biomolecular Science and Engineering Program, ¶Department of Molecular, Cellular and Developmental Biology University of California Santa Barbara, CA 93106, ¶ Department of Biology, Westmont, CA 93108*

This manuscript is under review with *Biochemistry and Molecular Biology Education*.

#### **Abstract:**

We developed an interactive exercise to teach students how to draw the structures of the 20 standard amino acids and to identify the one-letter abbreviations by modifying the familiar game of “Hangman”. Amino acid structures were used to represent single letters throughout the game. To provide additional practice in identifying structures, hints to the answers were written in “amino acid sentences” for the students to translate. Students were required to draw the structure of the corresponding letter they wished to guess on a whiteboard. Each student received a reference sheet of the structures and abbreviations, but was required to draw from memory when guessing a letter. Pre and post assessments revealed a drastic improvement in the students’ ability to recognize and draw structures from memory. This activity provides a fun, educational game to play in biochemistry discussion sections or during long incubations in biochemistry labs.

**Keywords:** Interactive Game, Amino Acid Structures, Amino Acid Abbreviations, Hangman, Active Learning

**Introduction:**

Biochemists proclaim that an intimate knowledge of chemical structures contributes informative insights into the molecular function and behavior of biochemical processes [1,2]. A typical requirement for introductory biochemistry classes is to learn the structure of the 20 standard amino acids and the single letter abbreviations. Students can then reference these throughout their academic and professional careers. Devoting structures to memory allows students to immediately recall properties and relative sizes of side chains without tediously sorting through mnemonics of which R groups are polar and uncharged or which absorb ultraviolet wavelengths, etc. Once comfortable with the amino acid structures, students can apply this knowledge to accomplish higher cognitive tasks such as readily explaining the steric and intermolecular consequences of a point mutation in an active site and specifically how it affects substrate specificity and enzyme activity without consulting a textbook.

Literacy in the single letter abbreviations is essential for analyzing professional protein papers. The International Union of Pure and Applied Chemistry (IUPAC) and the International Union of Biochemistry (IUB) developed a succinct alternative to the 3 letter code by establishing the single letter notation to achieve brevity and to compare large protein sequences [3,4]. Knowing the corresponding structure when reading the one letter code allows students to glean deeper insights into potential interactions or mechanisms. Compared to students who are structurally ignorant, for example, informed students can readily ascertain the nuances between the biomedically relevant mutations of R406W in tau for dementia and Alzheimer's Disease [5], E6V in hemoglobin for sickle cell anemia [6], Y402H in complement factor H for age-related macular degeneration[7] or R117H in cystic fibrosis [8].

Previous attempts to teach amino acid structure and single letter abbreviations have involved complicated rhymes [9], emphasis on structural similarities to acetyl-CoA, pyruvate, and other metabolic intermediates [10], and the rote memorization of nonsensical acronyms [2]. Once mastered, these approaches may confer a degree of comprehension, but some of these devices may require more tedious studying than just learning the structures and abbreviations directly.

Games have been identified as effective educational tools since the 1920s [11]. Interactive games have already been developed to teach aspects of protein folding such as hands-on activities in the classroom [12] and the online crowd-sourcing sensation, Foldit [13]. In the latter, gamers identify novel folding conformations with computational design, and many of these proteins have biomedical and renewable fuel applications. For example, the crowd-sourced players identified a new way to fold an alderase to increase its activity 18 fold [14]. However, these games provide information on the chemical properties of an amino acid sequence, and they do not rely on the players' knowledge of the monomeric structures. To specifically teach the structures and the single letter abbreviations of the 20 standard amino acids, the modified version of "Hangman" described here employs the three primary aspects that make games successful: motivation, practice and reinforcement [15]. Students are motivated to learn material destined to appear on exams, they practice drawing structures during the activity until they can confidently reproduce it in front of an audience, and they receive positive reinforcement by solving puzzles and thinking of their own Hangman clue(s). The only mnemonics employed during this game included the simple devices developed during the foundation of the single letter code such as pronouncing Asp as "aspar-*D*-ic acid" and Gln as "*Q*-tamine" [4] as well as an original, baby-like pronunciation of Trp as "t*W*yptophan". After playing four rounds of Hangman with amino

acid structures instead of English alphabet characters, students exhibited substantial improvement in both drawing the structures from memory and correctly labeling given structures with the single letter abbreviation.

## **Methods**

### *Preliminary instructions*

Students were informed during the first biochemistry class of the semester that the amino acid structures were cumulative material and would appear on the three exams throughout the course. Three weeks after the announcement, interactive Amino Acid Hangman was played in the lab section during the incubation periods of primary and secondary antibodies. The exercise was appropriate for lab sessions due to the relatively smaller class sizes compared to lecture and the longer periods of available time. Students were informed that the linear appearance of the “amino acid sentences” were NOT indicative of the actual stereochemistry formed by a peptide bond (Fig. 20).

### *Assessment*

In the beginning of the lab session, the instructor announced, “I like science and I like having fun and playing games. Since you will need to know your amino acid structures for the exams, we’re going to play a game to help you learn them. You will also have a chance to earn up to 12 points extra credit.”

Prior to receiving the reference sheet, students took 2 pre-tests. The first displayed the 20 single letter abbreviations, and the students were requested to draw the corresponding structure. The second pre-test displayed the 20 structures and the students were instructed to assign the correct single letter abbreviations. The instructions for both pretests were

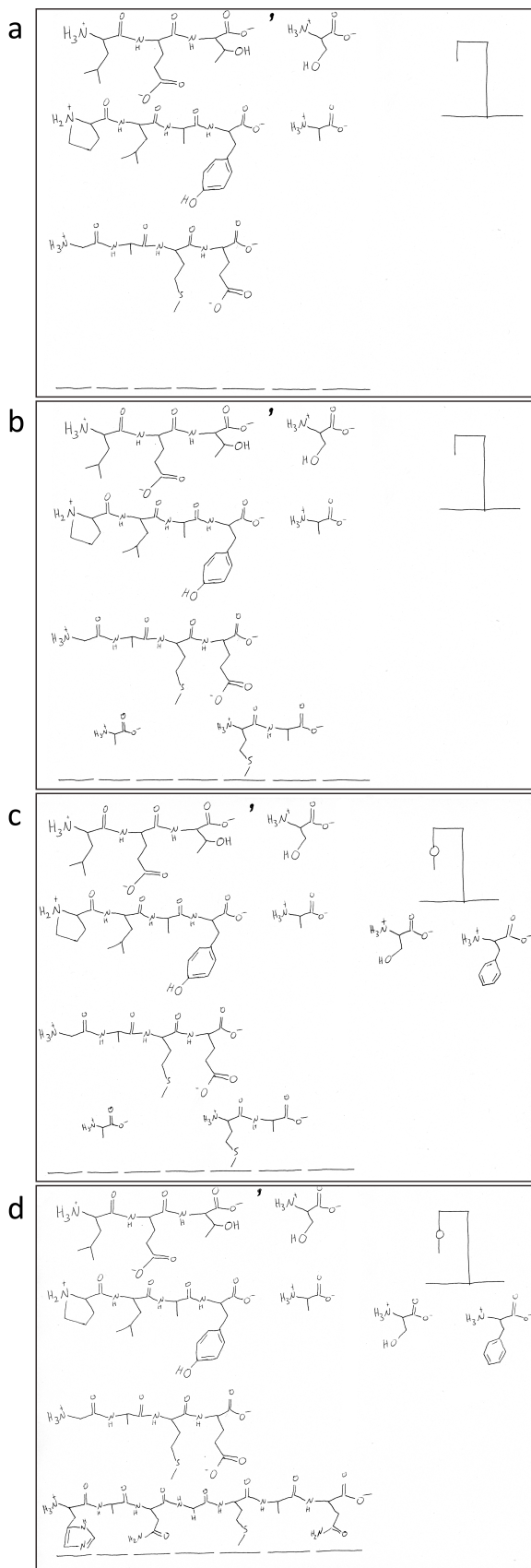


**Figure. 20.** Example of the Amino Acid Hangman game.

- A hint is drawn in “amino acid sentences” (LET’S PLAY A GAME) and spaces are drawn for each letter of the answer.
- Students guess letters by drawing the corresponding amino acid structure. If the letter appears in the answer, the student redraws the structure in the appropriate space(s) indicated by the instructor.
- If a proposed structure does not appear in the answer, the student redraws it in the corner and a body part is added to the hangman.
- The puzzle is solved when students draw correct structures in all of the available spaces.

“Drawing/Identifying >10 correct will earn +3 points extra credit. One wrong answer negates any extra credit.” The latter stipulation aimed to prevent rampant guessing based on the idea that grades, even extra points, are precious currency to the students [16].

After the activity, the exact same tests were distributed in the same order with the same instructions. Number of correct answers and structures were quantified.

### *Playing the Game*

To play traditional Hangman, one player picks a word or phrase for the audience to guess and draws horizontal dashes for each letter in the answer. The remaining players propose letters to fill in the blanks. If a letter appears within the word, the first player writes it in the appropriate spaces. If an incorrect letter is guessed, one body part is drawn on a cartoon gallows. The object of the game is to guess the word or phrase before a complete “hangman” is drawn.

To play Amino Acid Hangman, students first received a reference sheet with the amino acid structures and abbreviations (supplemental Fig. 7) and were allowed to refer to this sheet at their lab bench throughout the game. They were not permitted to bring it to the board. The instructor also wrote hints to the Hangman answers using structures instead of English alphabet characters (Fig. 20a, supplemental Table 1). Audible translation of the hint or the answer by a student would negate any extra credit. To guess a letter, students drew the corresponding structure from memory on the whiteboard in front of the class. If it appeared in the answer, the instructor indicated the appropriate space(s), and the student redrew the structure as it would appear at pH 7 in order to gain additional practice (Fig. 20b) [15]. If filling a space adjacent to a previously drawn amino acid, the student indicated which atoms participated in the dehydration reaction of the peptide bond formation, only referring to the instructor’s assistance when needed. If the proposed structure did not appear

within the answer however, the student drew it again in the top corner of the whiteboard and the instructor added a body part to the Hangman (Fig. 20c). To avoid discouraging or embarrassing the student, the instructor ensured that hands, feet and facial features would also be drawn. “Solving the puzzle” in one attempt was not allowed. The only way to complete the Hangman answer was for volunteers to draw individual structures, which maximized the number of participants.

After each puzzle was solved, the entire section went through the clue together: the instructor pointed to each structure and the students responded with the full amino acid name. While the instructor drew the hint for the next round, students were encouraged to practice drawing and identifying the amino acids from their reference sheet. Four rounds of Hangman were played in about 2 hours.

Surprisingly, a few students requested to draw their own hints for their own Hangman puzzle. One student was selected and was allowed to refer to the reference sheet while drawing her hint on the board (hint: SCARY SNAKES; answer: VIPERS). This student fulfilled the roles of the instructor for the entire round.

## **Results and Discussion:**

The post-test revealed a marked improvement in students’ ability to recognize and properly label the structures of all 20 amino acids (Fig. 21). Scarcely using a letter in the hints or answers did not preclude students from learning the single letter abbreviation. For example, F and V were accurately assigned to the corresponding structure by 41% and 58% more students after the activity respectively, despite only being used once during the game. Prior to Hangman, not one student correctly drew or identified M, but afterwards, over 40% of the class could accomplish both tasks. Methionine was only used 3 times. This suggests that students consulted the reference sheet with the structures and abbreviations and



practiced at their bench while playing the game. Therefore, the time devoted by the instructor to write the “structural sentences” of the next hint can be beneficial to students, and students should be encouraged to practice during the interludes between rounds.

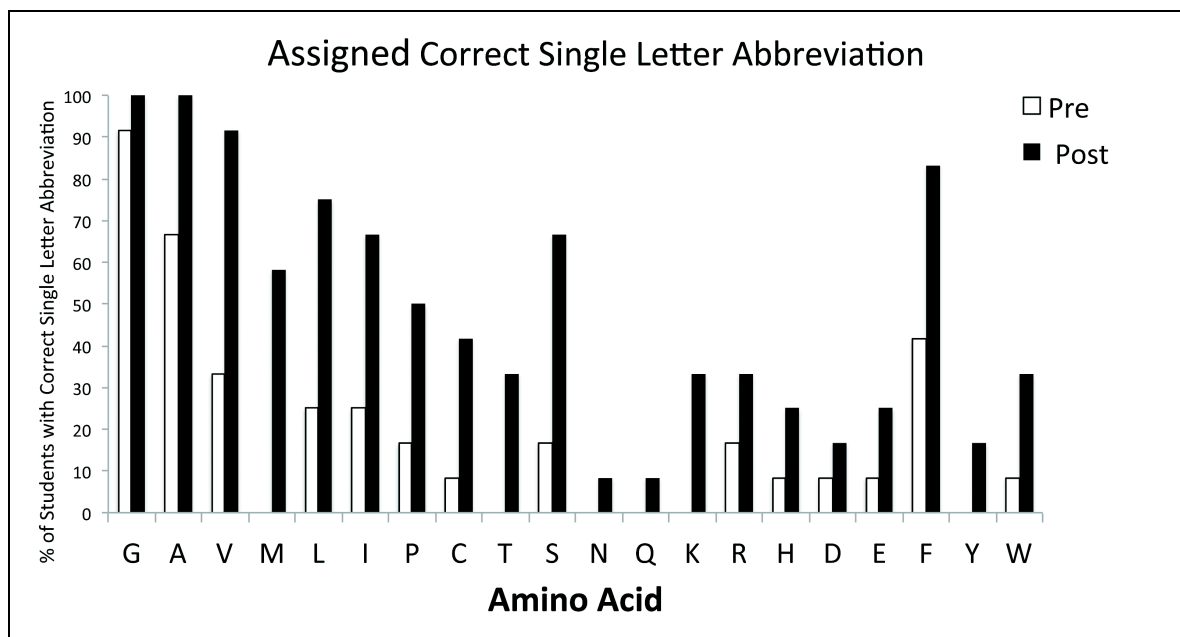


**Figure 21.** Students’ ability to assign the correct single letter abbreviation to a given structure improves after playing Amino Acid Hangman.

Students’ ability to draw structures from memory was also improved for 17 amino acids after they played the Hangman game (Fig. 22). Before the game, the majority of the class could only draw G, the simplest amino acid. Afterwards, more than half the class could accurately draw the structures of G, A, V, L, I, P, S, and F. Note that for 9 other amino acids, not one student drew the correct structure before the activity, but many students could properly draw these structures after the game. Interestingly, no student attempted to draw N, Q nor R for either the pre- or post-test. Perhaps this caution was due to the chance of losing extra credit. In order to incentivize mastery of complicated structures, additional points could be assigned to certain side chains. For each structure that

was attempted however, 5-65% more students were able to correctly sketch the amino acid after the activity than before playing Amino Acid Hangman. The higher number of accurate responses indicates that students improved their ability and perhaps even their confidence to draw and recognize the standard amino acid structures.

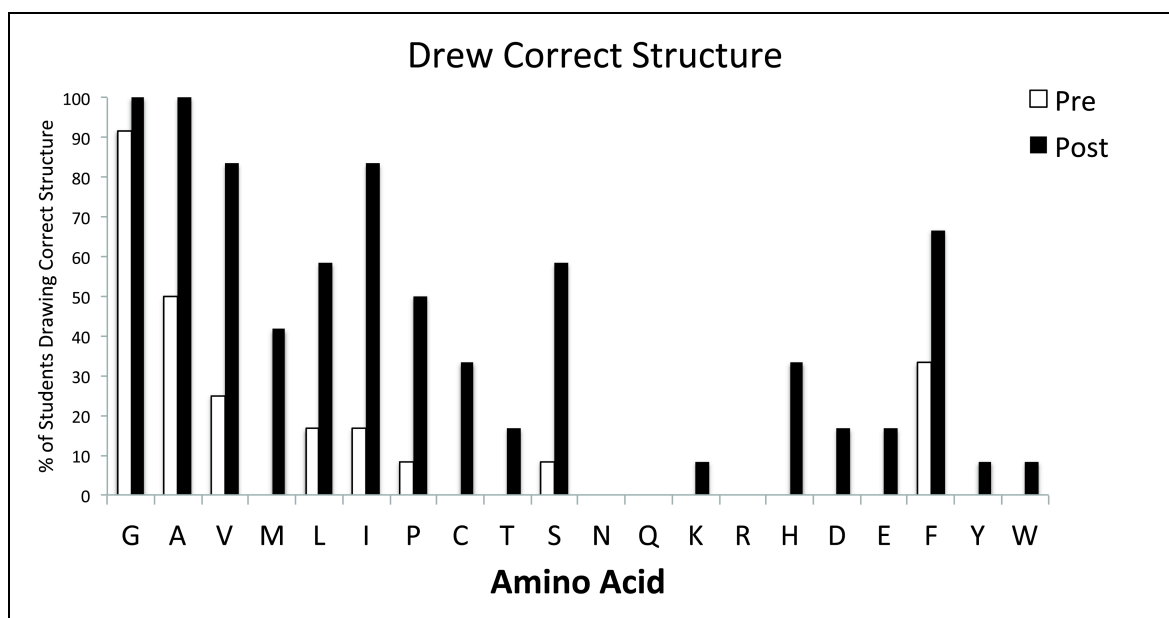


**Figure 22.** Students' ability to draw the correct amino acid structure improves after playing Amino Acid Hangman.

Students were enthusiastic to play when the game was presented as a means to extra credit while being a fun way to prepare them for relevant exam material. Humor and fun contribute to active learning [17,18]. For example, students were advised that they could write a love letter in amino acid structures if they had a particular nerdy sweetheart, or they could write clandestine, encrypted messages. Overall, we suggest that Amino Acid Hangman is a fun, educational, interactive exercise that improves students' ability to draw and correctly assign the single letter code to amino acids.

**Acknowledgements** – The authors wish to thank Jeffrey Bailey and Elmer Gomez for playing test versions of Amino Acid Hangman. We would also like to acknowledge Brittany McHargue for volunteering her own Amino Acid Hangman hint and answer during the exercise as well as all of the participating students in the Cell Biology course. BOP was

a fellow of the California Institute for Regenerative Medicine (CIRM) and the Richard & Katherine Gee Breau Fellowship in Vision Research and was also supported by the CIRM grants DR1-01444, CL1-00521, TG2-01151 and FA1-00616 (DOC).

## References

- [1] M. Saffran (1998) Amino acid names and parlor games: From trivial names to a one-letter code, amino acid names have strained students' memories. Is a more rational nomenclature possible? *Biochemical Education*, **26**(2), 116–118.
- [2] D. S. Moore (1987) Biochemically informative acronyms for the twenty common amino acids, *Biochemical Education* **15**(2), 74–76.
- [3] (1972) A one-letter notation for amino acid sequences, *Pure Appl Chem*, **31**(4), 641–645.
- [4] (1984) IUPAC-IUB Joint Commission on Biochemical Nomenclature (JCBN). Nomenclature and symbolism for amino acids and peptides. Recommendations 1983, *Biochem. J.* **219**(2), 345–373.
- [5] M. M. Hutton *et al.* (1998) Association of missense and 5'-splice-site mutations in tau with the inherited dementia FTDP-17, *Nature* **393**(6686), 702–705.
- [6] X. Li, U. A. Mirza, B. T. Chait, and J. M. Manning (1997) Systematic enhancement of polymerization of recombinant sickle hemoglobin mutants: implications for transgenic mouse model for sickle cell anemia, *Blood* **90**(11), 4620–4627.
- [7] G. S. Hageman *et al.* (2005) A common haplotype in the complement regulatory gene factor H (HF1/CFH) predisposes individuals to age-related macular degeneration, *Proc. Natl. Acad. Sci. U.S.A* **102**(20), 7227–7232.
- [8] P. Kristidis *et al.* (1992) Genetic determination of exocrine pancreatic function in cystic fibrosis, *Am. J. Hum. Genet.* **50**(6), 1178–1184.
- [9] V. A. Mezl (2001) The AAA amino acid list a mnemonic derivation of the structures and properties of the amino acids *Biochem. Mol. Biol. Educ.* **29**(2), 66–70.
- [10] L. J. Vanwinkle (1985) A Summary of Amino-Acid Metabolism Based on Amino-Acid Structure, *Biochemical Education* **13**(1), 25–26.
- [11] J. Henry (1997) Gaming: a teaching strategy to enhance adult learning, *Journal of Continuing Education in Nursing* **28**(5), 231–234 [Online]. Available: <http://web.b.ebscohost.com/ehost/detail/detail?sid=974a2bfe-da3a-40a8-8ab4-b0218f962e3a%40sessionmgr111&vid=5&hid=117&bdata=JnNpdGU9ZW9vc3QtbGl2ZQ%3d%3d#db=eue&AN=507587460>. [Accessed: 12-Aug-2014].
- [12] B. White (2006) A Simple and Effective Protein Folding Activity Suitable for Large Lectures, *Cell Biology Education* **5**(3), 264–269.
- [13] S. Cooper *et al.* (2010) Predicting protein structures with a multiplayer online game, *Nature* **466**(7307), 756–760.
- [14] C. B. Eiben *et al.* (2012) Increased Diels-Alderase activity through backbone remodeling guided by Foldit players, *Nature Biotechnology* **30**(2), 190–192.
- [15] M. Deck and J. Silva (1991) Games Manual: Getting Adults Motivated, Enthusiastic & Satisfied” [Online]. Available: <http://www.amazon.com/Games-Manual-Enthusiastic-Strategies-Instruction/dp/B000NGR0AE>. [Accessed: 12-Aug-2014].
- [16] H. Becker and E. Huges (1995) Making the Grade: The Academic Side of College, Transaction Publishers, pp. 55–59 [Online].
- [17] T. I. Poirier and M. Wilhelm, M (2014) Use of humor to enhance learning: bull’s eye or off the mark, *American journal of pharmaceutical education* **78**(2).article 27.
- [18] H. Baid and N. Lambert (2010) Enjoyable learning: The role of humour, games, and fun activities in nursing and midwifery education, *Nurse Education Today* **30**(6), 548–552.

## V. Conclusions

To me, it has been a privilege to work at the cutting edge of regenerative medicine, and I have been fortunate to occupy a specific, rare research niche during my six years in the Clegg Lab. On the one hand, I have collaborated with efforts of the California Institute for Regenerative Medicine (CIRM) and have experienced the laser-focused drive to generate a product that restores vision to the blind. On the other hand, I have also enjoyed the freedom to tinker with developmental mechanisms to radically expedite the derivation of potentially therapeutic cells. For me, this dichotomy encompasses the main objective of my doctorate program, Biomolecular Science and Engineering.

The work presented in this thesis primarily addresses two pertinent obstacles to the translation of stem cell therapies to the clinic. The first pertains to the *in vitro* culture conditions of stem cells and their derivatives. Currently, at the dawn of an upcoming era of treating human maladies with cellular therapies, it is acceptable to use xenogeneic reagents during production. As the field matures however, the primary convention for generating these treatments is expected to utilize defined xeno-free culture conditions to obviate the risk of exposing patients to animal-derived immunogens. Here, I have demonstrated that a synthetic, good manufacturing practices (GMP)-compliant peptide copolymer supports the growth of H9 and H14 human embryonic stem cells (hESCs). Due to the pluripotency of these cells, these findings can be applied to generate a wide range of therapeutic cell types.

A second obstacle to bringing cell-based therapies bench-to-bedside is the cost and duration of *in vitro* cell culture. I have assisted in developing a directed differentiation protocol that accelerates the derivation of hESC-RPE from several months to 14 days. By replacing the xenogeneic substrate and many of the expensive recombinant growth factors, I

have taken the preliminary steps to adapt this rapid protocol to less expensive xeno-free conditions. This directed differentiation procedure is expected to assist in the swift production of hESC-RPE as well as facilitate the study of RPE developmental mechanisms.

Lastly, how could we hope for future innovative breakthroughs without keen scientists and doctors? Educating the next generation of regenerative pioneers to approach problems with critical thought is essential for advancement. Experiments and discoveries are not created by memorizing a textbook. Therefore, we must provide undergraduate students with opportunities to practice critical thinking needed in a lab setting. Engaging, interactive exercises encourage students to train their higher cognitive skills of analysis, synthesis, and evaluation. And one should never underestimate the effects of having fun. In teaching. In science. In life.

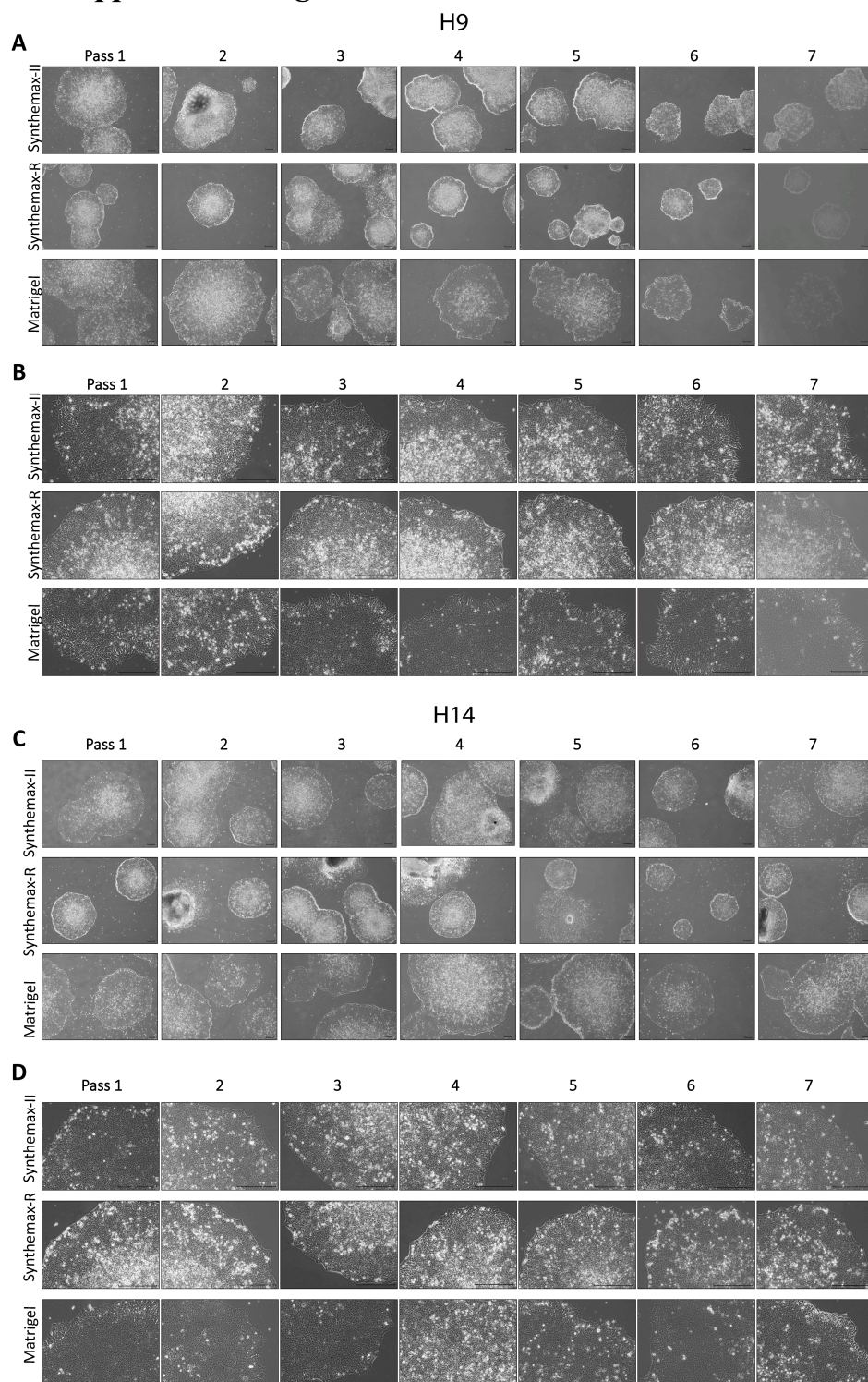
## Appendix

### *A. Supplemental Tables*

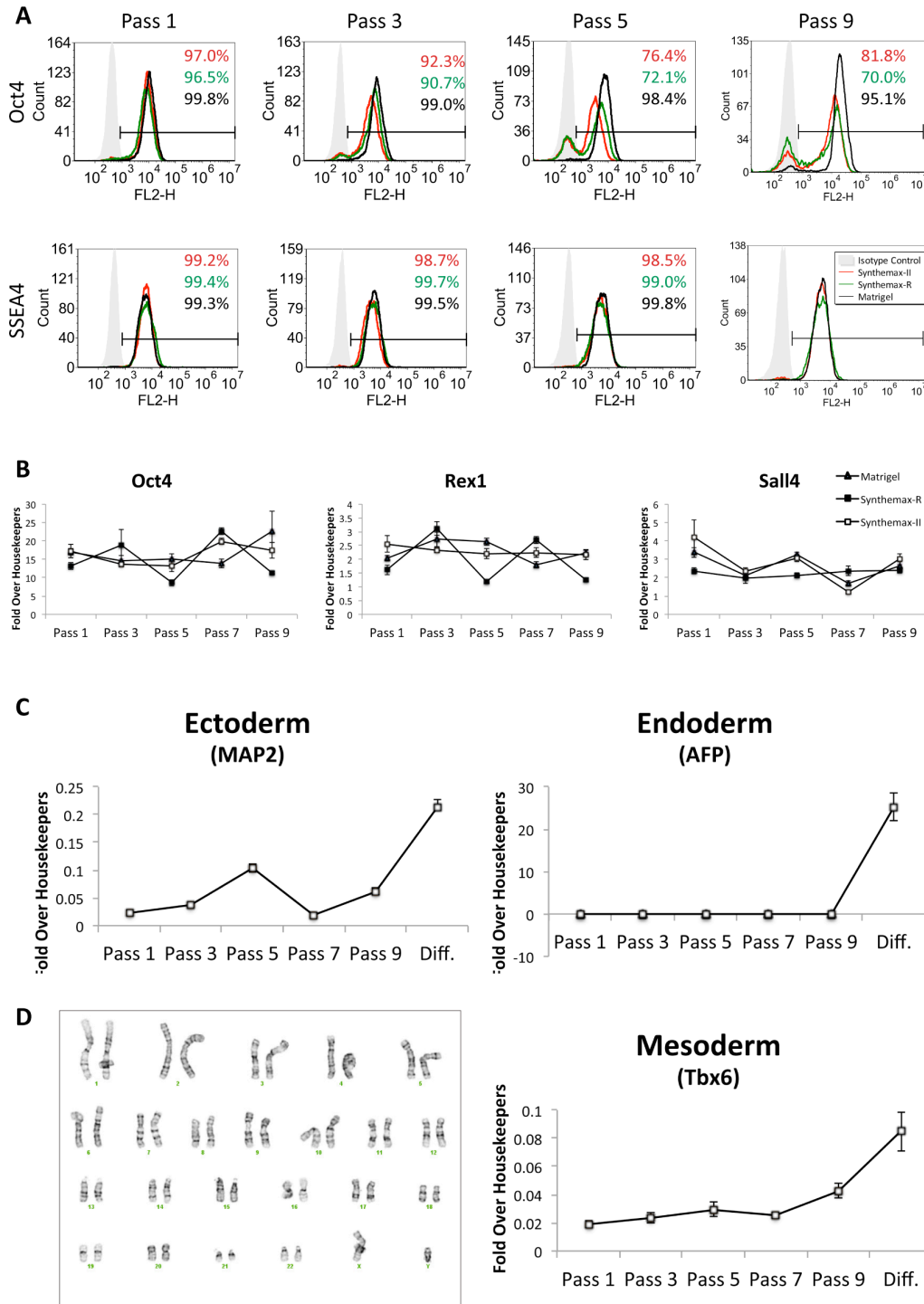
**Supplemental Table 1:** Examples of hints and answers that can be used in Amino Acid Hangman. Text in bold was used during the 4 rounds of Amino Acid Hangman described. Each letter is from the single letter code for amino acids developed by IUPAC and IUB.

Hint Written by Instructor	Answer
<b>LET'S PLAY A GAME</b>	<b>HANGMAN</b>
<b>ALIENS FLY IN</b>	<b>SPACESHIPS</b>
<b>MEAN SHIPS</b>	<b>PIRATES</b>
<b>SCARY SNAKE</b>	<b>VIPERS</b>
ANCIENT MEAT EATERS	CAVEMEN
AN INTERESTING CLASS	CHEMISTRY
TASTY GRAPES	WINE
SILLY MEMES	INTERNET CATS
TREES GIVE	SHADE
AFTER FALL	WINTER
AFTER WINTER	SPRING
WIND ANIMAL	WEATHERVANE
WILD ANIMAL	TIGER
IPAD	APPLE DEVICE
MARINE TV	SHARK WEEK
NICE PLANET	EARTH
MERRY CHRISTMAS	REINDEER
GAME CHEATER	CARD SHARK
W.M.D.	IRAQ

## B. Supplemental Figures

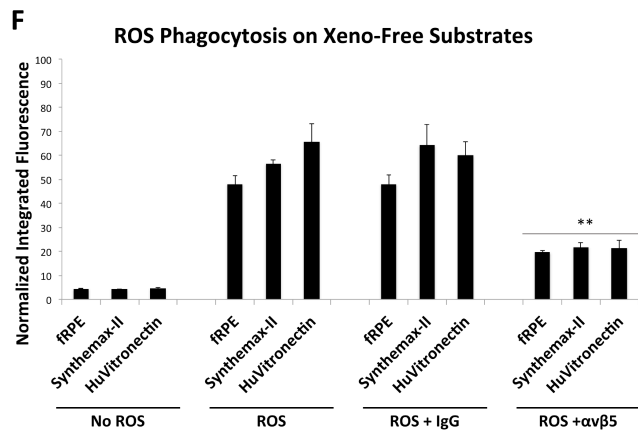
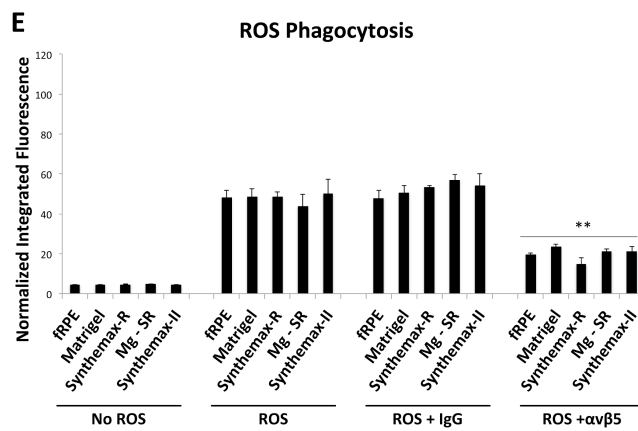
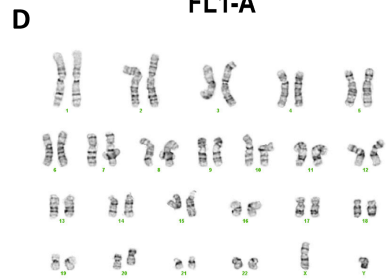
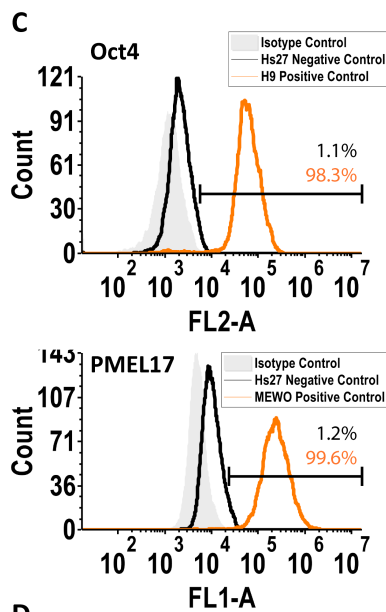
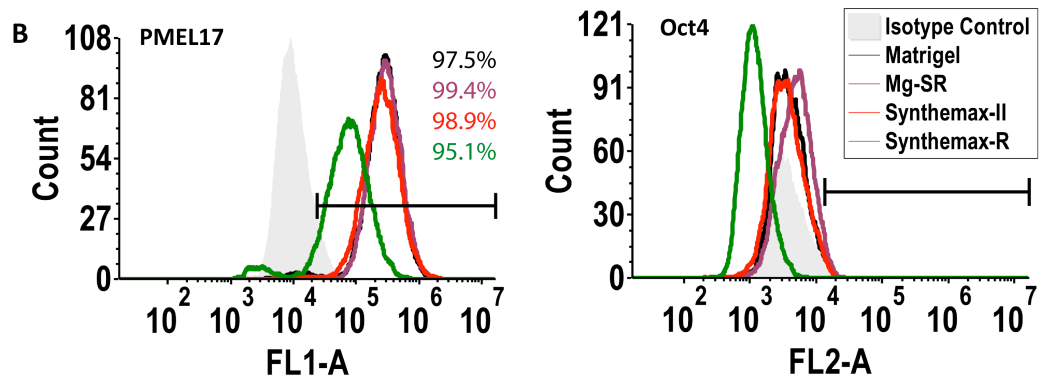
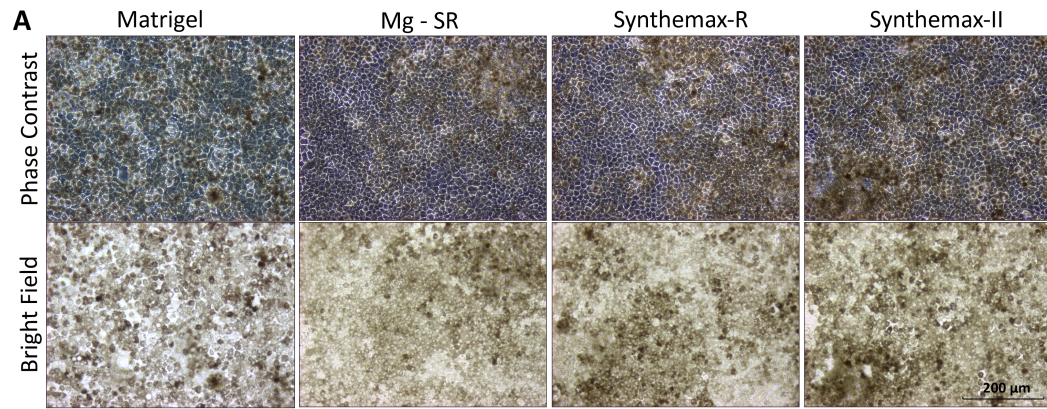


**Supplemental Figure 1:** Representative phase contrast images of H9 and H14 hESC colony morphology on Matrigel®, Synthemax®-R and Synthemax®II-SC during 7 passages. Images were taken 4-7 days post-seed. Scale bar = 200µm

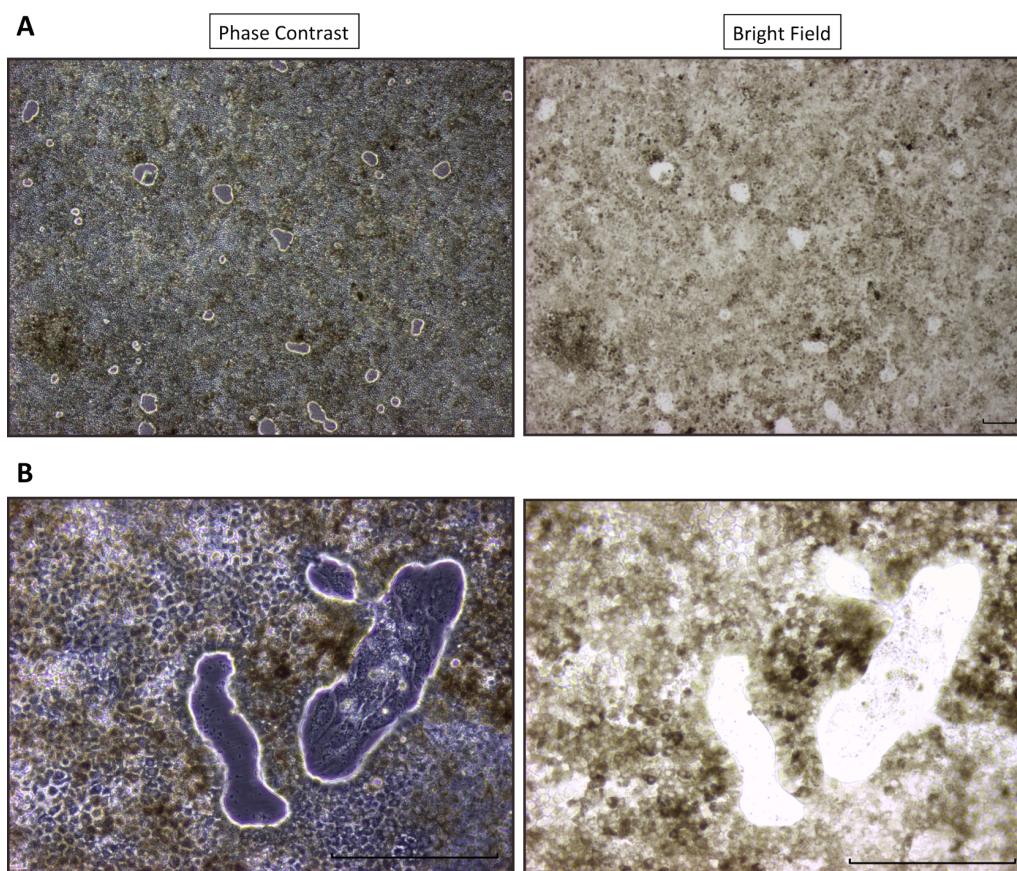


**Supplemental Figure 2:** Characterization of H14 hESCs maintained on Synthemax®II-SC  
**(A)** Representative flow cytometry histograms for pluripotency markers Oct4 and SSEA4 from H14 cultures grown on the indicated substrate at passages 1, 3, 5 and 9. **(B)** Relative mRNA expression of pluripotency genes in H14 cultures grown on Synthemax®II-SC, Synthemax®-R and Matrigel® at passages 1, 3, 5 and 9, as detected by qPCR. **(C)** Relative mRNA expression of germ layer markers in H14 hESCs differentiated on Synthemax®II-SC as detected by qPCR. **(D)** Normal karyotype of H14 hESCs maintained on Synthemax®II-SC for 16 passages.

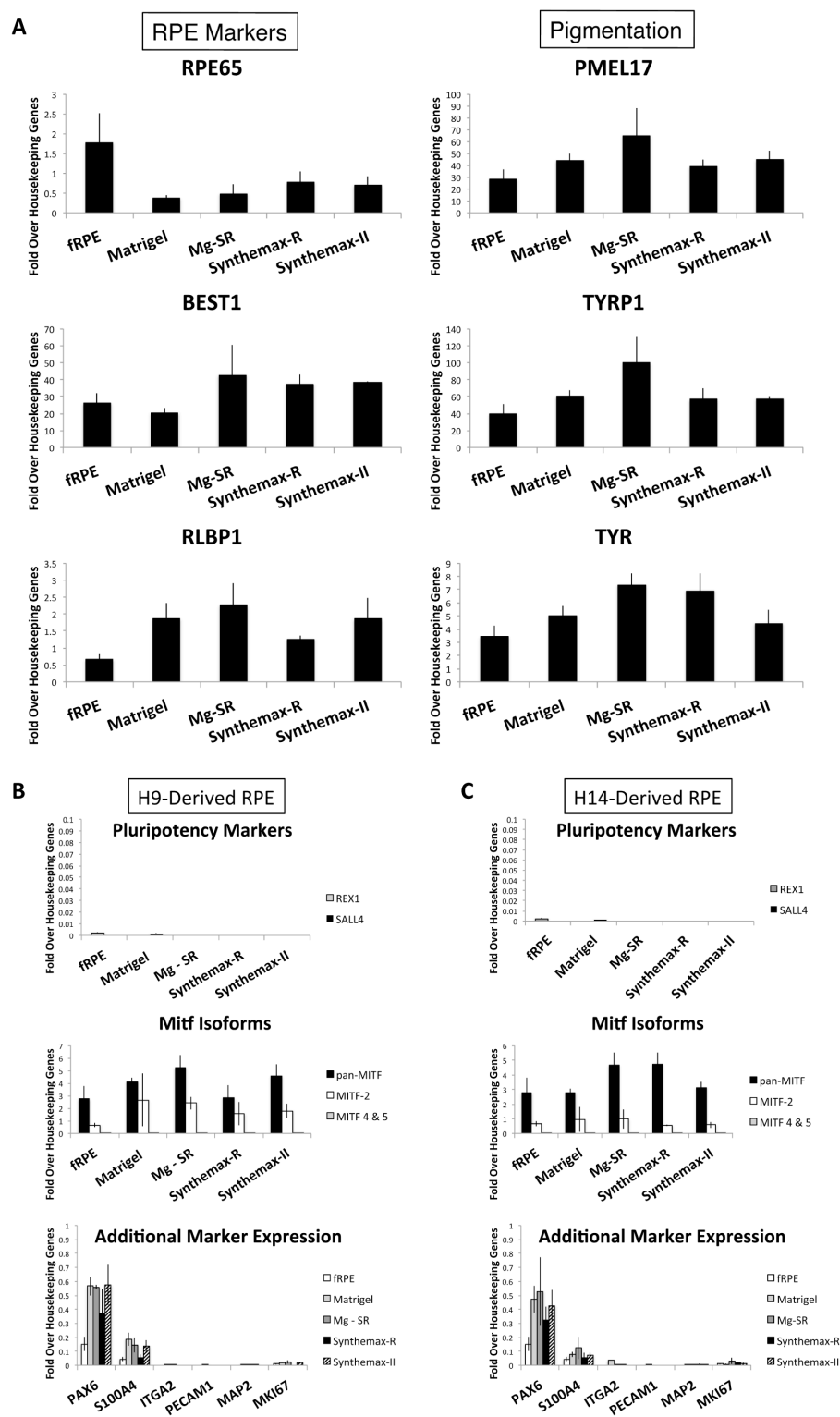




**Supplemental Figure 3:** Characterization of H14 hESC-RPE derived on Synthemax®II-SC. **(A)** Phase contrast and bright field images are shown of cells derived on different substrates. Mg-SR denotes the condition of hESCs grown and differentiated on Matrigel® then enriched as hESC-RPE on Synthemax®-R. Scale bar = 200µm. **(B)** Representative flow cytometry histograms are shown for the premelanosome pigmentation marker PMEL17 and the pluripotency marker Oct4 (not detected) for H14 hESC-RPE at passage 2, day 28 on the indicated substrate. **(C)** Validation of the flow cytometry antibodies. Oct4 antibody detects over 98% of the undifferentiated H9 positive control cells and 1.1% of Hs27 foreskin fibroblast negative control cells. PMEL17 antibody detects over 99% of MEWO human melanoma positive control cells and 1.2% of Hs27 negative control cells. **(D)** Normal karyotype of H14 hESC-RPE after spontaneous differentiation, enrichment and 3 passages on Synthemax®II-SC. **(E)** Quantification of ROS phagocytosis by H14 hESC-RPE derived on Synthemax®II-SC compared to H14 hESC-RPE derived on other substrates. Fetal RPE (fRPE) were used as a positive control. **(F)** Quantification of ROS phagocytosis by H14 hESC-RPE seeded onto surfaces coated with the defined substrates of Synthemax®II-SC or human vitronectin. The function-blocking antibody to integrin  $\alpha v \beta 5$  significantly hinders phagocytosis in all hESC-RPE cultures, \*\*  $p < 0.01$ , ttest.

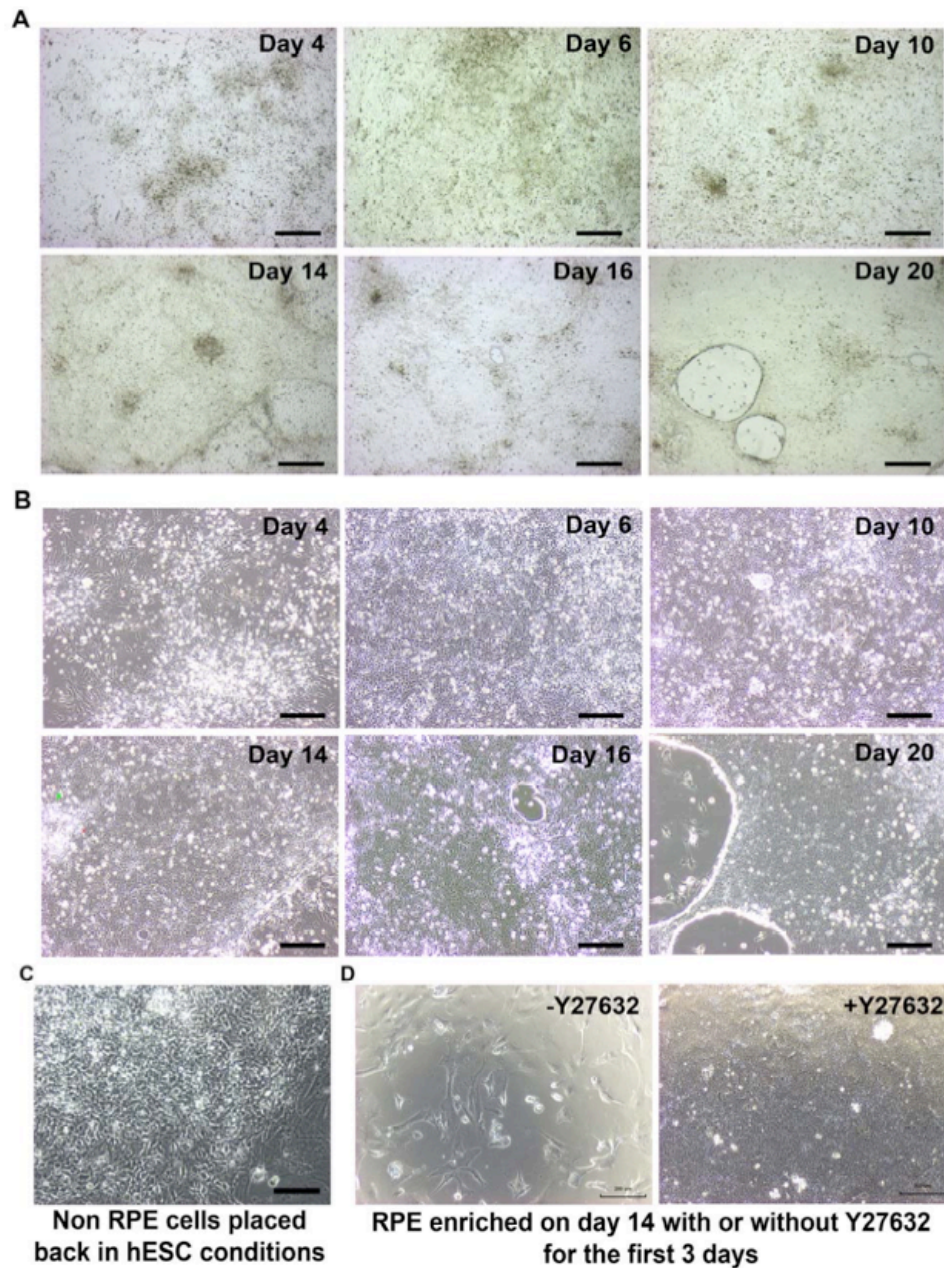


**Supplemental Figure 4:** Phase contrast and bright field images of lacunae in two hESC-RPE cultures on Synthemax®II-SC. **(A)** Lacunae in H9 hESC-RPE cultures on Synthemax®II-SC at passage 2 day 28. **(B)** Lacunae in H14 hESC-RPE cultures at passage 1 day 28. Scale bars = 200µm.

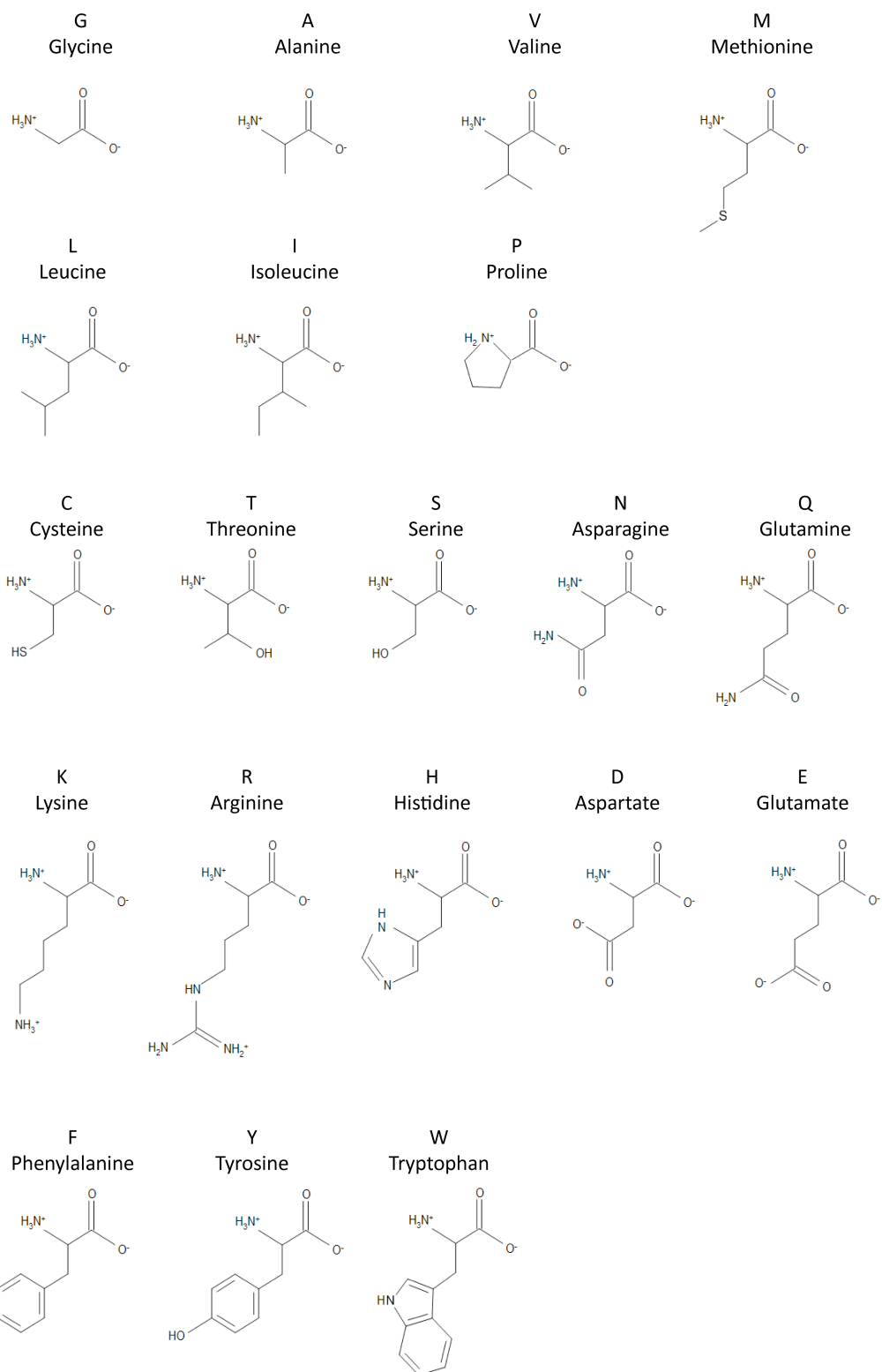


**Supplemental Figure 5:** Gene expression in H9 and H14 hESC-RPE (A) Expression of pigmentation and RPE marker genes in cells derived on the indicated substrate, as determined by qPCR. (B,C) Gene expression of genes indicated in H9 hESC-RPE and H14 hESC-RPE via PCR.





**Supplemental Figure 6.** The morphology of cells during differentiation and following enrichment. (A) 4X images of cells during differentiation. Scale bars = 500 $\mu$ m. (B) 10X images of cells during differentiation. Scale bars = 200 $\mu$ m. (C) Morphology of non-RPE cells enriched and culture under hESC conditions. Scale bar = 100 $\mu$ m. (D) Cells 21 days following enrichment on day 14 of differentiation with or without Y27632 during the first 3 days post enrichment. Scale bars = 200 $\mu$ m.



**Supplemental Figure 7:** Reference sheet with the 20 standard amino acids at pH7.  
Structures were drawn with Accelrys Draw 4.1 freeware.